Engineering Journal

American Institute of Steel Construction

Third Quarter 2013 Volume 50, No. 3

www.aisc.org

A Simplified Approach for Joist Girder Moment Frame Design Using Equivalent Beam Theory

PHILLIP A. KNODEL, ANDREA E. SUROVEK and JOSEPH J. POTE

ABSTRACT

The design of building structures has become a highly automated, computer-based process in which designers depend on the capabilities of commercial software for member strength checks and determination of deflections, drifts and member weights. Most commercial structural design software packages allow the user to build custom beam tables. The use of custom beam tables for joist girders requires the application of equivalent beam theory (EBT). Using EBT, section properties are determined in such a way that joist girder limit states are appropriately captured by strength checks employed by the software. By building custom beam tables, representing approximations of joist girders based on typical available chord sizes and typical ratios of weights, appropriate joist girder section properties can be estimated from almost any commercial structural software program. This paper presents the methodology for developing approximate section properties for steel joist girders that allow commercial software results to closely compare to joist manufacturers' designs.

Keywords: joist girder, beam theory, steel joist design.

INTRODUCTION

The design of building structures has become a highly automated, computer-based process in which designers depend on the capabilities of commercial software for member strength checks and determination of deflections, drifts and member/system weights. Currently available structural design software packages do not have the capabilities to estimate joist girder weight or section properties in an automated design process. For joist girders in moment frames, this is particularly critical because the stiffness of the joist girder affects the distribution of loads throughout the structure and the design of adjoining members, connections, etc. Consequently, selection of open-web steel joists and joist girders, as specified by the Steel Joist Institute (SJI), by commercially available software is typically limited to tabulated load tables for simply supported beams; estimates of joist girder properties and weights are unavailable. In particular, for complex loading, whether unequal loads at unequal spacing or lateral load-resisting frames with end moments and axial loads, the specifying professional has no automated tools for working with joist girders.

Joists and joist girders are custom designed for specific applications. Specific panel layouts and component sizes vary among manufacturers and may even vary among different plants or different design engineers for the same manufacturer. For this reason, it would be virtually impossible to provide accurate estimates of material sizes, weights and section properties in advance of the final joist or joist girder design. It is much more feasible to create a table of approximate joist girder material sizes, weights and section properties that can be used with commercial software programs.

The current design practice used for the design of joist girder moment frames (JGMFs) is detailed in *Technical Digest 11, Design of Lateral Load Resisting Frames Using Steel Joists and Joists Girders* (SJI, 2007). Additional discussion of JGMFs is provided in Green et al. (2009). There are two modeling issues in the approach that can cause problems in the design process:

- Computer software programs require the design engineer to input approximate values for moment of inertia, $I_{eff,}$ and area, A, based on estimated top and bottom chord sizes and joist girder depth. The estimation process is somewhat tedious and time-consuming, and the estimated properties must be checked and updated with each design iteration. Because the design engineer must estimate joist girder section properties without knowledge of the final joist girder design, the estimates for the moment of inertia used in the frame design may differ from the final joist girder design section property values by well over 20%, based on SJI anecdotal evidence.
- If the discrepancies between the properties determined from the final design by the joist engineer and those used in the analysis by the engineer of record (EOR)

Phillip A. Knodel, Design Engineer, New Millennium Building Systems, Butler, IN. E-mail: phillip.knodel@newmill.com

Andrea E. Surovek, Ph.D., P.E., Associate Professor, Civil and Environmental Engineering, South Dakota School of Mines and Technology, Rapid City, SD (corresponding). E-mail: surovek@sdsmt.edu

Joseph J. Pote, Director of Research and Development, New Millennium Building Systems, Hope, AR. E-mail: joe.pote@newmill.com

are large enough, redesign of multiple structural elements may be necessary based on the joist girder sizes determined by the joist engineer.

Most commercial structural design software allows the user to build custom beam tables with custom section properties. Custom beam tables for selection of virtual joist girders were developed for use in the design software STAAD.Pro (Bentley, 2007). The properties in these custom tables do not represent any specific joist girder or the exact properties of the final girder design. The properties are intended to be approximations, based on typical available chord sizes and some typical ratios of weights. The tables could be used in a wide range of applied design loads, including lateral-load-resisting moment frames. If an equivalent beam table for use in commercial software yields relatively close approximations of joist girder section properties and weights designed by the manufacturer, this tool would allow the EOR to easily include joist girders in their building design models in the same automated approach used for wide-flange beams.

The primary objective of this study was to validate a procedure to improve the ability of specifying engineers to accurately select joist girders for building design projects using commercially available design software. The research process was as follows:

- Testing and, where necessary, improvement of user input design tables that allow the EOR to select preliminary joist girders with estimates of moment of inertia values and member weights that have low variance from those designed using the proprietary joist design software.
- Computation of estimates of I_{zz}, shear area and member weight used in equivalent beam models in analysis software that closely match those provided by the joist manufacturer's software.
- Validation of the approach using realistic JGMF to show proof of concept.

BACKGROUND

Standard Joist Girder Design Procedure

Current methods for estimating sizes of joist girders in JGMFs can be tedious. In gravity frames, a joist girder and its equivalent properties can be input into a computer model of a structure by inputting data selected from a joist manufacturer's design catalog. While this method is not complex, it can become cumbersome with structures with a range of loading conditions or for in-progress projects that see changes to the load requirements being made as the structure is being designed.

The method for designing with joist girders in a moment-resisting load frame becomes much more complex because the stiffness of the joist girder affects the required strength and stiffness of the adjoined columns in the structural system. The method to accurately design a moment-resisting load frame with the use of joist girders is outlined in *SJI Technical Digest 11* (SJI, 2007) as follows:

1. Determine the loading (dead, live, wind, seismic) for every unique frame combination.

2. Make a preliminary selection of a joist girder of appropriate depth using the vertical loading only.

3. Approximate the moment of inertia using the following equation:

$$I_{eq} = 0.027NP_{npp}S_{jp}d \text{ (LRFD)} \quad (1a)$$

$$I_{eq} = 0.018NP_{npp}S_{jp}d \text{ (ASD)} \quad (1b)$$

where
I_{eq} = equivalent moment of inertia, in.^{4}
N = number of spaces between attached joists
P_{npp} = panel point load, kips
S_{jg} = joist girder span, ft
d_{jg} = effective joist girder depth, in.

4. Conduct a preliminary frame design to find the moments, shears and loadings in the frame, using the approximate joist girder moment of inertia. It is suggested to start with pinned base columns, with fixed rotation connections at the column–joist girder connection.

5. Use the lateral shear (the greater of the wind or seismic) per column value to calculate the maximum column moment, which is located at the bottom of the joist girder.

6. Select the load combinations that result in the worst loading, using the loads to select sufficient exterior and interior column sections.

7. Perform a computer analysis to determine forces, moments and deflections (both first- and second-order) for the load combinations prescribed by the applicable building code. The effects of leaning columns (if any) should be addressed in this analysis.

8. Use the end moments output by the analysis to calculate the maximum chord force in the joist girder. The chord force is the end moment divided by the depth of the girder, measured in between the centroids of the chords. It is assumed that the centroids of the chords are 1 in. from the top and bottom of the girder.

9. Use Table 2-1 in *SJI Technical Digest 11* (SJI, 2007) to choose a chord angle combination for the top and bottom of the joist girder. Calculate a new approximate joist girder moment of inertia, based on the chosen approximate chord angle section properties at the chosen joist girder depth.

10. Re-enter the new approximate moment of inertia into the model and re-analyze the model. If the new model fails to perform within the chosen drift and deflection parameters, the columns and chords must be approximated again.

Once a suitable design has been chosen for the columns and joist girders, the connections also need to be designed, and checks for local failures of the chords and webbing need to be completed. These last two steps would normally be the purview of the joist manufacturer unless special conditions need to be met.

As described, the method for joist girder design in moment frames is not automated, and the multistep process is iterative. Use of equivalent beam user tables allows this tedious manual approach to be replaced by an automated system of approximation that would yield similar, and potentially improved, results. The user table in this method is created using the entire practical range of chord sizes and a large range of depths. The equivalent beam properties of the joist girder are approximated using the properties from the top and bottom chords along with the selected joist girder depth.

Equivalent Beam Theory

Using equivalent beam theory (EBT), a complex flexural component such as a joist girder or other truss system is modeled as a single beam element with approximate equivalent beam properties. The use of an EBT model dramatically decreases the computational time of the software and the time required to input the joist girder into the structural model. As previously described, SJI provides the moment of inertia approximation given in Eq. 1 (SJI, 2007). As can be seen in Equations 1a and 1b, the approved EBT model is not applicable to joists or joist girders with uneven loading or unequally spaced loading.

Another method of utilizing equivalent beam theory explored by Giltner and Kassimali (2000) involves the direct modeling of a truss. The method involves designing a truss as one normally would for a structure. The loading and design configurations of the structure are considered, which are followed by a complete set of computer modeling under the applicable load cases. After the models are complete, the deflections of the truss are recorded. These deflections are then used to back-calculate the equivalent moment of inertia of a simple span beam with applied end moments. Once the equivalent moment of inertia is calculated, the equivalent beam can be used in the computer model for the entire structure wherever the comparative truss would have been placed. This method works well for a structure using custom trusses that are repeated often through a structure. The main benefit of using EBT is the reduction in processing time because the number of elements is reduced, as well as the time to enter the elements into the program. The method validates that the use of an equivalent beam model has the utility of decreasing the complexity of structural models while maintaining a good approximation of their behavior.

EQUIVALENT BEAM PROPERTY TABLES

In order to implement equivalent beam theory in a design program, a property table was developed for use in STAAD.Pro. Figure 1 presents a representation of the general configuration of a joist girder. The top and bottom chords are composed of two angles while the webbing can be either round or angle sections.

The properties included are typical of those required for user tables in commercial software, and the tables can be easily modified for use with other commercial software programs. Table 1 lists, in order, the properties included in the user table. A description of these properties and their approximations can be found in Appendix A.

Figure 2 displays a portion of the resultant virtual joist girder table. The file is simply a space-delineated text file. It is worth noting that in the virtual joist girder tables, the identifiers (e.g., 20GS1) call out the depth of the girders (e.g., the 20GS1 is 20 inches deep), but they otherwise do not have any significance other than to uniquely identify each data set.

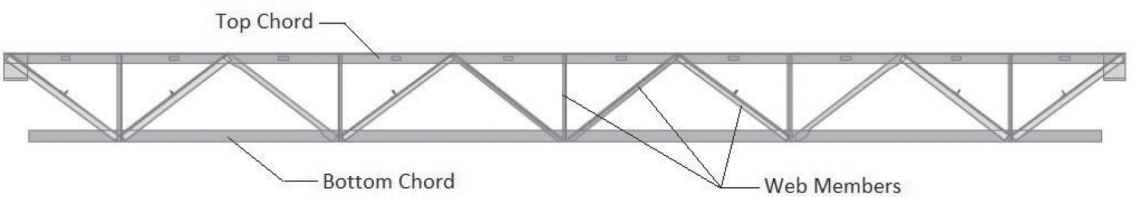

Fig. 1. Joist girder configuration.

The two properties of the most interest to the EOR and the joist designer are the moment of inertia, $I_{zz,}$ and the weight, the latter being approximately proportional to the chords area, A_x. The moment of inertia of a virtual joist girder is calculated using only the chords of the joist girder in the classical fashion. This value is then divided by 1.15 to account for shear deformation in the webbing. The webbing does not contribute any significant flexural stiffness.

The weight is calculated by using the cross-sectional area of the top and bottom chords, but the calculation does not explicitly consider the size of the webbing due to the large variation in webbing members used by joist manufacturers. The density of the virtual joist girder material is set to be the density of steel divided by 0.85 to account for the weight of the webbing. Joist girders with higher span-to-depth ratios will have more weight attributed to the chords, while joist girders with lower span-to-depth ratios will have more webbing and will therefore have less weight attributed to the chords. However, the 0.85 multiplier provides a simple method that represents an approximate average case, where 85% of the total joist girder weight is made up of the chord members.

STAAD.Pro calculates the member weight as a function of the member cross-sectional area and the material density. In order to correctly account for axial stresses in the STAAD.Pro code checks and material selections, it is essential to retain an accurate member cross-sectional area as the sum of the areas of the top and bottom chords. Therefore, the weight of the webs must be accounted for by adjusting the material density. Properties associated with out-of-plane limit states are not calculated in the tables but are set to unity. Lateral torsional buckling and weak-axis bending are not controlling limit states in joist girders due to industry standards for bracing; in instances where the design

Pseudo_Girder_Table - Notepad

File Edit Format View Help

```
UNITS INCHES
GENERAL
20GS1
3.548 20.000 0.667 6.000 0.224 271.802 7.315 1.000 32.730 2.438 0.887 0.887 32.730 1.000 1.000 2.500
22GS1
3.548 22.000 0.733 6.000 0.224 332.638 7.315 1.000 36.227 2.438 0.887 0.887 36.227 1.000 1.000 2.500
24GS1
3.548 24.000 0.800 6.000 0.224 399.644 7.315 1.000 39.724 2.438 0.887 0.887 39.724 1.000 1.000 2.500
26GS1
3.548 26.000 0.867 6.000 0.224 472.820 7.315 1.000 43.220 2.438 0.887 0.887 43.220 1.000 1.000 2.500
28GS1
3.548 28.000 0.933 6.000 0.224 552.166 7.315 1.000 46.717 2.438 0.887 0.887 46.717 1.000 1.000 2.500
30GS1
3.548 30.000 1.000 6.000 0.224 637.682 7.315 1.000 50.214 2.438 0.887 0.887 50.214 1.000 1.000 2.500
32GS1
3.548 32.000 1.067 6.000 0.224 729.368 7.315 1.000 53.710 2.438 0.887 0.887 53.710 1.000 1.000 2.500
34GS1
3.548 34.000 1.133 6.000 0.224 827.223 7.315 1.000 57.207 2.438 0.887 0.887 57.207 1.000 1.000 2.500
36GS1
3.548 36.000 1.200 6.000 0.224 931.249 7.315 1.000 60.704 2.438 0.887 0.887 60.704 1.000 1.000 2.500
38GS1
3.548 38.000 1.267 6.000 0.224 1041.444 7.315 1.000 64.200 2.438 0.887 0.887 64.200 1.000 1.000 2.500
40GS1
3.548 40.000 1.333 6.000 0.224 1157.809 7.315 1.000 67.697 2.438 0.887 0.887 67.697 1.000 1.000 2.500
42GS1
3.548 42.000 1.400 6.000 0.224 1280.344 7.315 1.000 71.194 2.438 0.887 0.887 71.194 1.000 1.000 2.500
44GS1
3.548 44.000 1.467 6.000 0.224 1409.048 7.315 1.000 74.691 2.438 0.887 0.887 74.691 1.000 1.000 2.500
46GS1
3.548 46.000 1.533 6.000 0.224 1543.923 7.315 1.000 78.187 2.438 0.887 0.887 78.187 1.000 1.000 2.500
48GS1
3.548 48.000 1.600 6.000 0.224 1684.967 7.315 1.000 81.684 2.438 0.887 0.887 81.684 1.000 1.000 2.500
50GS1
3.548 50.000 1.667 6.000 0.224 1832.181 7.315 1.000 85.181 2.438 0.887 0.887 85.181 1.000 1.000 2.500
52GS1
3.548 52.000 1.733 6.000 0.224 1985.566 7.315 1.000 88.677 2.438 0.887 0.887 88.677 1.000 1.000 2.500
54GS1
3.548 54.000 1.800 6.000 0.224 2145.119 7.315 1.000 92.174 2.438 0.887 0.887 92.174 1.000 1.000 2.500
56GS1
3.548 56.000 1.867 6.000 0.224 2310.843 7.315 1.000 95.671 2.438 0.887 0.887 95.671 1.000 1.000 2.500
58GS1
3.548 58.000 1.933 6.000 0.224 2482.737 7.315 1.000 99.168 2.438 0.887 0.887 99.168 1.000 1.000 2.500
60GS1
3.548 60.000 2.000 6.000 0.224 2660.800 7.315 1.000 102.664 2.438 0.887 0.887 102.664 1.000 1.000 2.500
62GS1
3.548 62.000 2.067 6.000 0.224 2845.034 7.315 1.000 106.161 2.438 0.887 0.887 106.161 1.000 1.000 2.500
64GS1
3.548 64.000 2.133 6.000 0.224 3035.437 7.315 1.000 109.658 2.438 0.887 0.887 109.658 1.000 1.000 2.500
```

Fig. 2. Excerpt of user table file.

Table 1. Equivalent Beam Properties			
A_x	Total area of the chords	S_z	Elastic section modulus about strong axis
D	Girder depth	S_y	Elastic section modulus about weak axis
TD	Web thickness	A_y	Shear area in y direction
B	Flange width	A_z	Shear area in z direction
TB	Flange thickness	P_z	Plastic section modulus about strong axis
I_{zz}	Joist girder strong-axis moment of inertia	P_y	Plastic section modulus about weak axis
I_{yy}	Joist girder weak-axis moment of inertia	HSS	Warping constant
I_{xx}	Torsional constant	DEE	Depth of web

requirements require out-of-plane limit states to be considered, this method is not recommended.

VALIDATION STUDIES

A three-stage process was used to establish the validity of the equivalent beam user tables for commercial design use. First, simply supported isolated joist girder designs were considered, eliminating the effect of support conditions or adjoining members on the results, to establish if the user tables were effective in the most fundamental design case. Next, isolated fixed-end joist girders were considered to include the effect of end moment. Finally, simple frames were designed to establish proof of concept, including the effects of adjoining beam-columns and leaning columns.

Because final joist girder design is always performed by the joist manufacturer, the objective was to determine if the moment of inertia and weight of the design software selected virtual joist girders were within an acceptable range of error from the joist girders designed by the robust proprietary joist design software. The primary difference in the two design processes is that the general commercial design software chooses a single-member equivalent beam with approximate property values, whereas the proprietary design software utilizes the actual joist girder truss configuration with multiple members.

Parameters for the isolated joist girder studies (simply supported and fixed) were chosen to represent a reasonably comprehensive, yet practical, range of design conditions. The intent was not to consider every possible permutation, but rather a representation of the practical values in design. The range of parameters was suggested by an advisory group consisting of members of the SJI Research Committee and Engineering Practice Committee based on their years of experience in joist and joist girder design. The ranges for the parameters considered in the single beam studies were as follows:

- Span: 20 ft to 80 ft at 10 ft intervals.
- Panel-point loads: 10 kips to 90 kips at 20-kip intervals.
- Panel-point spacing: 4, 5, 6 and 8 ft.

The joist depth was not an independent parameter, but was determined by design. Span-to-depth ratios were limited to between 12 and 24.

Based on the chosen parameters, there were 105 possible practical permutations of the span, spacing and loading. Combinations that cause overstressed members in the proprietary design program were removed from consideration, as were panel point spacings that did not equally divide the joist length, and joist girders using chords with leg lengths greater than 6 in.

The user table created to provide STAAD.Pro with equivalent beams includes a reasonably comprehensive selection of realistic combinations of chords and depths in joist girders. The two most relevant properties are computed based on SJI suggested values as follows:

$$I_{zz} = \frac{I_{chords}}{1.15} = \frac{\sum (I_{chord} + A_{chord} d^2)}{1.15} \tag{2}$$

$$\text{Material density} = \frac{\text{Density of steel}}{0.85} \tag{3}$$

where

I_{zz} = moment of inertia of the joist to be used in calculations
I_{chords} = moment of inertia calculated from the joist chords not considering web deformation
I_{chord} = moment of inertia of the chord members
A_{chord} = area of chord members
d = distance from the centroid of the chord to the centroid of the joist

The following procedure was used in the verification of the equivalent beam model:

1. Span, spacing and load configuration are chosen. The design is entered into STAAD.Pro, and the program is allowed to choose a joist girder with a depth that is within range of span-to-depth ratios from 12 to 24.

2. The unique identifier, total weight, moment of inertia

Table 2. Pinned-End Virtual Joist Girders with Partial Bracing			
Acceptable variance (±)	10%	15%	20%
Number considered	76	76	76
I acceptable	76%	80%	84%
Weight acceptable	63%	72%	83%
Both acceptable	62%	71%	82%

and end moments (if fixed ends) of the joist girder selected by STAAD.Pro are recorded.

3. The depth of the selected joist girder, along with the same span and loading configuration, is entered into the proprietary joist girder design software.

4. The corresponding results are compared and the variation in results is calculated.

To provide a full set of test permutations, the same procedure was run for joist girders of the same span, spacing and loading configuration, except a depth was specified in STAAD.Pro. This produced values that might be encountered in situations where architectural constraints might affect allowable joist depth.

Simply Supported Joist Girders

The model used for the simply supported joist girder studies is shown in Figure 3. Here, S_{pp} is equal to the panel point spacing; the other variables are defined in Equations 1a and 1b.

The first set of simply supported beam studies were run according to the previously described equivalent beam testing procedure. At the end of the study, 76 cases produced designs with an angle leg of 6 in. or smaller; this limit was recommended by the SJI advisory group and imposed in these studies. The results are summarized in Table 2. Complete results are reported in Knodel (2011). Results of a single beam test were deemed "acceptable" if the value of Equation 4 was within a designated variance from the proprietary software values and given by:

$$\frac{\text{STAAD\_value} - \text{P.Software\_value}}{\text{P.Software\_value}} \times 100\% \qquad (4)$$

where

STAAD_value = moment of inertia or weight of joist girder selected by STAAD.Pro

P.Software_value = moment of inertia or weight of joist girder designed by SJI proprietary software

The initial set of simply supported beam studies presented a practical limitation of the virtual joist girder tables. After completing 102 tests on pinned-end joist girders, 76 were included in the results. These did not exceed a 6-in. maximum chord leg, an upper limit suggested by SJI for this study.

Initial examination of the results determined that a number of the joist girders were failing in STAAD.Pro due to lateral torsional buckling (LTB). The parametric study was then re-run with the bracing in STAAD.Pro changed from panel point bracing to continuous lateral support. While the equivalent beam theory works well for in-plane bending of joist girders, the equivalent beam section properties that control lateral torsional buckling—including C_W, I_y and J—have not been well defined for steel joists and are consequently not correctly modeled in the user tables. Additionally, typical steel joists designs have adequate lateral bracing, so LTB

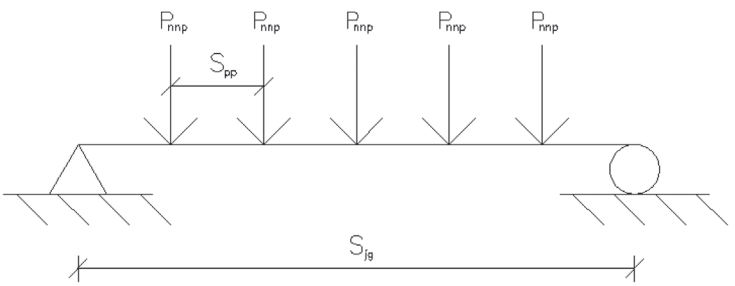

Fig. 3. Simply supported isolated joist girder.

Table 3. Pinned-End Virtual Joist Girders			
Acceptable variance (±)	10%	15%	20%
Number considered	78	78	78
I acceptable	97%	99%	99%
Weight acceptable	72%	86%	97%
Both acceptable	72%	86%	97%

Table 4. Fixed-End Virtual Joist Girders			
Acceptable variance (±)	10%	15%	20%
Number considered	82	82	82
I acceptable	91%	100%	100%
Weight acceptable	71%	91%	99%
Both acceptable	70%	91%	99%

is typically not considered to be a limit state in joist girder design. Changing the lateral support condition changed the controlling limit state to in-plane bending; this represented the joist behavior and allowed for direct comparison with the proprietary joist girder design software results.

Once tests were re-run with continuous lateral bracing, a significant improvement was noted in agreement between the designs of the two programs. With continuous lateral bracing, STAAD.Pro selected lighter joist girders in many instances, resulting in 78 joist girders within the 6-in. maximum chord size limit. These results are summarized in Table 3.

As can be seen in Table 3, the acceptability of the moment of inertia approximation for pinned-end virtual joist girders is close to complete acceptability at a ±10% acceptable variance. It can be seen that increasing the acceptability criteria to ±20% increased the weight approximations acceptability by 25%. It is clearly demonstrated in the overall results that the decision to use a completely braced model results in a much more accurate approximation of actual joist girder behavior.

Fixed-End Joist Girders

The trials on fixed-end joist girders utilized the same virtual joist girder user table as the pinned-end, single beam trials. Out of the 105 joist girders designed, 82 of the designs were at or below the 6-in. maximum chord size limit. A summary of the results is given in Table 4.

As can be seen in Table 4, the acceptability of the moment of inertia approximation for fixed-end virtual joist girders is acceptable 91% of the time when considering ±10% variance. Increasing the acceptability criteria to ±15% increased the weight approximations acceptability from 71 to 91% and the moment of inertia approximation to complete acceptability (100%).

Trends in Variance of Isolated Joist Girder Designs

The results of the beam studies were examined to determine if improvements could be made to the approximate properties typically used by SJI to provide for better estimates in the virtual joist girder user table, particularly with respect to weight. Variance was plotted with respect to depth and length/depth ratios to establish any trends in error that could lead to better estimates for the properties. Figures 4 and 5 show representative plots of the variance data for the fixed-end joist girders comparing moment of inertia and weight to depth, respectively.

As expected, a minor correlation was seen in the variance when considering weight versus span/depth ratio. On average, 85% of a joist girder's weight is from the top and bottom chords. In a more shallow joist girder (span-to-depth ratio of 24), 90% of the joist girder weight will typically come from the chords. In a deeper joist girder (span-to-depth ratio of 12), typically only 80% of the total weight may come from the chords, and the equivalent beam will typically underestimate the weight of deep joist girders. Because the span-to-depth ratio is not a known parameter prior to preliminary design, it was not considered a practical parameter for any possible adjustments to the weight approximation for use in the tables.

Based on the scatter of the data, no significant correlation was established that would provide a means to adjust the weight or moment of inertia approximation. The SJI recommended approach of increasing density by dividing the

value of steel by 0.85 was not changed for the remainder of the study nor was the moment of inertia approximation of $I_{chords}/1.15$.

MOMENT FRAME STUDY

To study the behavior of the virtual joist girder method in a system where the effects of adjoining members are considered, a series of frames were run in the same manner as the single beam studies. The parameters of the tests can be seen in Figure 6 and include bay width, L; frame height, H; and leaning column load, αP. Specifically, the value αP represents the destabilizing effect of leaning columns on the frame, where P is an equivalent one-bay load applied as a point load to the column and α is the number of columns "leaning" on the moment frame. The parameters were chosen to represent a typical joist girder design. The parameters of the frame study resulted in 24 unique frames, each with three virtual joist girder spans. Frames with 40-ft spans were designed with a joist spacing of 8 ft. Frames with 50-ft spans were designed with a joist spacing of 5 ft. The frame studies followed the same procedure as the isolated joist girder studies, with one additional step. Once the proprietary software design was complete, the specific properties of that design were input in STAAD.Pro, and the resulting frame designed was analyzed. A comparison of the interaction value of the controlling limit state was made between the preliminary design and the proprietary design to determine the impact of the variation in joist girder properties on the beam-column designs.

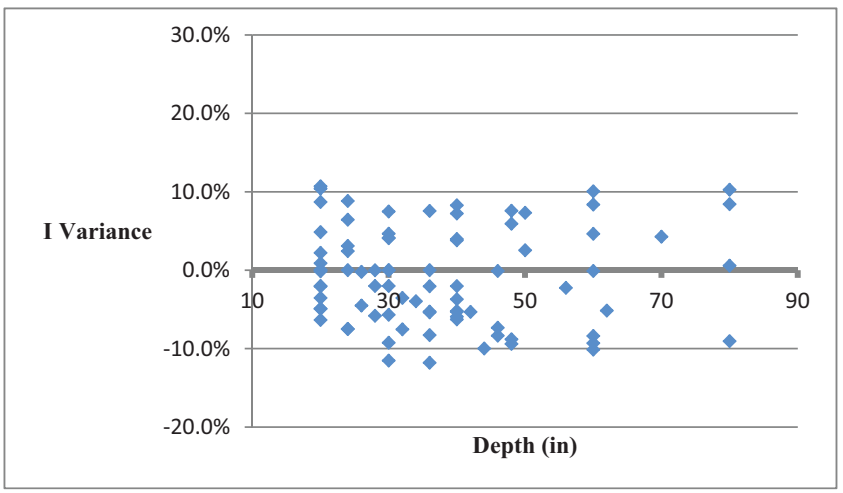

Fig. 4. Fixed-end condition moment of inertia variance versus joist girder depth.

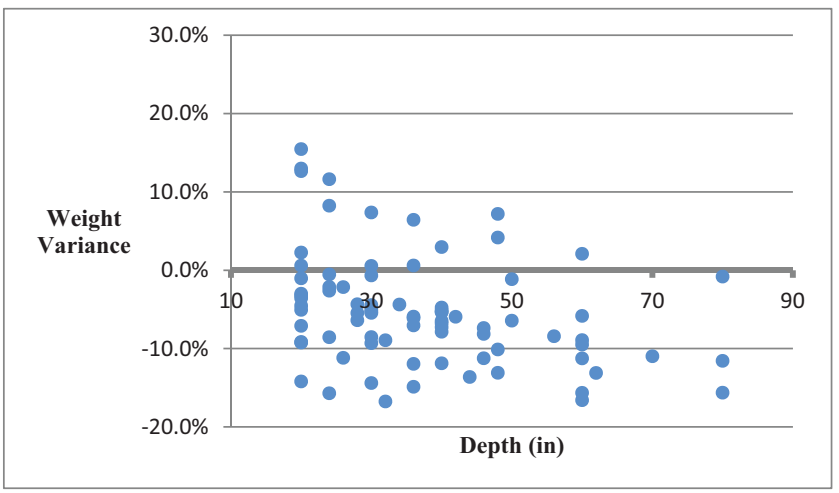

Fig. 5. Fixed-end condition weight variance versus joist girder depth.

Table 5. Fixed-End Virtual Joist Girders in Frames			
Acceptable variance (±)	10%	12.5%	15%
Number considered	72	72	72
I acceptable	88%	96%	100%
Weight acceptable	90%	100%	100%

Frame Study Results

The results from the frame study resulted in a total of 72 tested virtual joist girders. The virtual joist girders selected by STAAD.Pro included no overstressed joists girders or designs with chord sizes with legs longer than 6 in. Table 5 provides a summary of the variances. A summary of all results from the parametric studies is presented in Knodel (2011).

As in the fixed-beam study, the virtual joist girder study results show a high level of acceptability when considering the initial ±10% variance with 100% acceptable variance when considering a ±15% variance. Over the course of the frame study, the column stress ratios and story drifts were recorded. As reported in Knodel (2011), the story drift for all 24 frames never exceeded $H/100$, and 17 of the 24 frames did not exceed an $H/200$ story drift. It can also be seen that the stress ratios for columns never changed more than 5% between the first and second design iterations with the average difference being insignificant (0.2%).

OUTLIER INVESTIGATION

A review was performed of the individual cases in which the variance exceeded 10% in order to establish the specific reasons for the design variations. The review looked at five individual cases and resulted in four different design situations. The reader should note that the five cases examined were above 10% variance when comparing the proprietary software data to the STAAD.Pro data. The final results of the virtual joist girder study are reported using the proprietary software as the baseline.

The first two cases with the greatest variance examined showed that STAAD.Pro picked a virtual joist girder with larger chord sizes than the proprietary software. It was found that when STAAD.Pro picked an initial member size, there was a small overstress that resulted in STAAD.Pro choosing a new, larger section size. Coincidently, the next larger size was a chord with a longer leg length, which dramatically changed the properties. This relatively large change in size pushed the variance over the 10% limit. With further investigation, it was found that the initial small overstress in STAAD.Pro was caused by the approximately 2% increase in loading due to self-weight of the virtual joist girder. Because the self-weight is neglected in the proprietary joist design software settings, the extra stress was not detected and the chords were not upsized. It can be noted that the initial pick by STAAD.Pro—before self-weight calculation—was the same as the proprietary software. It was noticed after the project had been completed that this inconsistency in self-weight inclusion had occurred. While introducing error into the overall results, that error renders the results an upper bound of variance between EOR and joist designer results.

The other three cases examined were very close to the 10% variance limit. In all cases, the STAAD.Pro chord pick

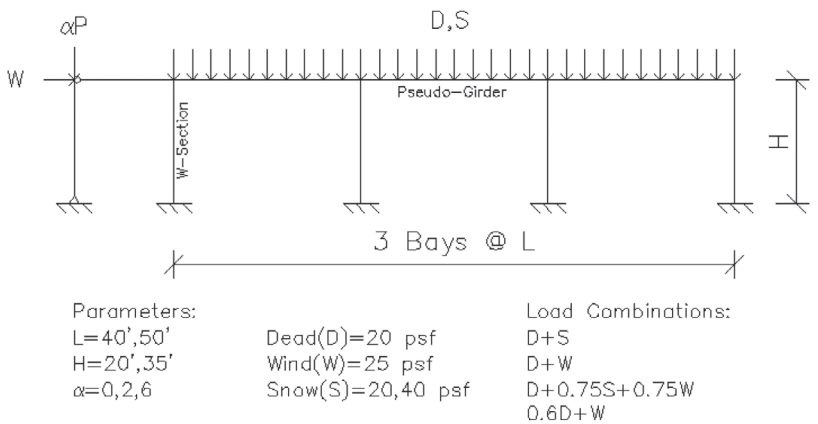

Fig. 6. Moment frame configuration and parameters.

was smaller than the pick from the proprietary joist design software. In two of the cases, clear reasons could be identified for the discrepancies in the designs, as follows:

- In the first case, the joist girder had a localized failure on the chord angle under the high 30-kip loading, which controlled the top chord selection in the proprietary software. If stiffeners were used to support the horizontal leg of the top chord, or some other means were used to minimize the localized bending stress effects, then the STAAD.Pro chord choice would be acceptable.
- The next case suffered in-plane buckling of the four panels nearest the mid-span, which controlled the design of the top chord in the proprietary software. If two panels were added to either side of the midspan, halving the effective panel length, the STAAD.Pro pick would be suitable.

Overall, it is concluded that the outlier conditions found in the study were no different than the typical variance found between the designs of different SJI member companies for the same loading and geometric configuration.

CONCLUSIONS AND RECOMMENDATIONS

Designing with steel joist girders is currently a labor-intensive task, especially when considering design timetables that force early assumptions or designs with complex loadings. An automated design process utilizing a pseudo–joist girder section table allows for changing and complex projects to consider joist girders more readily. The virtual joist girder method provided designs within 10% of the joist girder manufacturer's design approximately 90% of the time, when considering the design moment of inertia, and weight approximations were within 20% variance more than 90% of the time. The single beam studies provide a wide range of possible design configurations. The frame studies showed particularly good results with 100% of the frame designs falling within 15% variance levels; in addition, there was little to no effect on the column response to the variance in the joist girder selections.

Overall, this study suggests that the virtual joist girder user tables provide a straightforward and user-friendly approach for automated preliminary design of joist girders by the specifying engineer. The method for using the tables STAAD.Pro is included in Appendix B, although the tables are easily adaptable for other commercial design programs. Also, although no seismic load conditions were run in the frame studies, there appears to be no reason the approach could not be used for seismic designs utilizing equivalent static seismic loads; design examples with seismic loading will be developed as part of an upcoming SJI research project to determine if any specific limitations are required.

The virtual joist girder tables are available as of this writing (2012) from SJI for use by design engineers, and may be downloaded by visiting http://steeljoist.org/virtual-joist-girder-table. SJI is currently examining extension of the tables to include all open web joists (including K-, LH-, and DLH-series joists) to facilitate improved selection and weight estimation of joists by the EOR when using commercially available structural design software.

ACKNOWLEDGMENTS

This research was sponsored by the Steel Joist Institute. The opinions presented are solely those of the authors and not of SJI or any other organizations. Bentley Systems Inc. provided a seat license for STAAD.Pro for this project, and Phil Hodge provided the HABCO joist design software package currently in use by several SJI member companies.

The authors wish to acknowledge the input and assistance offered by members of the SJI Research Committee, in particular David Samuelson of Nucor Research and Development for Downstream Products and Walter Worthley of Valley Joist Inc.

REFERENCES

Bentley (2007), Staad.Pro Software V7, Bentley Systems Inc., Exton, PA.

Giltner, Brian and Kassimali, Aslam (2000), "Equivalent Beam Method for Trusses," *Practice Periodical on Structural Design and Construction,* ASCE, Vol. 5, No. 2, pp. 70–77.

Green, Perry S., Fisher, James M. and Pote, Joe (2009), "Design of Lateral Load Resisting Frames Using Steel Joists and Joist Girders," *Don't Mess with Structural Engineers: Expanding Our Role, Proceedings of the 2009 Structures Congress,* April 29–May 2, ASCE.

Knodel, Phillip (2011), *Development of an Improved Design Method for Joist Girder Selection in a Generalized Structural Design Program*, M.S. Thesis, South Dakota School of Mines and Technology, Rapid City, SD.

SJI (2007), *Technical Digest 11, Design of Lateral Load Resisting Frames Using Steel Joists and Joist Girders,* Steel Joist Institute, Myrtle Beach, SC.

APPENDIX A
Virtual Joist Girder Properties

A_x Total area of top and bottom chords: Sum of top and bottom chord areas.

D Total joist girder depth.

TD Web thickness: Total depth/30; ensures that the section is treated as compact when considering web shear.

B Flange width: 2 × Chord angle leg + 1 in. chord gap.

TB Flange thickness: (Chord angle thickness/Chord angle leg) × B/2; this value results in the correct width-to-thickness ratio when STAAD.Pro checks (B/2)/TB.

I_{zz} Joist girder strong-axis moment of inertia: Classically calculated moment of inertial then divided by 1.15 to reduce to obtain an effective I.

I_{yy} Joist girder weak-axis moment of inertia: 2 × Top chord moment of inertia; based on flange (chord) that would typically be in compression; not required in open web joist design.

S_z Elastic section modulus about strong axis: Minimum chord area × Joist effective; reduces the overestimation of chord (flange) stresses. The method substitutes an effective section modulus based on a stress distribution used in classis truss theory of uniform stress distribution across the cross section of the member.

S_y Elastic section modulus about weak axis: Section modulus of top chord; a reasonable conservative value used when joist girder is used in out-of-plane bending.

A_y Shear area in y direction: A_x × 0.25; based on an approximation of the shear area used by SJI for chord shear checks.

A_z Shear area in z direction: A_x × 0.25; based on an approximation of the shear area used by SJI for chord shear checks.

P_z Plastic section modulus about strong axis: Equals S_z; stress distribution is always uniform across the chord in classical truss analysis, whether in a plastic or elastic state.

P_y Plastic section modulus about weak axis: Unity; not required in open web joist design.

HSS Warping constant: Unity; not required in open web joist design.

DEE Depth of web: Equals top chord angle leg length.

APPENDIX B
User Manual

The following instructions are applicable for the use of the virtual joist girder user table in STAAD.Pro.

Installing User Table File

1. Create directory (folder) for STAAD.Pro design files that will be using the virtual joist girder user table.
2. Place a copy of the user table file into the same directory.
3. Any design files saved in a directory without the user table file will not be able to access the user table data.

Activating User Table

1. In modeling mode select *Tools*.
2. Select *Create User Table*.
3. In the pop-up window select the *New Table* button.
4. Checkmark the *External Table* box and select the *Browse* button.
5. Select the user table file and click *Open*.
6. In the *Select Section Type* drop down menu, choose *General* and press *OK*.
7. The user table should automatically be given a number. Press *Close*.

Assigning User Table Data

1. In modeling mode, select the *General* tab.
2. In the Properties–Whole Structure window, select the *User Table* button.
3. Choose the previously assigned user table number.
4. Select a section and assign the appropriate material.
5. Select *Add* and close the window.
6. Assign virtual joist girder sections from the Properties–Whole Structure window in the same manner as with ordinary sections.

Virtual Joist Girder Material Properties

Virtual joist girders use the same material properties as steel, except with a higher density. Then density modification is required to accurately approximate the weight of a steel joist girder.

To create a new material in STAAD.Pro:

1. In modeling mode, select the *General* tab.
2. Select the *Material* tab.
3. Select the *Create* button in the pop-up window.
4. Name the new material and enter the following data:
   Young's modulus, $E = 2.9e+007$ lb/in.^{2}
   Poisson's ratio, $\nu = 0.3$
   Density = 0.333 lb/in.^{3}
   Thermal coefficient, $\alpha = 6e{-}006$
   Critical damping = 0.03
   Shear modulus, $G = 1.1154e+007$ lb/in.^{2}

Notes on Using the Virtual Joist Girder User Table

1. All virtual joist girders must be modeled as having an unbraced length of zero.
2. Virtual joist girder designations shown in STAAD.Pro and in the .txt user table file do not correspond to specific joist girders. The virtual joist girders user table is for initial design approximation only.

Stability Design of Cross-Bracing Systems for Frames

ERIC M. LUI and XIAORAN ZHANG

ABSTRACT

In this study, the inelastic load-carrying capacity of the compression diagonal of a typical cross-bracing system used in concentrically braced frames under gravity and wind loads is investigated, taking into consideration its interaction effect with the tension diagonal. Depending on the lateral stiffness of the tension diagonal, the compression diagonal can be fully or partially braced by the tension diagonal at their intersection point. An expression for the transition lateral stiffness, k_{st}, that demarcates the fully and partially braced conditions is derived. When the compression diagonal is fully braced, its maximum load-carrying capacity is a function of its member slenderness, L/r, only. However, when the compression diagonal is partially braced, its load capacity is dependent upon both its member slenderness, L/r, and the lateral stiffness, k_s, of the tension diagonal. Once the equations for the maximum load-carrying capacity of the compression diagonal are established, design guidelines are proposed and design examples are given to demonstrate how the proposed guidelines can be used for the design of cross-bracing systems in steel frames. The consideration of the lateral bracing effect will result in a more economical and logical design for such bracing systems.

Keywords: cross-bracing systems, steel frames, inelastic analysis, stability design.

INTRODUCTION

Cross braces are used in concentrically braced steel frames to provide resistance against excessive sway caused by horizontal loads. They are also used in industrial buildings to resist crane surge and in roof trusses to account for load reversal under wind uplift (Kitipornchai and Finch, 1986).

Under a lateral load, one member of this cross-bracing system is often under tension, while the other is subjected to compression. However, in conventional design of cross-bracing systems for wind load, a common yet conservative assumption is that only the tension diagonal resists the applied lateral load. The contribution of the compression diagonal to resist frame sway is neglected (El-Tayem and Goel, 1986). Although this assumption can simplify the design, the result is an overdesign of the bracing system. A somewhat less conservative approach is to design the compression diagonal as a column supported at midspan by the tension diagonal. Timoshenko and Gere (1961) derived the relationship for the elastic buckling load of a column braced at mid-point. However, the nonlinear relationship is rather complicated and is therefore difficult to apply in a design situation.

Eric M. Lui, Ph.D., Meredith Professor, Department of Civil and Environmental Engineering, Syracuse University, Syracuse, NY (corresponding). E-mail: emlui@syr.edu

Xiaoran Zhang, MSCE, Graduate Assistant, Department of Civil and Environmental Engineering, Syracuse University, Syracuse, NY. E-mail: xzhang42@syr.edu

To achieve a more concise and practical method for design, Picard and Beaulieu (1987, 1988) carried out a series of analytical and experimental studies to establish the relationship between the ultimate strength of the bracing system and the internal forces in both diagonals. They recommended the use of an effective length factor K of 0.5 applied to the full length of the member in the design of the compression diagonal. Nevertheless, their research is limited to the condition in which no out-of-plane translational movement is experienced by either diagonal at their intersection point.

Stoman (1989) provided a set of effective length spectra for cross bracing within the elastic range. However, Stoman's study did not provide any formula to quantify the lateral support to the compression diagonal by the tension diagonal. Moon et al. (2008) proposed values for the effective length factor K for use in an elastic design of the compression diagonal and checked the validity of the proposed K factors with the AISC equation for the inelastic case. However, no direct mathematical relationship relating the inelastic ultimate strength of the compression diagonal with other system parameters is given. The objectives of this article are, therefore, to investigate the interaction effect between the compression and tension diagonals of a typical cross-bracing system under combined gravity and wind loads and to develop equations suitable for use in the design of such system.

If the compression and tension diagonals are connected at their intersection point and if all the connections are properly designed for strength and ductility (Sabelli and Hohbach, 1999), the ultimate strength of the cross bracing is mostly controlled by the out-of-plane buckling capacity of the compression diagonal. This out-of-plane buckling capacity can be more accurately determined if the tension diagonal is

taken into consideration in design. Even though the tension diagonal may not always have the necessary lateral stiffness to enable the compression diagonal to buckle in its second mode, it often provides sufficient out-of-plane restraint to the compression diagonal at the intersection point so that the ultimate strength of the compression diagonal will be higher than that predicted based on its first buckling mode (i.e., by ignoring the bracing effect provided by the tension diagonal altogether).

The amount of increase in the buckling capacity is a function of the slenderness ratios, L/r, boundary conditions and effective stiffness (stiffness accounting for the axial force effect) of both the compression and tension diagonals. In addition, geometrical imperfections and inelastic behavior of the cross-braced members will also have an effect on system stability. The objective of this study is to investigate the effects these factors have on the ultimate strength of a typical cross-bracing system. This study will focus on cross-bracing systems primarily used for concentrically braced frames, that is, a symmetrical system in which the intersection point occurs at the braces' half-lengths and that the connection provides full continuity (e.g., the use of welded or fully bolted connections) for both braces as shown in Figure 1. In the current analysis, it is assumed that system behavior is controlled by out-of-plane buckling of the braces as depicted in Figure 2. As will be discussed in more detail in a later section, the symmetric out-of-plane buckling mode corresponds to the partially braced condition and the anti-symmetric out-of-plane buckling mode corresponds to the fully braced condition. Unless both diagonals are subjected to the same compressive force, one will provide lateral support to the other. Normally, the brace that is providing the lateral support is in tension, but even when both braces are in compression, the brace that is subjected to a lower compressive force can still brace the one with a higher compressive force, although the amount of lateral support that can be relied upon in this scenario will undoubtedly be lower.

CROSS-BRACING SYSTEM MODEL

In reference to a diagonal cross-bracing system shown in Figure 3, if the beam-column joints to which the ends of the cross-bracing system are connected are braced against out-of-plane deflections, the support conditions of the cross-bracing system can conservatively be idealized as pinned. If we denote P as the compressive force acting on the compression diagonal with length L and flexural rigidity EI, and $\overline{P}$ as the tensile force acting on the tension diagonal with length $\overline{L}$

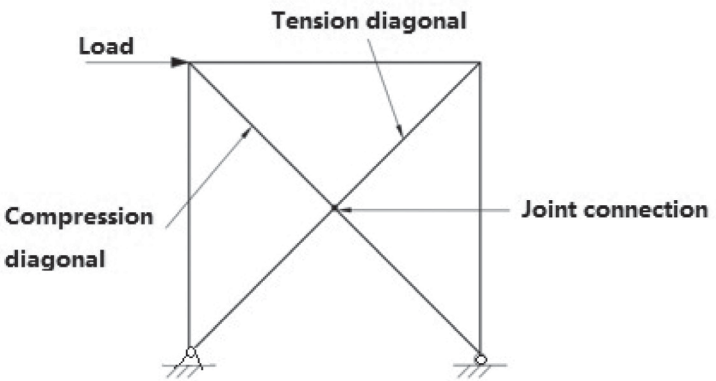

Fig. 1. Steel frame with a cross-bracing system.

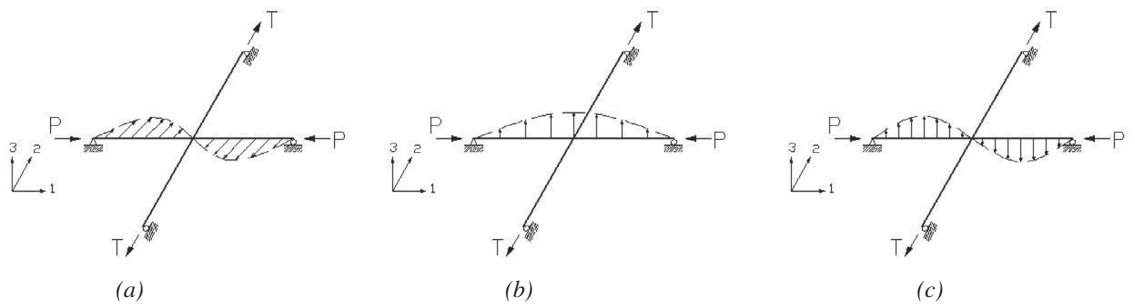

Fig. 2. Buckling modes of a cross-bracing system: (a) in-plane; (b) symmetric out-of-plane; (c) anti-symmetric out-of-plane.

and flexural rigidity $\overline{EI}$, the differential equations that govern the out-of-plane instability behavior of the first half (i.e., $0 \le \overline{x} \le L/2$, $0 \le \overline{x} \le \overline{L}/2$) of the compression and tension diagonals (Figures 4a and 4b) can be written, respectively, as (Chen and Lui, 1987)

$$\frac{d^2y}{dx^2} + k^2 y = \frac{Q}{2EI}x \tag{1}$$

$$\frac{d^2\overline{y}}{d\overline{x}^2} - \overline{k}^2\overline{y} = -\frac{\overline{Q}}{2\overline{EI}}\overline{x} \tag{2}$$

where $k^2 = \frac{P}{EI}$, $\overline{k}^2 = \frac{\overline{P}}{\overline{EI}}$, and $Q = \overline{Q}$ is the action/reaction internal force pairs acting at the midpoints of the two diagonals.

By using the pinned support condition and symmetry at midpoint, the solutions to the differential Equations 1 and 2 that satisfy the boundary conditions of $y_{x=0} = \overline{y}_{\overline{x}=0} = 0$, $\frac{dy}{dx}_{x=\frac{L}{2}} = \frac{d\overline{y}}{d\overline{x}}_{\overline{x}=\frac{\overline{L}}{2}} = 0$ are

$$y = -\frac{QL^3\sin(kx)}{2(kL)^3 EI\cos\left(\frac{kL}{2}\right)} + \frac{QL^2x}{2(kL)^2 EI} \quad 0 \le x \le L/2 \tag{3}$$

$$\overline{y} = -\frac{\overline{Q}\overline{L}^3\sinh(\overline{k}\overline{x})}{2(\overline{kL})^3\overline{EI}\cosh\left(\frac{\overline{kL}}{2}\right)} + \frac{\overline{Q}\overline{L}^2\overline{x}}{2(\overline{kL})^2\overline{EI}} \quad 0 \le \overline{x} \le \overline{L}/2 \tag{4}$$

Because the two braces are connected at midpoint, compatibility requires that $y_{x=\frac{L}{2}} = \overline{y}_{\overline{x}=\frac{\overline{L}}{2}}$, and because $Q = \overline{Q}$, we have

$$\frac{Q}{y_{x=\frac{L}{2}}} = \frac{\overline{Q}}{\overline{y}_{\overline{x}=\frac{\overline{L}}{2}}} \tag{5}$$

and with respect to the compression diagonal, the above equation can be written as

$$\frac{2EIk^3}{\frac{kL}{2} - \tan\left(\frac{kL}{2}\right)} = k_s \tag{6}$$

where

$$\begin{aligned} k_s &= \frac{\overline{Q}}{\overline{y}_{\overline{x}=\frac{\overline{L}}{2}}} = \frac{2\overline{EI}\overline{k}^3}{\frac{\overline{kL}}{2} - \tanh\left(\frac{\overline{kL}}{2}\right)} \\ &= \left[\frac{\left(\overline{kL}\right)^3}{24\left[\frac{\overline{kL}}{2} - \tanh\left(\frac{\overline{kL}}{2}\right)\right]}\right]\frac{48\overline{EI}}{\overline{L}^3} \\ &\approx \left[1 + \frac{\left(\overline{kL}\right)^2}{10} - \frac{\left(\overline{kL}\right)^4}{8400}\right]\frac{48\overline{EI}}{\overline{L}^3} \end{aligned} \tag{7}$$

is the lateral stiffness the tension diagonal is imparting to the compression diagonal when the system is experiencing out-of-plane instability. A plot of Equation 7 is shown in Figure 5 as a solid line. Also shown in the figure as a dashed line is the case when the "tension" diagonal is also under compression. This condition may occur when the superimposed dead and live gravity loads are high compared to the wind load. In this case, k_s is given by

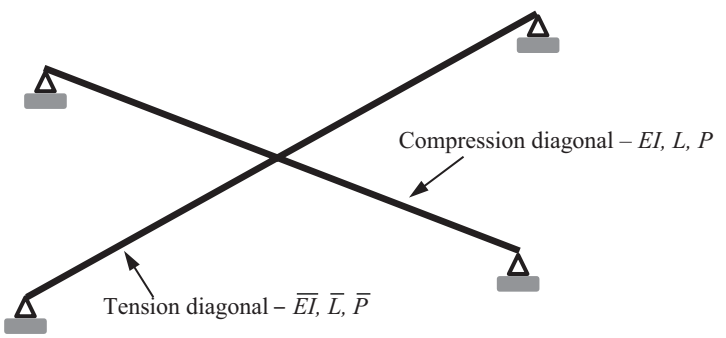

Fig. 3. Analytical model of a cross-bracing system.

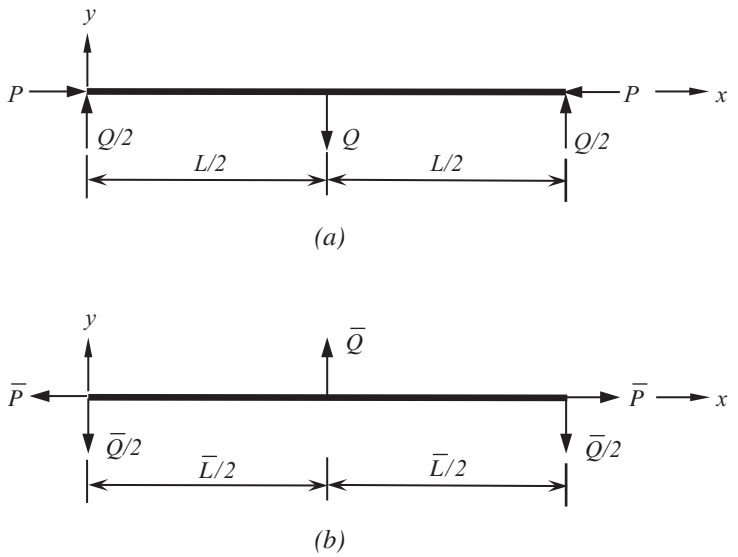

Fig. 4. Free-body diagrams of (a) compression diagonal and (b) tension diagonal.

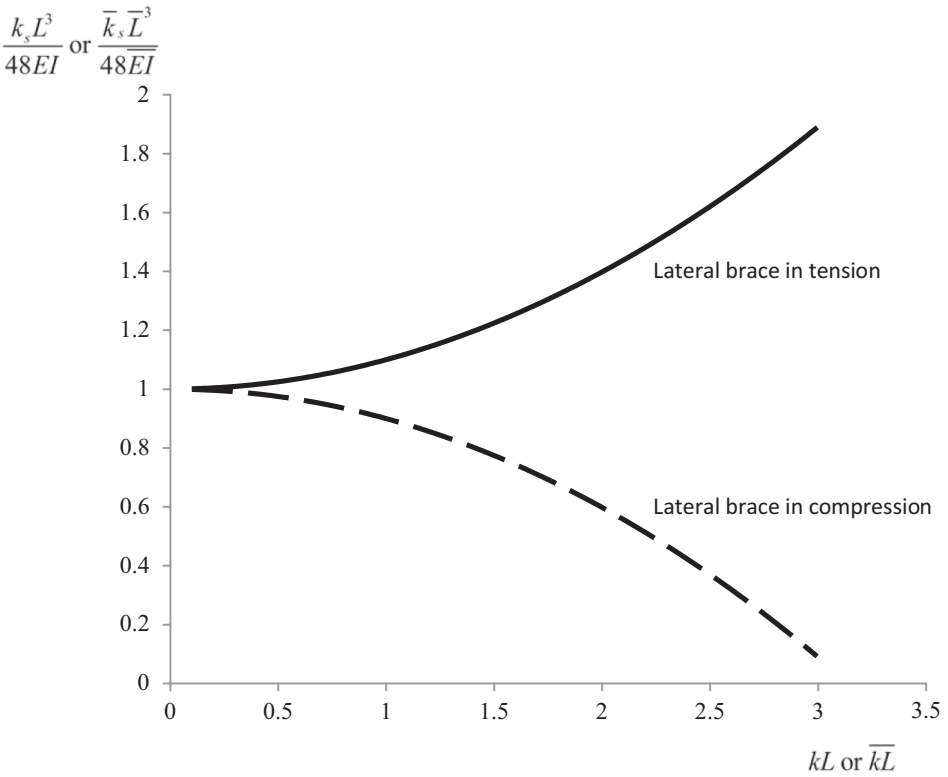

Fig. 5. Lateral bracing stiffness variation.

$$k_s = \frac{2\overline{EI}\overline{k}^3}{\tan\left(\frac{\overline{kL}}{2}\right) - \frac{\overline{kL}}{2}} = \left[\frac{\left(\overline{kL}\right)^3}{24\left[\tan\left(\frac{\overline{kL}}{2}\right) - \frac{\overline{kL}}{2}\right]}\right]\frac{48\overline{EI}}{\overline{L}^3} \quad (8)$$

$$\approx \left[1 - \frac{\left(\overline{kL}\right)^2}{10} - \frac{\left(\overline{kL}\right)^4}{8400}\right]\frac{48\overline{EI}}{\overline{L}^3}$$

In the preceding equations, $\frac{48\,\overline{EI}}{\overline{L}^3}$ is the lateral stiffness of the supporting brace when $\overline{P} = 0$. If the force in the supporting brace is tensile, the terms inside the brackets of Equation 7 represent the magnification effect of tension stiffening, whereas if the force in the supporting brace is compressive, the terms inside the brackets of Equation 8 represent the reduction effect of compression softening. The first three terms of a Taylor series expansion of the bracketed terms are provided in Equations 7 and 8 as well. They are accurate to within 1.2% of the theoretical values in the range ($0 \le \overline{kL} \le 3$) and should be used when $\overline{kL} = 0$ because the theoretical expressions become indeterminate at $\overline{kL} = 0$. If the axial compressive force in the bracing member exceeds $0.4P_y$ where P_y is the yield load, the tangent modulus should be used in place of the elastic modulus in Equation 8.

If we substitute $k = \sqrt{\frac{P}{EI}} = \frac{\pi}{L}\sqrt{\frac{P}{P_e}}$, where $P_e = \frac{\pi^2 EI}{L^2}$, into Equation 6, the equation can be expressed in a nondimensional form (Timoshenko and Gere, 1961) as

$$\frac{2\pi\left(\sqrt{\frac{P}{P_e}}\right)^3}{\frac{\pi}{2}\sqrt{\frac{P}{P_e}} - \tan\left(\frac{\pi}{2}\sqrt{\frac{P}{P_e}}\right)} = \frac{k_s L}{P_e} \quad (9)$$

In the event that yielding has occurred in the compression diagonal, the concept of tangent modulus can be used, and for design purposes, the nominal compressive strength, P_n, can be used in place of P_e in Equation 9. Thus, we have

$$\frac{2\pi\left(\sqrt{\frac{P}{P_n}}\right)^3}{\frac{\pi}{2}\sqrt{\frac{P}{P_n}} - \tan\left(\frac{\pi}{2}\sqrt{\frac{P}{P_n}}\right)} = \frac{k_s L}{P_n} \quad (10)$$

where, according to the AISC 360-10,

$$P_n = \begin{cases} \left(0.658^{\frac{F_y}{F_e}}\right)P_y & \text{when } \frac{KL}{r} \le 4.71\sqrt{\frac{E}{F_y}} \text{ or } \frac{F_y}{F_e} \le 2.25 \\ \left(0.877\frac{F_e}{F_y}\right)P_y & \text{when } \frac{KL}{r} > 4.71\sqrt{\frac{E}{F_y}} \text{ or } \frac{F_y}{F_e} > 2.25 \end{cases} \quad (11)$$

in which F_y is the yield stress, $F_e = \frac{\pi^2 E}{\left(\frac{KL}{r}\right)^2}$ with $K = 1$ for a pinned-pinned member, L is the full length of the compression diagonal, r is the radius of gyration, $P_y = AF_y$ is the yield load, and A is the cross-sectional area. Because P_n as expressed in Equation 11 takes into consideration the member out-of-straightness effect, the effect of geometrical imperfections on member strength is implicitly accounted for. Because the compression diagonal is conservatively assumed to be pinned at both ends in this study, its effective length factor K is equal to 1. As a result, L will be used in place of KL in the discussion to follow.

It is important to note that as k_s increases, there comes a point when the compression diagonal becomes fully braced (Winter, 1960; Yura, 1996) in that the compression diagonal will buckle in its second mode as shown in Figure 2c. When this happens, any further increase in k_s will not bring about an increase in its buckling capacity. This represents a limiting condition for the cross-bracing system, and the value of k_s that corresponds to this condition is referred to as the transition brace stiffness k_{st}. The computation of this transition brace stiffness will be given in the next section. In the discussion to follow, the system is said to be fully braced when this limiting condition is attained, and it is said to be partially braced when this limiting condition has not been reached.

TRANSITION BRACE STIFFNESS

As mentioned in the preceding section, as the lateral brace stiffness increases, a limiting condition will be reached in which the capacity of the compression diagonal will remain stationary. The magnitude of P for this limiting state, denoted as P_{peak}, can be obtained by evaluating P_n in Equation 11 using the unbraced length (i.e., $L/2$) of the compression diagonal. The transition brace stiffness, k_{st}, can then be evaluated from Equation 10 by substituting P_{peak} for P in the equation. If we denote P_o as the capacity of the compression diagonal when the lateral brace stiffness, k_s, is 0 (i.e., when P_n in Equation 11 is evaluated using the full length L of the compression diagonal), the following equation for k_{st} can be derived:

$$\frac{k_{st}L}{P_o}=\frac{2\pi\left(\sqrt{\frac{P_{peak}}{P_o}}\right)^3}{\frac{\pi}{2}\sqrt{\frac{P_{peak}}{P_o}}-\tan\left(\frac{\pi}{2}\sqrt{\frac{P_{peak}}{P_o}}\right)} \quad (12)$$

where P_{peak}/P_o, obtained by taking the ratio of P_n evaluated for the unbraced length $L/2$ to P_n evaluated for the full length L of the compression diagonal, is given by

$$\frac{P_{peak}}{P_o}=\begin{cases} 1.369^{\frac{F_y}{F_e}} & \text{when} \quad \frac{F_y}{F_e}\le 2.25 \quad (13a) \\ \dfrac{0.901^{\frac{F_y}{F_e}}}{0.877\left(\frac{F_e}{F_y}\right)} & \text{when} \quad 2.25<\frac{F_y}{F_e}\le 9.00 \quad (13b) \\ 4 & \text{when} \quad \frac{F_y}{F_e}>9.00 \quad (13c) \end{cases}$$

and F_y and F_e are as defined in Equation 11.

A plot of Equation 12 as a function of F_y/F_e, using the expressions for P_{peak}/P_o given in Equations 13a, 13b and 13c, is shown in Figure 6. It can be seen that the nondimensional transition brace stiffness, $k_{st}L/P_o$, varies as a function of F_y/F_e when F_y/F_e is less than or equal to 9, but becomes a constant when F_y/F_e exceeds 9. Because F_e is inversely proportional to the square of L/r, it can be concluded that $k_{st}L/P_o$ increases with L/r until it reaches $3\pi\sqrt{E/F_y}$, when $k_{st}L/P_o$ becomes a constant.

CROSS-BRACING SYSTEM BEHAVIOR

Figure 7 shows how the load-carrying capacity, P_{max}, of a typical compression diagonal varies with the lateral brace stiffness, k_s, for several slenderness ratios L/r. With reference to this figure, the following observations can be made:

1. All the curves consist of an initial nonlinear portion, as described by Equation 10, before the transition brace stiffness is attained followed by a horizontal line that represents the limiting condition when the transition brace stiffness is reached. When the brace stiffness is less than its transition value, the compression diagonal buckles in a symmetric mode (Figure 2b). Once the brace stiffness is equal to or larger than its transition value, the buckling mode of the compression diagonal will become anti-symmetric (Figure 2c).

2. The load capacity of the compression diagonal is a function of L/r only if it is fully braced, but it is a function of both L/r and k_s if it is partially braced.

3. When the slenderness ratio of the compression diagonal is large (e.g., $L/r = 400$), the member behaves elastically, and so the relationship between the load capacity and the lateral brace stiffness follows that of Equation 9 with a limiting value for $P_{max}/P_o = 4$. As L/r decreases, P_{max}/P_o falls below 4. This is because compression

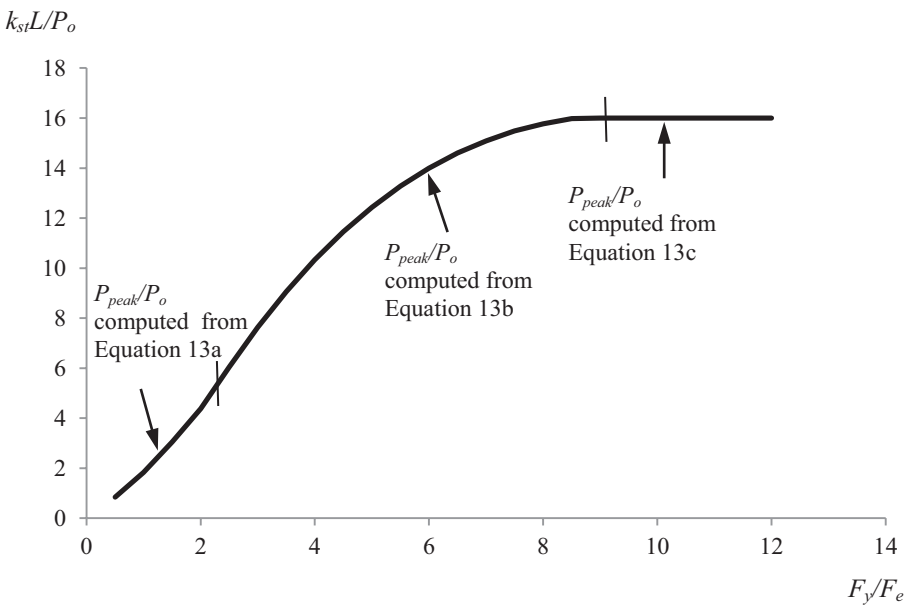

Fig. 6. Transition bracing stiffness variation.

members with low slenderness ratios tend to fail in the inelastic range. In the extreme case when the compression diagonal is so short that cross section yielding becomes the limit state, P_{max}/P_o will approach 1, meaning the bracing effect from the cross diagonal will be totally ineffective.

4. Although different slenderness ratios will lead to different limiting values for P_{max}/P_o, the slenderness effect on P_{max}/P_o is not apparent when k_s is less than k_{st}—that is, the ascending (nonlinear) portion of the curves shows very little change regardless of L/r.

DESIGN RECOMMENDATIONS

In this section, design equations for a cross-bracing system when the compression diagonal is under fully or partial braced condition will be presented.

Fully Braced Condition

When a compression diagonal is fully braced (i.e., when $k_s \geq k_{st}$), its capacity is a function of its slenderness ratio, L/r, only and is independent of the brace stiffness, k_s. Under this condition, the capacity denoted as P_{peak} can be calculated from Equation 11 by replacing KL with $l = L/2$—that is,

$$P_{peak} = \begin{cases} \left(0.658^{\frac{F_y}{F_e}}\right)P_y & \text{when } \dfrac{l}{r} \leq 4.71\sqrt{\dfrac{E}{F_y}} \text{ or } \dfrac{F_y}{F_e} \leq 2.25 \\ \left(0.877\dfrac{F_e}{F_y}\right)P_y & \text{when } \dfrac{l}{r} > 4.71\sqrt{\dfrac{E}{F_y}} \text{ or } \dfrac{F_y}{F_e} > 2.25 \end{cases} \quad (14)$$

where $F_e = \dfrac{\pi^2 E}{\left(\dfrac{l}{r}\right)^2}$, and $l = L/2$ is the unbraced length (i.e., half the full length) of the compression diagonal.

Partially Braced Condition

When the fully braced condition has not been reached (i.e., when $0 \leq k_s < k_{st}$), the compression diagonal is said to be partially braced. For the partially braced condition, P_{max} is a function of both L/r and k_s. To simplify matters, it is assumed that P_{max}/P_n of the compression diagonal varies linearly with k_sL/P_n—that is, a linearized form of Equation 10 will be used. This assumption will result in a conservative estimate for P_{max}. The proposed linearization involves determining the intercept and slope of a straight line that can approximate the curve given by Equation 10 and plotted in Figure 7 for a given L/r.

Intercepts

Because the intercept represents the capacity of the compression diagonal when $k_s = 0$, its value can be obtained directly from Equation 11 by using the full-length L of the compression diagonal. Therefore, if we denote P_o as the intercept, we have

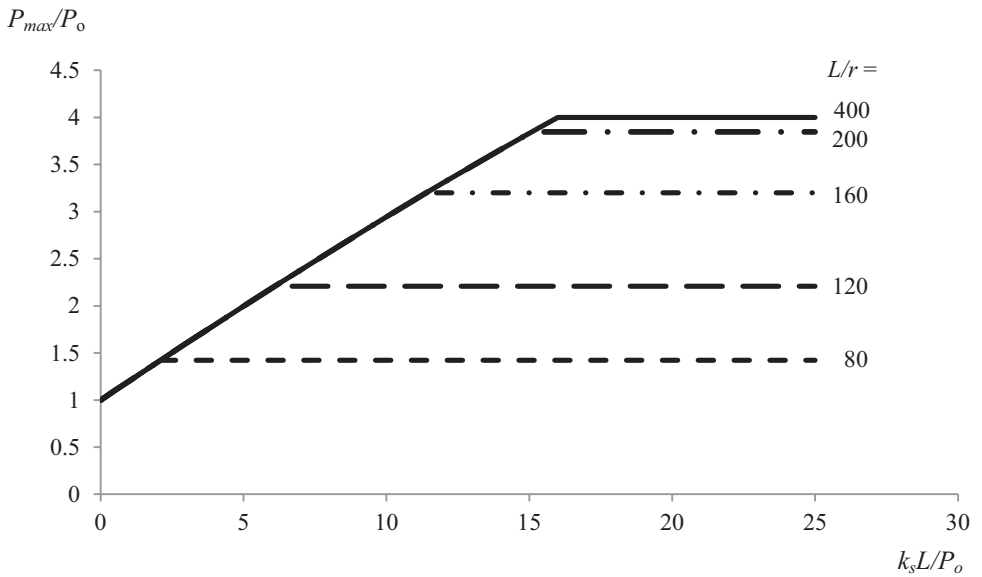

Fig. 7. Plot of P_{max}/P_o *versus* k_sL/P_o.

$$P_o = \begin{cases} \left(0.658^{\frac{F_y}{F_e}}\right) P_y & \text{when } \dfrac{L}{r} \le 4.71\sqrt{\dfrac{E}{F_y}} \text{ or } \dfrac{F_y}{F_e} \le 2.25 \\ \left(0.877\dfrac{F_e}{F_y}\right) P_y & \text{when } \dfrac{L}{r} > 4.71\sqrt{\dfrac{E}{F_y}} \text{ or } \dfrac{F_y}{F_e} > 2.25 \end{cases} \quad (15)$$

where F_y and F_e are as defined in Equation 11.

Slopes

Slopes represent the ratio of the increase in P_{max} as k_s increases in the range $0 \le k_s < k_{st}$. If we denote S_o as the slopes, we have from Figure 7 (with $P_n = P_o$ at $k_s = 0$),

$$S_o = \frac{\dfrac{P_{peak}}{P_o} - 1}{\dfrac{k_{st}L}{P_o}} \quad (16)$$

Upon substitution of Equation 12 and Equation 13 into Equation 16, S_o can be expressed as a function of F_y/F_e. A plot of S_o versus F_y/F_e is given in Figure 8. Because the variation (from 0.202 to 0.188) is not significant, it is recommended that a constant value of 0.188 be used for design. Note that this value can also be obtained by approximating the full length of the curved inclined line in Figure 7 by a straight line that shares the same end points as the curved line and taking its slope—that is, $S_o = (4 - 1)/16 = 0.188$.

Using the intercept and slope equations presented earlier, the load capacity of a partially braced compression diagonal can be written as

$$P_{max} = S_o \times k_s L + P_o \quad (17)$$

In summary, the load carrying capacity of the compression diagonal of a cross-brace system is

$$P_{max} = \begin{cases} P_{peak} & \text{for the fully braced condition} \\ S_o \times k_s L + P_o & \text{for the partially braced condition} \end{cases} \quad (18)$$

where S_o = 0.188; L is the full length of the compression diagonal; P_{peak} and P_o are to be computed from Equations 14 and 15, respectively; and k_s is calculated from Equation 7 or 8, depending on whether the supporting brace is in tension or compression.

BRACE FORCE

The brace force, denoted as Q in Figure 4, is a function of k_s and the amount of out-of-plane deformation of the cross-bracing system when P_{max} is reached. Based on a parametric study (Lui and Khanse, 2008) in which a series of pinned-end compression members having different slenderness ratios, supported by a spring with different stiffness placed at different locations and considering inelasticity and initial geometric imperfections, were analyzed numerically, the upper- and lower-bound envelope curves for Q/P_{max} plotted as a function of k_sL/P_e are shown in Figure 9. From the figure, a conservative Q/P_{max} value of 4% was recommended. This is different from the 1% value recommended in the AISC specification (2010) for a nodal bracing system. This is because the 1% value is applicable only if the lateral stiffness provided is twice that of the critical brace stiffness defined

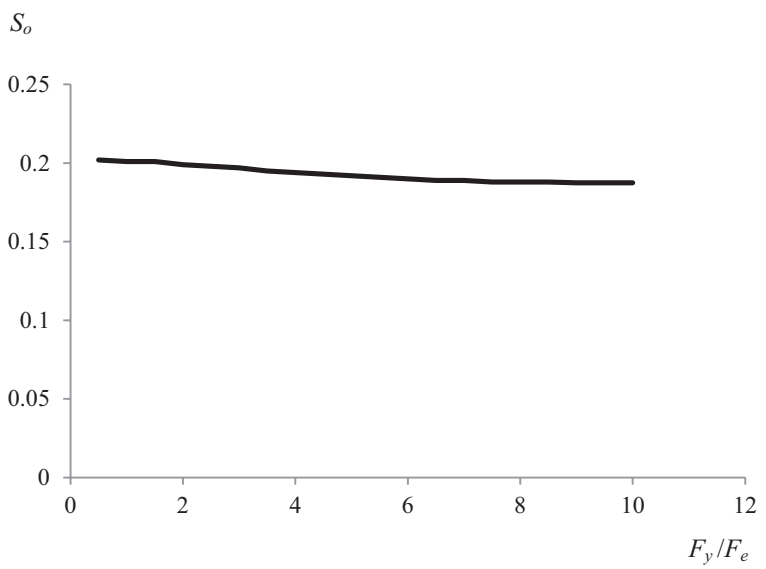

Fig. 8. Variation of S_o *with* F_y/F_e.

as the stiffness needed to develop $P_e = \pi^2 EI/l^2$, where l is the unbraced length (i.e., length between adjacent braced points) of the compression member. In the current context, this condition cannot be guaranteed because the same size section has to be used for both the tension and compressional diagonals because wind direction can reverse. In other words, unlike a typical nodal bracing problem when the design of the brace can be separated from the design of the member it braces, the design of the tension and compression diagonals is dependent on each other.

DESIGN PROCEDURE

In this section, design guidelines that take into consideration the interaction effect of the two diagonals of a cross-bracing system will be proposed. Design examples will then be given to demonstrate how the proposed procedure can be used for the design of cross-bracing systems for concentrically braced frames. In some applications, the cross-bracing members can be prestrained or prestressed during installation to enhance their stiffness. The pretensioned stress is usually in the range of 1 to 5% of the material yield stress. If such prestress is present, it should be accounted for in the analysis in obtaining the internal axial forces in the cross diagonals.

The following procedure is recommended for the design of a cross-bracing system:

1. Determine the required axial strength, P_u, for both diagonals.

2. Select a trial section based on the compression, P_u, and if both diagonals are in compression, select a trial section based on the larger of the two compressive, P_u. Because the load capacity of the compression diagonal, P_{max}, is not a constant but varies with L/r for the fully braced condition, and with L/r and k_s for the partially braced condition as shown in Figure 7, an assumed increase of the unbraced (i.e., first mode) capacity of the compression diagonal P_o by a certain percentage should be used. In terms of design, this means a reduction in P_u can be used. In the example problems, a trial section is selected based on a reduced required compressive strength of $P_u/1.25$, but depending on the expected L/r and k_s values, other reduction factor for P_u can be used as well.

3. Using the trial section properties, calculate L/r for the compression diagonal, and determine k_s from Figure 5 or, alternatively, from Equation 7 if the supporting diagonal is in tension and from Equation 8 if the supporting diagonal is in compression.

4. Calculate the transition brace stiffness, k_{st}, from Equation 12.

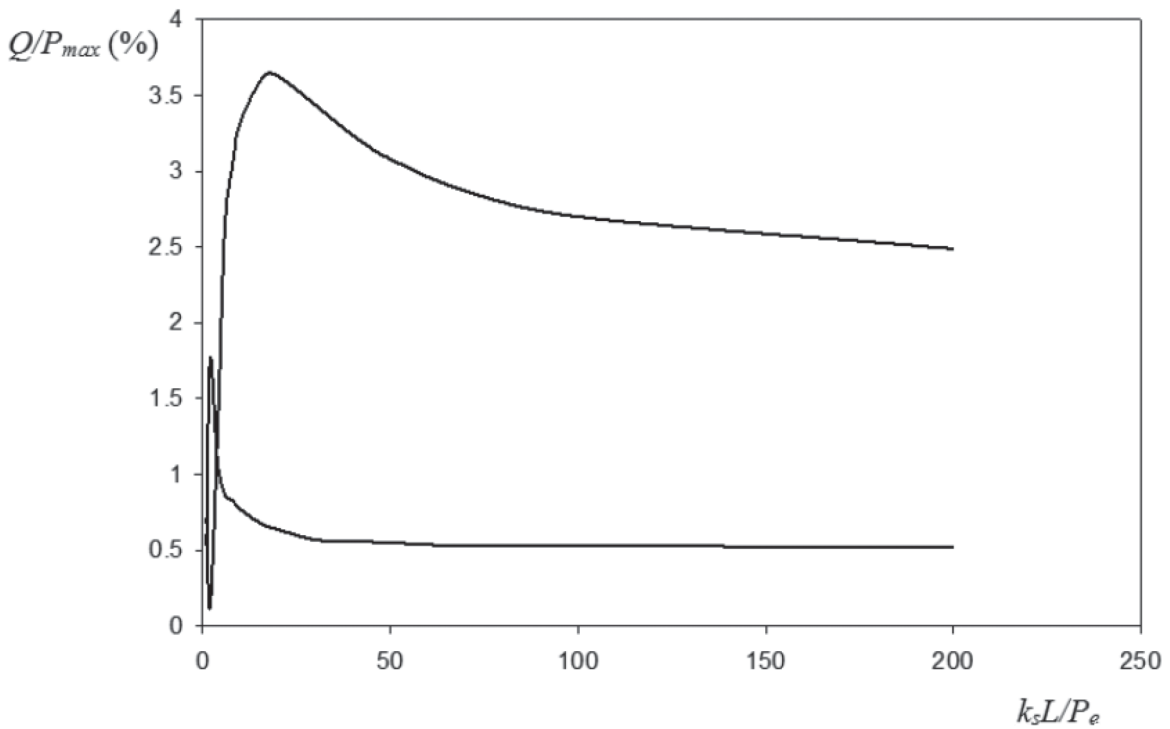

Fig. 9. Upper- and lower-bound curves for the braced force.

5. If $k_s \geq k_{st}$, the compression diagonal is fully braced and so P_{max} (= P_{peak}) is to be computed from Equation 14. However, if $k_s < k_{st}$, the compression diagonal is only partially braced, so P_{max} is to be computed from Equation 17.
6. Check the adequacy of both the compression and tension diagonals using the axial force–flexure interaction equation by subjecting the members to their respective P_u and to a lateral force equal to 4% of the compressive P_u. If the interaction equation is not satisfied, select a new trial section and repeat steps 3 through 6.

DESIGN EXAMPLES

Example 1

A square hollow structural section (HSS) is to be used for the cross braces of a diagonal bracing system of an industrial building to resist wind load. If the length of the members is 20 ft and the required axial strengths in the tension and compression diagonals are computed to be 10 and 35 kips, respectively, select an appropriate HSS. Assume the members are pinned at both ends and welded together at their intersection point. Use ASTM A500 Grade B steel.

Solution:

As a first trial, use a reduced required axial compressive strength of:

$$P_{u,reduced} = \left(\frac{35}{1.25}\right) = 28 \text{ kips}$$

Using the AISC Compression Member Selection Tables with KL = (1)(20) = 20 ft, select HSS 4×4×¼ as a trial section for the compression diagonal. Because the wind can blow in either direction, the same section is to be used for the tension diagonal.

Material properties: ASTM A500 Grade B steel: F_y = 46 ksi, E = 29,000 ksi.

Geometric properties: A = 3.37 in.^{2}, I = 7.80 in.^{4}, r = 1.52 in., Z = 4.69 in.^{3}, L = 240 in.

Determine the lateral stiffness of the tension diagonal from Equation 7:

$$k_s = \left[\frac{\left(\overline{kL}\right)^3}{24\left[\frac{\overline{kL}}{2} - \tanh\left(\frac{\overline{kL}}{2}\right)\right]}\right]\frac{48\overline{EI}}{\overline{L}^3} = 0.985 \text{ kip/in.}$$

Calculate the transition lateral stiffness from Equation 12.

Because F_y/F_e = 4.01, P_{peak}/P_o = 3.01 from Equation 13b and P_o = 33.9 kips from Equation 15. Hence, using Equation 12 we have

$$\frac{k_{st}L}{P_o} = \frac{2\pi\left(\sqrt{\frac{P_{peak}}{P_o}}\right)^3}{\frac{\pi}{2}\sqrt{\frac{P_{peak}}{P_o}} - \tan\left(\frac{\pi}{2}\sqrt{\frac{P_{peak}}{P_o}}\right)} = 10.4, \text{ or } k_{st} = 10.4\frac{P_o}{L} = 1.47 \text{ kip/in.}$$

Because $k_s < k_{st}$, the compression diagonal is only partially braced.

Compute P_{max} using Equation 17:

$$P_{max} = S_0 \times k_s L + P_o = 78.3 \text{ kips}$$

The design compressive strength is therefore

$$\phi_c P_{max} = (0.90)(78.3) = 70.5 \text{ kips}$$

Because the lateral interaction force, F_s, between the compression and tension diagonals is assumed to be 4% of P_u, $F_s = (0.04)(35) = 1.4$ kips.

Now, check the adequacy of the compression and tension diagonals for combined axial force and flexure.

The AISC interaction equation that needs to be checked is:

$$\text{If } \frac{P_r}{P_c} \geq 0.2, \quad \frac{P_r}{P_c} + \frac{8}{9}\frac{M_r}{M_c} \leq 1.0 \tag{19a}$$

$$\text{If } \frac{P_r}{P_c} < 0.2, \quad \frac{1}{2}\frac{P_r}{P_c} + \frac{M_r}{M_c} \leq 1.0 \tag{19b}$$

For the compression diagonal,

$$\begin{aligned} P_r &= 35 \text{ kips} \\ P_c &= \phi_c P_{max} = 70.5 \text{ kips} \\ M_r &= \frac{1}{4} F_s L = 84 \text{ kip-in.} \\ M_c &= \phi_b F_y Z = 0.90 F_y Z = 194 \text{ kip-in.} \end{aligned}$$

Thus,

$$\frac{P_r}{P_c} + \frac{8}{9}\frac{M_r}{M_c} = \frac{35}{70.5} + \frac{8}{9}\left(\frac{84}{194}\right) = 0.881 < 1.0$$

The compression diagonal is OK.

For the tension diagonal,

$$\begin{aligned} P_r &= 10 \text{ kips} \\ P_c &= \phi P_y = 139.5 \text{ kips} \\ M_r &= \frac{1}{4} F_s L = 84 \text{ kip-in.} \\ M_c &= \phi F_y Z_y = 0.90 F_y Z = 194 \text{ kip-in.} \end{aligned}$$

Thus,

$$\frac{1}{2}\frac{P_r}{P_c} + \frac{M_r}{M_c} = \frac{10}{2(139.5)} + \frac{84}{194} = 0.47 < 1.0$$

The tension diagonal is OK.

Therefore, use the HSS4×4×¼ section for both the compression and tension diagonals of the cross-bracing system.

Example 2

A cross-bracing system is to be designed using a W-section and ASTM A992 steel for the frame shown in Figure 10. The frame is designed to support a dead load of 20 kips, a live (or roof live) load of 60 kips, and a wind load of 10 kips. All loads are to be applied to the top joints as concentrated loads as shown in the figure. The column and beam sections used for the frame are W8×31 and W6×20, respectively. They are oriented so that their webs are parallel to the plane of the frame. The two diagonals of the bracing system are assumed to be pin connected to the frame and are joined at their mid-points using a welded connection. The diagonals are 32 ft in length and are oriented in such a way that their webs are perpendicular to the plane of the frame.

Solution:

Because the frame is statically indeterminate, the analysis results will depend on the relative sizes of the members. Assuming the members used for the cross-bracing system are both W4×13, the axial forces calculated for these members from two controlling load combinations are summarized here.

Load Combination	**Diagonal *AC***	**Diagonal *BD***
$1.2D + 1.6L$	15.6 kips (compression)	15.6 kips (compression)
$1.2D + 1.6L_r + 0.5W$	12.8 kips (compression)	19.2 kips (compression)

Note that there is no "tension" diagonal for this frame. However, for the gravity plus wind load case, because the two diagonals are not subjected to the same axial force, diagonal *AC* can still provide lateral bracing to diagonal *BD*.

For the W4×13 section,

Material properties: ASTM A992 steel: $F_y = 50$ ksi, $E = 29{,}000$ ksi.

Geometric properties: $A = 3.83$ in.^{2}, $I_x = 11.3$ in.^{4}, $r_x = 1.72$ in., $I_y = 3.86$ in.^{4}, $r_y = 1.00$ in., $L = 384$ in.

For the gravity load case, both diagonals are subjected to the same axial force. As a result, neither diagonal can provide out-of-plane lateral restraint to the other diagonal, so $k_s = 0$ for both diagonals. However, they do provide in-plane translational restraint to each other as shown in Figure 2a.

Using Equation 11, and with $(KL/r)_x = (1)(384)/1.72 = 223$ and $(KL/r)_y = (1)(192)/1.00 = 192$, the design compressive strength is determined to be $\phi_c P_n = (\phi_c P_n)_x = 17.4$ kips, which is larger than the required compressive strength of $P_u = 15.6$ kips.

For the gravity plus wind load case, the lateral stiffness that diagonal *AC* can provide to diagonal *BD* can be determined from Equation 8 as

$$k_s = \left[\frac{\left(\overline{kL}\right)^3}{24\left[\tan\left(\frac{\overline{kL}}{2}\right) - \frac{\overline{kL}}{2}\right]}\right]\frac{48\overline{EI}}{\overline{L}^3} = 0.117 \text{ kip/in.}$$

and because $F_y/F_e = 8.68$, $P_{peak}/P_o \approx 4$ from Equation 13b, and $P_o = 19.3$ kips from Equation 15. Hence, by using Equation 12,

$$\frac{k_{st}L}{P_o} = \frac{2\pi\left(\sqrt{\frac{P_{peak}}{P_o}}\right)^3}{\frac{\pi}{2}\sqrt{\frac{P_{peak}}{P_o}} - \tan\left(\frac{\pi}{2}\sqrt{\frac{P_{peak}}{P_o}}\right)} = 16, \text{ or } k_{st} = 16\frac{P_o}{L} = 0.804 \text{ kip/in.}$$

Because $k_s < k_{st}$, diagonal *BD* is only partially braced, so its capacity is to be calculated from Equation 17 as:

$$P_{max} = S_o \times k_s L + P_o = 27.7 \text{ kips}$$

The design compressive strength is therefore

$$\phi_c P_{max} = (0.90)(27.7) = 24.9 \text{ kips}$$

The lateral interaction force, F_s, between the two diagonals is assumed to be 4% of P_u, so $F_s = (0.04)(19.2) = 0.768$ kips.

Now, check the adequacy of diagonal *BD* for the combined axial force and flexure under the gravity plus wind load case. Because $P_r/P_c = P_u/\phi_c P_{max} = 19.2/24.9 = 0.771$, use Equation 19a with

$$P_r = 19.2 \text{ kips}$$
$$P_c = \phi_c P_{max} = 24.9 \text{ kips}$$
$$M_r = \frac{1}{4} F_s L = 73.7 \text{ kip-in.}$$
$$M_c = \phi_b \times \text{AISC Eq. (F2-2)} = 283 \text{ kip-in.}$$

In calculating M_c, C_b is taken as 1.67, so $\phi_b M_p$ controls, and

$$\frac{P_r}{P_c} + \frac{8}{9}\frac{M_r}{M_c} = \frac{19.2}{24.9} + \frac{8}{9}\left(\frac{73.7}{283}\right) \approx 1.0$$

The design is therefore is OK. Note that diagonal *AC* need not be checked because it has a lower P_u than diagonal *BD*.

Use W4×13 for the diagonals of the cross-bracing system. It should be noted that the W4×13 would have been considered inadequate for the gravity plus wind load case if the lateral bracing effect of the cross-bracing system had not been considered.

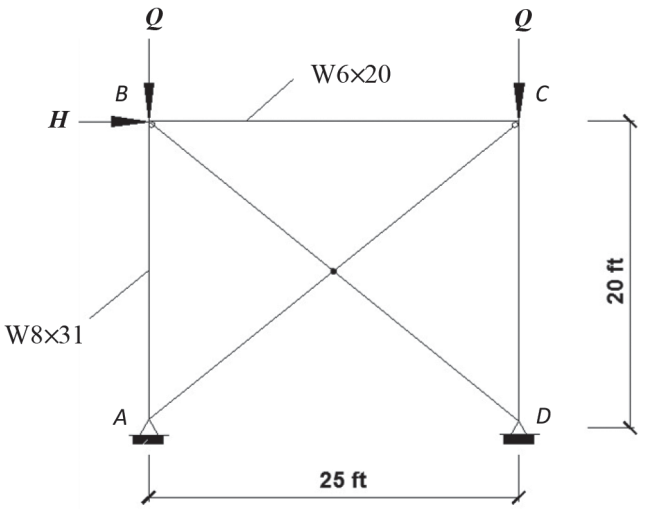

Fig. 10. Example frame.

SUMMARY AND CONCLUSIONS

In a conventional design of cross-bracing systems for braced frames, two relatively simple but somewhat unrealistic approaches are often used. One is a conservative approach in which only the tension diagonal is assumed to be active in controlling frame sway. The contribution of the compression diagonal is totally ignored. On the other extreme, the tension diagonal is assumed to have sufficient stiffness to brace the compression diagonal to allow it to attain a compressive strength that corresponds to its second buckling mode. In reality, the behavior of the system often falls somewhere between these two extreme cases. In this study, the partially braced strength of a typical cross-bracing system is investigated and design guidelines are proposed. Examples are then given to demonstrate how the proposed procedure can be applied for the design of cross-bracing systems. Based on the current study, the following conclusions can be drawn:

1. The compression diagonal is fully braced and can develop a compressive strength corresponding to its second buckling mode only if the tension diagonal possesses sufficient stiffness referred to as the transition stiffness, k_{st}, given by Equation 12.

2. The transition brace stiffness increases with F_y/F_e or L/r, and for large slenderness (when the compression diagonal remains elastic at incipient instability) becomes asymptotic at $16P_o/L$, where P_o is the axially capacity of the compression diagonal when the lateral bracing stiffness $k_s = 0$, and L is the full length of the member.

3. If $k_s \geq k_{st}$, the compression diagonal is said to be fully braced. The compressive strength of a fully braced compression diagonal, given by Equation 14, is a function its slenderness ratio, L/r, only.

4. If $k_s < k_{st}$, the compression diagonal is said to be partially braced. The compressive strength of a partially braced diagonal, given by Equation 17, is a function of both its slenderness ratio, L/r, and the lateral bracing stiffness, k_s.

5. In cases when both diagonals are in compression, the diagonal with the lower compressive force can still provide bracing to the diagonal with the higher compressive force (see Figure 5) as long as the axial forces in the diagonals are not the same.

6. The internal out-of-plane force developed at the intersection point of the two diagonals when instability occurs can be conservatively taken as 4% of the required compressive strength, P_u, of the compression diagonal. This force is assumed to act on both diagonals and their adequacy is checked using the AISC interaction equation for combined axial force and flexure.

REFERENCES

AISC (2010), *Specification for Structural Steel Buildings*, ANSI/AISC 360-10, American Institute of Steel Construction, Chicago, IL.

Chen, W.F. and Lui, E.M. (1987), *Structural Stability: Theory and Implementation,* Elsevier, NY.

El-Tayem, A.A. and Goel, S.C. (1986), "Effective Length Factor for the Design of X-Bracing Systems." *Engineering Journal,* AISC, Vol. 23, No. 1, pp. 41–45.

Kitipornchai, S. and Finch, D.L. (1986), "Stiffness Requirement for Cross Bracing," *Journal of Structural Engineering,* ASCE, Vol. 112, No. 12, pp. 2703–2707.

Lui, E.M. and Khanse, A.C. (2008), "Behavior and Design of Laterally Braced Inelastic Compression Members," *Advanced Steel Construction,* Vol. 4, No. 4, pp. 260–283.

Moon, J., Yoon, K., Han, T. and Lee, H. (2008), "Out-of-Plane Buckling and Design of X-Bracing Systems with Discontinuous Diagonals," *Journal of Constructional Steel Research,* Vol. 64, No. 3, pp. 285–294.

Picard, A. and Beaulieu, D. (1987), "Design of Diagonal Cross Bracings, Part 1: Theoretical Study," *Engineering Journal,* AISC, Vol. 24, No. 3, pp. 122–126.

Picard, A. and Beaulieu, D. (1988), "Design of Diagonal Cross Bracings, Part 2: Experimental Study, *Engineering Journal,* AISC, Vol. 25, No. 4, pp. 156–160.

Sabelli, R. and Hohbach, D. (1999), "Design of Cross-braced Frames for Predictable Buckling Behavior," *Journal of Structural Engineering,* ASCE, Vol. 125, Issue 2, pp. 163–168.

Stoman, S.H. (1989), "Effective Length Spectra for Cross Bracings," *Journal of Structural Engineering,* ASCE, Vol. 115, No. 12, pp. 3112–3122.

Timoshenko, S. and Gere, J.M. (1961), *Theory of Elastic Stability,* McGraw-Hill, NY.

Yura, J.A. (1996), "Winter's Bracing Approach Revisited," *Engineering Structures,* Vol. 18, No. 10, pp. 821–825.

Winter, G. (1960), "Lateral Bracing of Columns and Beams," *Transactions of the ASCE,* Vol. 125, Part 1, pp. 809–825.

Notes on the Nodal and Relative Lateral Stability Bracing Requirements of AISC 360

LOUIS F. GESCHWINDNER and ANDRES LEPAGE

ABSTRACT

The requirements for stability bracing of columns and beams have been included in AISC specifications since 1999. These requirements are intended to permit properly braced columns and beams to attain the buckling strength of the member as if braced by immovable supports and thus be designed as braced members according to the requirements of the *Specification*. The *Specification* addresses lateral stability bracing of columns and beams and torsional stability bracing of beams. This paper will address only the requirements for lateral stability bracing.

Although these requirements appear to be fairly straightforward, one question is regularly asked by those trying to put them into practice: What is the difference between "nodal" and "relative" bracing? This paper looks at the background of the provisions, describes how they have been obtained from the theoretical equations and then suggests how best to distinguish between these "nodal" and "relative" braces. It also shows that the approach taken by the *Specification* is safe and permits simple rules to be applied to a wide range of bracing problems. In addition, recommendations are made for revision of the requirements.

Keywords: beam bracing, column bracing, brace force, brace stiffness, lateral bracing.

INTRODUCTION

Lateral bracing for columns and beams sufficient to permit them to attain the buckling strength of the member as if braced by immovable supports is called stability bracing. The stability bracing requirements found in Appendix 6 of the AISC *Specification for Structural Steel Buildings* (AISC, 2010a) have remained essentially unchanged since they were first introduced in the 1999 LRFD *Specification for Structural Steel Buildings* (AISC, 2000). George Winter (1958) appears to have been the first to recognize that stability bracing must not only develop sufficient strength but must also have sufficient stiffness to provide the necessary stability bracing of columns and beams. This stability bracing is equivalent in effectiveness to an immovable support and in this paper is also referred to as bracing.

Although the *Specification* requirements appear to be fairly straightforward, practicing engineers often ask about the difference between "nodal" and "relative" bracing. This paper will first look at the background of the provisions and then suggest how best to distinguish between these "nodal" and "relative" braces. It will also show that the approach taken by the *Specification* is safe and permits simple rules to be applied to a wide range of bracing problems.

Louis F. Geschwindner, Ph.D., P.E., Professor Emeritus of Architectural Engineering, The Pennsylvania State University, University Park, PA (corresponding). E-mail: lfg@psu.edu

Andres Lepage, Ph.D., P.E., S.E., Associate Professor, Department of Civil, Environmental and Architectural Engineering, University of Kansas, Lawrence, KS. E-mail: alepage@ku.edu

Figure 1 shows four ways to provide lateral bracing for a column; three are identified as nodal bracing and one as relative bracing. Case (a) shows braces that are immovable supports. The column is divided into two segments with length L_b. Thus, the Euler buckling load (flexural buckling) for this column is $P_e = \pi^2 EI/L_b^2$. The column of case (b) is braced at the midpoint with a spring. Thus, if the given spring has sufficient stiffness and strength, this column will also buckle at the load P_e as for case (a). Case (c) column is similar to case (b) except that the immovable support at the top has been replaced by a spring. If these springs have sufficient stiffness and strength, this column will also buckle at the same load as in case (a). The last column to consider is that given as case (d). This structure shows a column that is braced by a series of diagonal braces, interconnected in such a way that the column on the right is sufficiently braced to permit it to buckle at the same load as the column of case (a).

COLUMNS WITH NODAL BRACES

Column Case (b)

Timoshenko (1936) used the basic theory of elastic stability to determine the ideal bracing stiffness for the column given as case (b) and similar columns with numerous equally spaced braces. Winter (1958) recognized that it would not be necessary to determine the exact stiffness and strength requirement if a practical and simple method could be developed that would also account for initial imperfections of the column. The column shown in Figure 2 is the column addressed initially by Winter. The column is shown in its perfectly straight position as a solid line. The assumed

imperfect column is shown as a dashed line with an initial displacement at the point of the spring, δ_o. As a compressive load is applied to the column, it will deform as shown by the second dashed line with an additional displacement, δ. The corresponding force in the spring is $F = \beta\delta$, where β is the spring stiffness at the brace point. If the spring stiffness is sufficient to permit buckling as defined in case (a), the stiffness will be defined as β_{req}. The column will snap through to the two half-wave modes shown as a thin solid line in Figure 2, and the load will be equal to the Euler buckling load, $P_e = \pi^2 EI/L_b^2$. In this buckled shape, considering small displacements, placing a hinge at the point of the spring causes little loss of accuracy because the moment at this point may be taken as zero. Taking moments about this hinge for either half of the column gives

$$M = \frac{\beta_{req}\delta}{2} L_b - P_e\left(\delta_o + \delta\right) = 0 \tag{1}$$

which leads to

$$\beta_{req} = \frac{2P_e}{L_b}\left(\frac{\delta_o}{\delta} + 1\right) \tag{2}$$

For the perfect or ideal column, $\delta_o = 0$, and the ideal stiffness can be defined as

$$\beta_{ideal} = \frac{2P_e}{L_b} \tag{3}$$

The ideal stiffness given in Equation 3 is the minimum brace stiffness needed for the column to attain the Euler buckling load if the column were perfectly straight. For real braces, this brace stiffness will include the influence of all components that make up the brace between the column being braced and the immovable support. This would include connections and any other structure the brace might be connected to.

It will be shown later that providing the ideal stiffness leads to a very large spring force at buckling. However, given that a real column is not ideal, the required brace stiffness can be determined by combining Equations 2 and 3, thus

$$\beta_{req} = \beta_{ideal}\left(\frac{\delta_o}{\delta} + 1\right) \tag{4}$$

and the brace force is given by

$$F = \beta_{req}\delta = \beta_{ideal}\left(\delta_o + \delta\right) \tag{5}$$

Winter (1958) proceeds to determine the ideal stiffness for columns similar to Figure 1b with two, three and four equally spaced springs while having an immovable support at the top of the column. These values are identical to those presented by Timoshenko (1936) and are given here in Table 1, where

$$\beta_{ideal} = \eta_0 P_e/L_b \tag{6}$$

A value of $n = 1$, which leads to $\eta_0 = 2.0$, corresponds to the condition that led to Equation 3 as shown in Figure 2. The subscript of η refers to the lateral degree of freedom at the top of the column.

More recently, Zhang, Beliveau and Huston (1993) published a single equation that provides the ideal stiffness for any number of springs. Their equation is

$$\beta_{ideal} = 4\sin^2\left[\frac{\pi}{2}\left(\frac{n}{n+1}\right)\right]\frac{P_e}{L_b} = \lambda\frac{P_e}{L_b} \tag{7}$$

The coefficient λ in Equation 7 provides identical values to those given by Timoshenko (1936).

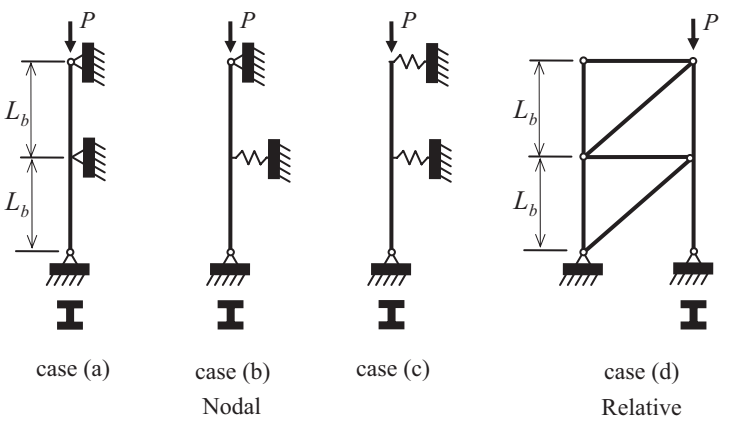

Fig. 1. Lateral bracing for column stability.

Table 1. Coefficient, η_0, for Determination of Ideal Spring Stiffness, Case (b) n = number of springs (Timoshenko, 1936)								
n	1	2	3	4	5	6	10	infinite
η_0	2.00	3.00	3.41	3.62	3.73	3.80	3.92	4.00

Table 2. Coefficient, η_1, for Determination of Ideal Spring Stiffness, Case (c), n = number of springs (Zhang et al., 1993)								
n	1	2	3	4	5	6	10	infinite
η_1	1.00	2.62	3.25	3.53	3.68	3.77	3.91	4.00

Column Case (c)

The column of case (c) behaves differently than the column of case (b) because, in addition to the intermediate braced points, the top of this column is permitted to displace laterally. This column was treated by Timoshenko and Gere (1961) for the case of only one spring, which was located at the top of the column as shown in Figure 3. Taking Winter's (1958) equilibrium approach and using the same definitions as previously, the moment about the column base is

$$M = \beta_{req}\delta L_b - P_e\left(\delta_o + \delta\right) = 0 \tag{8}$$

which gives the required stiffness as

$$\beta_{req} = \frac{P_e}{L_b}\left(\frac{\delta_o}{\delta} + 1\right) \tag{9}$$

For the ideal column with $\delta_o = 0$, the ideal stiffness is

$$\beta_{ideal} = \frac{P_e}{L_b} \tag{10}$$

Although Timoshenko and Gere (1961) do not provide results for more than one spring in the arrangement of case (c), Zhang et al. (1993) provide an equation for the ideal spring stiffness for any number of springs as

$$\beta_{ideal} = 4\sin^2\left[\frac{\pi}{2}\left(\frac{2n-1}{2n+1}\right)\right]\frac{P_e}{L_b} = \eta_1\frac{P_e}{L_b} \tag{11}$$

The ideal stiffness given by Equation 11 is the minimum stiffness if the column were ideal. Note that multiplier η_1 (Table 2) starts at 1.0 for a single spring and increases to 4.0 for an infinite number of springs. The multiplier η_0 (Table 1) starts at 2.0 for a single spring and also increases to 4.0 for an infinite number of springs.

As was the situation with the column of case (b), a real column is not ideal, and the brace stiffness can be determined by combining Equations 9 and 10, thus

$$\beta_{req} = \beta_{ideal}\left(\frac{\delta_o}{\delta} + 1\right) \tag{12}$$

and the brace force is given by

$$F = \beta_{req}\delta = \beta_{ideal}\left(\delta_o + \delta\right) \tag{13}$$

Equation 12 is identical to Equation 4. Thus, regardless of

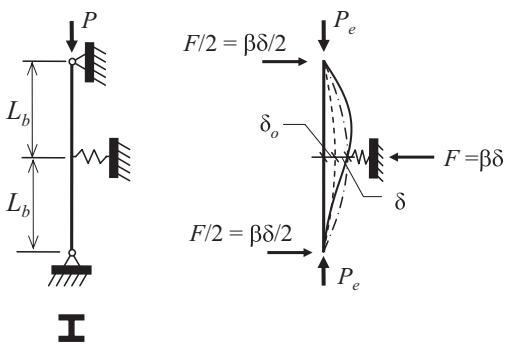

Fig. 2. Column buckling (Winter, 1958).

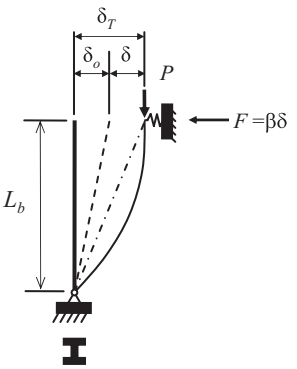

Fig. 3. Brace at top of column (Timoshenko and Gere, 1961).

which spring arrangement is used, the relationship between the required stiffness and the ideal stiffness is the same and is a function of the relationship between the initial displacement and the final displacement at buckling.

To investigate the relationship between spring stiffness and column buckling strength, the column of Figure 3 will again be used. Taking moments about the pin at the base of the column gives

$$P\delta_T = \beta L_b\left(\delta_T - \delta_o\right) \tag{14}$$

Using the ideal stiffness from Equation 10 and rearranging yields

$$\frac{P}{P_e} = \frac{\beta}{\beta_{ideal}}\left[\frac{\left(\delta_T - \delta_o\right)}{\delta_T}\right] = \frac{\beta}{\beta_{ideal}}\left[1 - \frac{1}{\delta_T/\delta_o}\right] \tag{15}$$

From Equation 15 it can be seen that, for a brace with ideal stiffness, δ_T/δ_o must approach infinity in order for the column buckling load to approach P_e. This is illustrated in Figure 4 for the column with a spring of ideal stiffness through the curve labeled β_{ideal}. With the deflection approaching infinity, the brace force will also approach infinity. This, of course, is an untenable solution. However, if the spring stiffness is taken as $1.5\beta_{ideal}$, it can be shown that the column will attain the buckling load with a displacement of $\delta_T/\delta_o = 3$. If the spring stiffness is $2\beta_{ideal}$, the column will attain the buckling load when $\delta_T/\delta_o = 2$, and when the spring stiffness is $3\beta_{ideal}$, the column will attain the buckling load when $\delta_T/\delta_o = 1.5$. These curves are illustrated in Figure 4.

For a column to attain $P = P_e$, Equation 15 leads to a brace (spring) stiffness of

$$\beta = \frac{\delta_T/\delta_o}{\left(\delta_T/\delta_o - 1\right)}\beta_{ideal} \tag{16}$$

Combining Equations 10 and 16, the brace force, $F = \beta(\delta_T - \delta_o)$, simplifies to

$$F = \frac{\delta_T}{\delta_o}\left(\frac{\delta_o}{L_b}P_e\right) \tag{17}$$

Both Equations 16 and 17 are plotted in Figure 5 as a function of $\delta_T/\delta_o = 0$. The figure shows that for $\delta_T/\delta_o = 2$, the combination of required brace stiffness and brace force is optimal for design.

The case of $\delta_T/\delta_o = 2$ means that the displacement at buckling will be equal to the initial deflection. Thus, $\delta = \delta_o$, for which Equation 12 is simplified to

$$\beta_{req} = \beta_{ideal}\left(1+1\right) = 2\beta_{ideal} \tag{18}$$

Equations 5 and 13, which give the required brace force, are also identical for the two arrangements of bracing. Thus, regardless of arrangement of nodal braces, the required brace force is a function of the ideal stiffness and the displacement at the brace point. To determine the brace force, it is not sufficient to establish the relationship between the initial imperfection and the final deflection; actual numerical values must be established. With the column length defined as in these cases, the permitted out-of-plumbness tolerance is usually taken as $0.002L_b$, based on the AISC *Code of Standard Practice* (AISC, 2010b). For the assumption of $\delta = \delta_o$, the brace force is

$$\begin{aligned} F &= \beta_{ideal}\left(\delta_o + \delta\right) \\ &= \beta_{ideal}\left(0.002L_b + 0.002L_b\right) = 0.004L_b\beta_{ideal} \end{aligned} \tag{19}$$

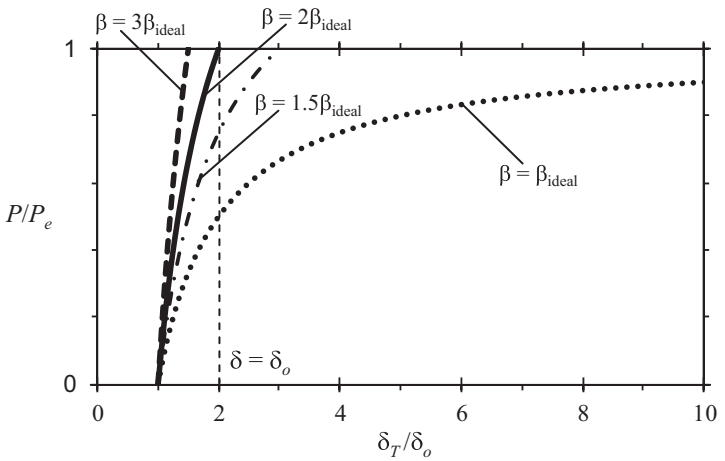

Fig. 4. Influence of brace stiffness, β*, on column buckling load,* P.

This coincides with the value obtained using Equation 17, with $\delta_T/\delta_o = 2$ and $\delta_o/L_b = 0.002$.

Specification Provisions for Nodal Braces

The required brace stiffness and force for column nodal braces are given in Appendix 6.2.2 of the *Specification*. Winter (1958) noted that "the small magnitudes of both rigidity and strength of bracing which are sufficient to provide extremely large effects…suggest that it is not necessary to compute these two characteristics with great accuracy." The largest required brace stiffness occurs as the number of braces approaches infinity for the columns of cases (b) and (c). In both cases, the coefficient, η_0 or η_1, is equal to 4.0. Thus, the *Specification* adopted this condition as a simple and conservative requirement and from Equation 18, with $\beta_{ideal} = 4P_e/L_b$,

$$\beta_{req} = \beta_{ideal}(1+1) = 2\beta_{ideal} = \frac{8P_e}{L_b} \tag{20}$$

In the elastic buckling region of column behavior, the nominal strength is given by *Specification* Equation E3-3. In terms of force this can be written as

$$P_n = 0.877P_e \tag{21}$$

Because the designer will be starting with the column required strength, P_r, it will be useful to establish a relationship between P_r and P_e. If the required strength of the column is exactly equal to the available strength, then

$$P_r = \phi P_n = 0.9(0.877P_e) = 0.789P_e \tag{22}$$

Solving Equation 22 for P_e and defining a resistance factor for design of bracing stiffness, $\phi = 0.789$, yields

$$P_e = \frac{P_r}{0.789} = \frac{P_r}{\phi} \tag{23}$$

Substituting Equation 23 into Equation 20 gives

$$\beta_{req} = \frac{8P_r}{\phi L_b} \tag{24}$$

Conservatively defining $\phi = 0.75$ yields *Specification* Equation A-6-4 for LRFD. A similar substitution with Ω will give the ASD equation. The same requirements apply to columns controlled by inelastic buckling. The *Specification* Commentary provides a way to reduce the required stiffness to account for the actual number of intermediate braces but does not distinguish between the columns of Figures 1b and 1c.

Although the *Specification* establishes the required brace stiffness based on an infinite number of equally spaced braces, the required brace force is based on the two-story column shown in Figure 2. Using Equation 19 and substituting the ideal stiffness for a single spring at mid-height, from Table 1, which is $\eta_0 = 2.0$, yields

$$F = 0.004L_b\beta_{ideal} = 0.004L_b\left(\frac{2P_e}{L_b}\right) = 0.008P_e \tag{25}$$

Because the column will only be called upon to provide the required strength, P_r, this required strength will be directly substituted in place of P_e. Design for brace strength will utilize the safety and resistance factors associated with design of the specific bracing members.

Winter (1958) assumed that the shape of the initial

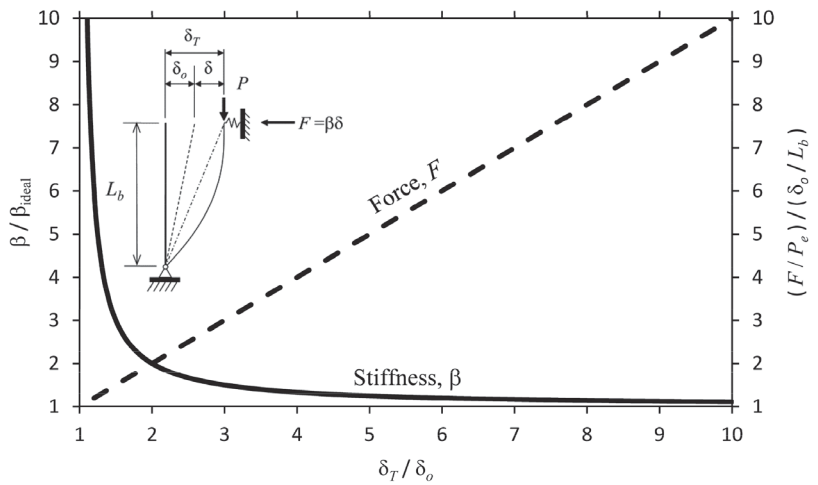

Fig. 5. Required brace stiffness, β*, and brace force,* F*, for column load* $P = P_e$.

imperfections followed the same sine wave as the buckled column. Plaut (1993) showed that Equation 25, based on Winter's approach, can be unconservative for assumed displacements with shapes other than that assumed by Winter. To account for this, *Specification* Equation A-6-3 for the required brace force uses the multiplier of 0.01 rather than 0.008:

$$P_{rb} = 0.01P_r \tag{26}$$

COLUMNS WITH RELATIVE BRACES

Column Case (d)

The approach to development of the requirements for relative braces usually starts with the structure shown in Figure 6. A review of that structure shows that the diagonal bracing member connects the top of the column to an immovable support. Thus, this structure can be modeled like the structure in Figure 3. The only difference is that the stiffness and force requirements relate to the horizontal direction, and they must be converted for design to the longitudinal direction of the brace. Accepting that Figure 3 is a simplification of the structure in Figure 6, the required stiffness for the structure of Figure 6 is derived from equilibrium:

$$\beta_{req} = \frac{P_e}{L_b}\left(\frac{\delta_o}{\delta} + 1\right) \tag{27}$$

which is identical to Equation 9. For the perfect or ideal column, $\delta_o = 0$ and the ideal stiffness is

$$\beta_{ideal} = \frac{\rho_1 P_e}{L_b} \tag{28}$$

where $\rho_1 = 1.0$. The required brace force is then given by

$$F = \beta_{ideal}\left(\delta_o + \delta\right) \tag{29}$$

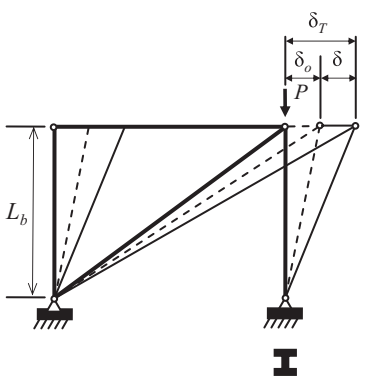

Fig. 6. Relative column brace.

The extension of the one-story structure of Figure 6 to a multistory structure similar to that in Figure 1d is rarely presented in the literature. It is that extension that causes difficulty in understanding exactly what a relative brace is because, clearly, the two cases just discussed could both be called nodal braces.

Zhang et al. (1993) presented a study of column bracing stiffness that addressed both nodal and relative braces through an energy analysis. They first showed that for a single-degree-of-freedom system, as shown here in Figures 3 and 6, the ideal stiffness is as given in Equation 28. They then proceed to address multi-degree-of-freedom systems and found, again through an energy analysis, that for systems similar to that shown in Figure 1d, ρ_1 is always 1.0. In addition to the multi-degree-of-freedom system shown in Figure 1d, they also studied a system similar to that in Figure 1d but with an immovable support at the top of the structure. They found that the coefficient for this case, taken here as ρ_0, was also always 1.0, regardless of the number of brace points. Thus, the ideal stiffness (case with $\delta_0 = 0$) for all these relative bracing systems is given as

$$\beta_{ideal} = \frac{\rho P_e}{L_b} \tag{30}$$

with $\rho = \rho_0 = \rho_1 = 1.0$.

The condensed stiffness matrix for the multistory nodal brace system in Figure 1c (with identical braces at each story) is the constant brace stiffness times the identity matrix. Thus, there is no interaction between the displacement at one brace point and the displacement at any other brace point. The stiffness matrix for the relative brace system shown in Figure 1d is the constant brace stiffness times a diagonal matrix with a bandwidth of 3. Thus, there is interaction between adjacent braced points. It is this interaction that separates a relative brace system from a nodal brace system.

Specification Provisions for Relative Braces

Using Equations 27, 28 and 29, the equations for relative braces found in the *Specification* can be developed. If the final deflection is again taken equal to the initial imperfection, as was done for nodal braces, $\delta = \delta_o$ and from Equation 27 the required brace stiffness is

$$\beta_{req} = \frac{2P_e}{L_b} = 2\beta_{ideal} \tag{31}$$

Substituting for P_e, as was done earlier for nodal braces, yields the required brace stiffness as given by *Specification* Equation A-6-2:

$$\beta_{req} = \frac{2P_r}{\phi L_b} \tag{32}$$

As with the derivation of Equation 25 for nodal braces, if a tolerable value of displacement at buckling, δ, is assumed equal to the initial out-of-plumbness, $\delta = \delta_o = 0.002L_b$, and P_e is replaced by P_r, the required brace force becomes

$$P_{rb} = \beta_{ideal}\left(\delta_o + \delta\right) = 0.004P_r \tag{33}$$

which is *Specification* Equation A-6-1.

NUMERICAL EXAMPLES

A three-story column will be used to confirm that the ideal spring stiffness results in the column buckling at the Euler buckling load. Figure 7 shows four possibilities for bracing of the column, similar to the four columns shown in Figure 1. For the column, $I = 18.3$ in.^{4} (I_y for a W8×24) and $L_b = 10.0$ ft, SAP2000 (CSI, 2011) is used to determine the buckling load for each column considering only flexural deformations of the column.

Case (a): Immovable Supports

The Euler buckling load for this column with a length of 10.0 ft is

$$P_e = \frac{\pi^2 EI}{L^2} = \frac{\pi^2(29{,}000)(18.3)}{\left[10(12)\right]^2} = 363.7 \text{ kips}$$

With immovable supports, the buckling load for the three-story column, as determined by SAP2000, is $P_{critical} = 363.8$ kips.

Case (b): Two Intermediate Spring Supports, $n = 2$, $\eta_0 = 3.00$

Again, with the Euler buckling load at 363.7 kips, the ideal stiffness is

$$\beta_{ideal} = \frac{\eta_0 P_e}{L_b} = \frac{3.00P_e}{L_b} = \frac{3.00(363.7)}{10(12)} = 9.09 \text{ kips/in.}$$

The minimum spring stiffness for these two intermediate springs resulting in a buckling load of 363.7 kips, as determined by SAP2000, is $\beta = 9.09$ kips/in.

Case (c): Two Intermediate Spring Supports Plus Top Spring Support, $n = 3$, $\eta_1 = 3.25$

Again, with the Euler buckling load at 363.7 kips, the ideal stiffness is

$$\beta_{ideal} = \frac{\eta_1 P_e}{L_b} = \frac{3.25P_e}{L_b} = \frac{3.25(363.7)}{10(12)} = 9.85 \text{ kips/in.}$$

The minimum spring stiffness for these three springs resulting in a buckling load of 363.7 kips, as determined by SAP2000, is $\beta = 9.84$ kips/in.

Case (d): Three-Story Column with Truss Type Bracing, $\rho = 1.0$

For this structure, the horizontal and vertical members are assumed axially rigid. Thus, the bracing stiffness will all be

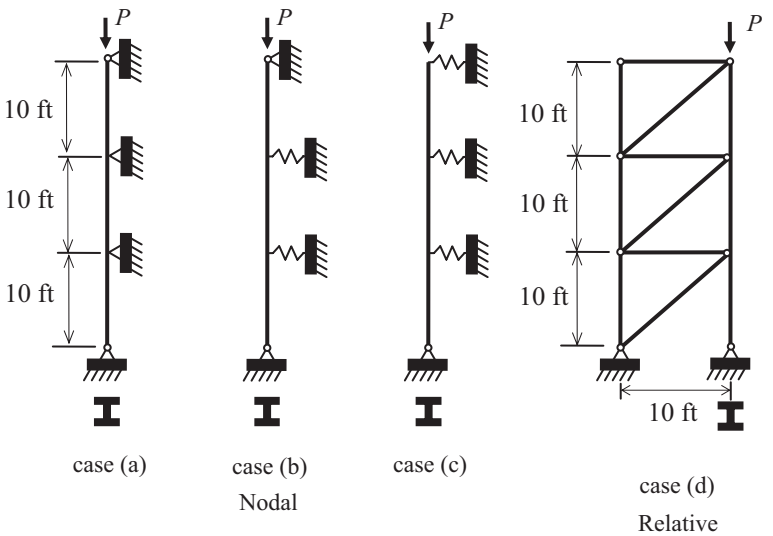

Fig. 7. Structures for lateral bracing for column stability examples.

contributed by the diagonal braces. Again, with the Euler buckling load at 363.7 kips, the ideal stiffness is

$$\beta_{ideal} = \frac{\rho P_e}{L_b} = \frac{1.00P_e}{L_b} = \frac{1.00(363.7)}{10(12)} = 3.03 \text{ kips/in.}$$

The minimum spring stiffness for the three diagonals resulting in a buckling load of 363.7 kips, as determined by SAP2000, is $\beta = 3.03$ kips/in., which corresponds to a brace area of 0.0355 in.^{2}

RECOMMENDED REVISIONS TO APPENDIX 6 REQUIREMENTS FOR COLUMN BRACES

Based on the development presented here, there appear to be two inconsistencies in the *Specification* requirements. The first has to do with determination of the required brace force for nodal braces and the second the brace force for relative braces.

The required brace stiffness given in Equation 24 (Equation A-6-4) is based on the assumption of an infinite number of nodal braces, $\eta_0 = 4.0$, while the required brace force given in Equation 25 is based on a single intermediate nodal brace, $\eta_0 = 2.0$. It would seem to be a more reasonable assumption to base both the required stiffness and strength on the same structure. Because the assumption of an infinite number of braces is conservative for all cases, use of that same assumption for required brace force would mean that Equation 25 should be

$$F = 0.004L_b\beta_{ideal} = 0.004L_b\left(\frac{4P_e}{L_b}\right) = 0.016P_e \quad (34)$$

Using the increase for a variation in the shape of the initial imperfections based on the work of Plaut (1993) and how that work was used to get from Equation 25 to Equation 26 (Equation A-6-3), the required brace force should be

$$P_{rb} = 0.02P_r \quad (35)$$

It is interesting to note that this recommended requirement is the same as what had been used historically (before 1999); brace force equals 2% of the force in the column.

The *Specification* Commentary provides an approach to reduce the required brace stiffness to account for the actual number of braces. However, because the required brace force is already based on the presence of a single brace, there can be no reduction of the brace force to account for the actual number of braces.

Although no studies have been found to illustrate the impact of the variation in shape of the initial imperfections on the relative bracing system, it would seem logical that there is an influence and that it would be similar to that on a nodal brace system. That being the case, Equation 33 (Equation A-6-1) should be

$$P_{rb} = 0.005P_r \quad (36)$$

WHICH IS IT, NODAL OR RELATIVE?

The *Specification* makes the distinction between nodal and relative braces in order to provide simplified equations for design of braces. Using the definitions of nodal and relative braces found in the *Specification* Commentary, the brace of Figure 3 is a nodal brace, and the brace of Figure 6 is a relative brace. Yet, as was shown here, for the case of this one-story structure, the brace points are identical in how they behave and, thus, have the same theoretical strength and stiffness requirements. For a nodal bracing system, all braces are nodal. For a relative bracing system, all diagonal braces are relative braces, while all other members are axially rigid. There are many other ways to provide bracing for columns. However, based on the derivations illustrated here, the *Specification* requirements do not directly apply to those situations.

As the number of brace points increases, the ideal stiffness coefficient for nodal braces approaches 4, while the ideal stiffness coefficient for relative braces remains at 1. This difference is also reflected in the required brace strength. Thus, it is desirable to distinguish between the two types of bracing systems. A nodal brace connects a column to an immovable support. The condensed stiffness matrix for a multistory nodal brace system (Figures 1a, 1b and 1c) with identical braces at each story is the constant brace stiffness times the identity matrix. Thus, there is no interaction between the displacement at one brace point and the displacement at any other brace point. A relative brace system, however, braces a column in such a way that there is interaction between the displacements at each end of the column unbraced length. In this system (Figure 1d), the stiffness matrix is the constant brace stiffness times a diagonal matrix with a bandwidth of 3, showing the interaction between adjacent brace points. It is this interaction that defines a relative brace system and distinguishes it from a nodal brace system.

Another way to identify the type of bracing is by examining the braced member and assuming that it is hinged at the brace points. These hinges lead to a structural mechanism when any single brace point is considered laterally unsupported. If the mechanism accommodates a deflected shape involving the displacement of more than one brace point, then the bracing is relative. When investigating possible mechanisms, only diagonal braces or spring supports may be removed. This is consistent with the assumption that these members are the only source of axial deformations.

This can be illustrated by considering the column of

Figure 7d as if it were hinged at each brace point. The removal of the bottom diagonal brace triggers a mechanism where all three brace points above the base displace laterally as a rigid body. This is an indication that the bottom diagonal provides relative bracing. If the diagonal brace at the second level is removed, a mechanism is formed where the two brace points above this brace are displaced laterally. Thus, this too is a relative brace. If this same approach is applied to any of the examples of nodal braces, it will be seen that the only brace point to displace is the point actually braced, thus confirming it is a nodal brace.

Once the required force at the brace points is determined, it is generally sufficient to consider that this force acts nonconcurrently at each of the brace points. This is consistent with the assumption that the braced member acts as if it were hinged at brace points and that instability occurs with buckling of a single segment between hinges.

To simplify design, the *Specification* provisions for a nodal brace use the worst-case stiffness requirement of an infinite number of braces. This means that when using the requirements of *Specification* Appendix 6, the required stiffness of a nodal brace is 4 times that of a relative brace (comparing Equations 20 and 31) and, using the approach detailed here, the required strength of the nodal brace is 2.5 times that of a relative brace (comparing Equations 26 and 33). Because the option is available in the *Specification*, it is desirable to design braces like those of Figures 1d and 6 as relative braces. However, for any column bracing system, if there is a question as to how to classify the brace, a nodal bracing solution will generally be conservative. Because the required stiffness and strength are usually small in magnitude, this extra conservatism is not likely to be a burden on the design.

The recommended revisions presented in the previous section make both the stiffness and strength requirements of nodal braces equal to four times that of relative braces.

Beams with Lateral Braces

Two types of lateral braces are defined for beams, nodal braces and relative braces as shown in Figure 8. The *Specification* provisions are derived from the same models previously discussed for columns. However, there are a number of factors that affect the requirements for beam braces that were not a part of the discussion for columns. These include the conversion of the beam moment to an equivalent axial force, the presence of load applied to the top flange of the beam and the possibility of double curvature bending. The *Specification* Commentary shows how these factors are incorporated as Equation C-A-6-5, based on the presentation by Yura (2001):

$$\beta_{br} = \frac{2N_i C_t \left(C_b P_f\right) C_d}{\phi L_b} \tag{37}$$

In this equation, the 2 represents the relationship between the required and ideal brace stiffness as shown for columns by Equations 18 and 31; N_i is equivalent to η_0 given in Table 1 for nodal braces of columns and is given in the *Specification* Commentary by the approximate equation, $N_i = (4 - 2/n)$; C_t accounts for top flange loading and is taken as 1.0 when the beam is loaded at its centroid and $1 + (1.2/n)$ otherwise; and C_d accounts for reverse curvature bending. The term $C_b P_f$ uses the flexural moment gradient factor, C_b, *Specification* Equation F1-1, to increase the possible flange force, $P_f = \pi^2 E I_{yc} / L_b^2$, due to a moment diagram less severe than uniform moment, where $I_{yc} = t_f b_f^3/12$, the out-of-plane moment of inertia of the compression flange.

For the *Specification* requirements, the term $C_b P_f$ in Equation 37 is replaced by an equivalent flange force, M_r/h_o, where M_r is the maximum required flexural strength of the beam as if it were under a uniform moment and h_o is the distance between beam flange centroids. For nodal braces, N_i varies from 2 to 4 based on the number of braces. The upper limit of 4 was selected for columns. However, for beams, C_t also varies with the number of braces. Therefore it is helpful to look at the range of the product of these terms. Table 3 shows the multipliers η_0, N_i, C_t and $N_i C_t$.

Recognizing that the range of the product $N_i C_t$ is from 4.00 to 4.80 and remembering Winter's original goal was to find a simple yet conservative approach, for the *Specification* requirement this product is conservatively taken as 5.

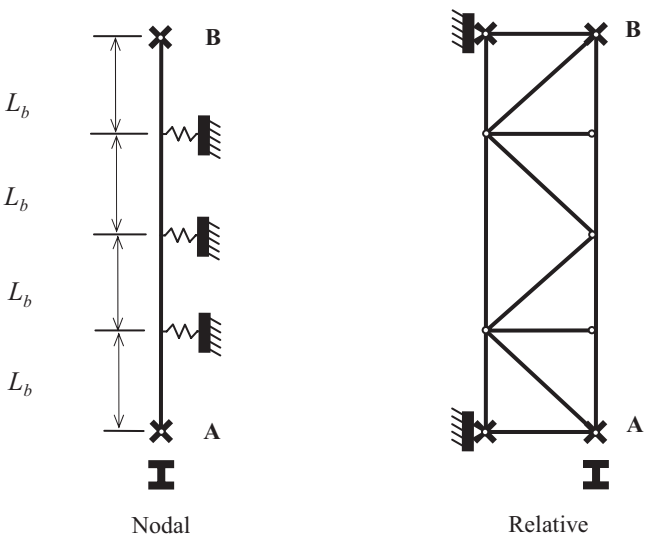

Fig. 8. Plan view of beam AB *with compression flange lateral brace.*

Table 3. Coefficients for Nodal Beam Braces *n* = number of springs (Yura, 2001)								
n	1	2	3	4	5	6	10	infinite
η_0	2.00	3.00	3.41	3.62	3.73	3.80	3.92	4.00
N_i	2.00	3.00	3.33	3.50	3.60	3.67	3.80	4.00
C_t	2.20	1.60	1.40	1.30	1.24	1.20	1.12	1.00
N_iC_t	4.40	4.80	4.67	4.55	4.46	4.40	4.26	4.00

With these two substitutions, Equation 37 for nodal beam braces becomes *Specification* Equation A-6-8:

$$\beta_{br} = \frac{1}{\phi}\left(\frac{10M_rC_d}{L_bh_o}\right) \tag{38}$$

For a column relative brace, it was shown in Equation 30 that $\beta_{ideal} = \rho P_e/L_b$ and $\rho = 1.0$. Thus, for a relative beam brace, N_i will be taken as 1.0. From Table 3 it is seen that the maximum value of C_t is 2.2 for a single brace with top flange loading. For simplicity, C_t is taken as 2.0 for relative bracing according to Yura (2001), so Equation 37 becomes, for a relative beam brace, *Specification* Equation A-6-6:

$$\beta_{br} = \frac{1}{\phi}\left(\frac{4M_rC_d}{L_bh_o}\right) \tag{39}$$

A similar approach can be followed to obtain the *Specification* equations for ASD.

The brace force requirements are the same as they were for columns, with the addition of the influence of location of load on the cross section and reverse curvature bending, if applicable. From Equations 38 and 39, recognizing that $\beta_{br} = 2\beta_{ideal}$ and using $\delta = \delta_o = 0.002L_b$ as was done for columns, the required nodal brace force is obtained using $F = \beta_{ideal}(\delta_o + \delta)$, which gives *Specification* Equation A-6-7:

$$P_{rb} = 0.02\,M_rC_d\,/\,h_o \tag{40}$$

For a relative brace, *Specification* Equation A-6-5 is

$$P_{rb} = 0.008\,M_rC_d\,/\,h_o \tag{41}$$

In each of these required stiffness and strength equations, according to the *Specification*, $C_d = 2$ for the brace closest to the inflection point and $C_d = 1$ for all other braces on a beam in double curvature and for all braces of a beam in single curvature. As was the case for column bracing design, the resistance and safety factors, ϕ and Ω, will be applied in the brace strength design.

The distinction between nodal braces and relative braces for beams is the same as it was for columns. If there is an interaction between braced points, then the braces can be treated as relative braces. However, treating all cases of bracing as nodal will always be conservative and, as was the case for columns, will not be a burdensome requirement.

It is important to note that for beams loaded at their centroid, $C_t = 1$ and the stiffness and strength requirements of nodal beam braces would be equal to four times that of relative beam braces.

CONCLUSIONS

The intent of the lateral stability bracing requirements of *Specification* Appendix 6 is to provide a simple yet conservative approach for sizing braces. This paper has shown how these requirements were developed, has described the distinction between nodal and relative braces, and has pointed out two apparent inconsistencies. Recommendations have been offered for changes in two of the *Specification* equations. It was recommended that *Specification* Equation A-6-3 be changed to

$$P_{rb} = 0.02P_r \tag{35}$$

and *Specification* Equation A-6-1 be changed to

$$P_{rb} = 0.005P_r \tag{36}$$

One additional requirement should be discussed. If the bracing is included in a second-order analysis that incorporates the initial out-of-straightness of the member, the results of that analysis may be used in lieu of the lateral stability bracing requirements of *Specification* Appendix 6. Because *Specification* Chapter C requires that a second-order analysis, including initial out-of-straightness, be carried out for the lateral-load-resisting system and because column bracing will be included in that analysis, application of the requirements of *Specification* Appendix 6 for column bracing can often be avoided.

Because beam bracing is normally not included in a second-order analysis, the beam bracing provisions usually cannot be avoided. In addition to the lateral bracing requirements for beams discussed in this paper, *Specification* Appendix 6 includes provisions for torsional bracing.

SYMBOLS

C_b Lateral-torsional buckling modification factor for nonuniform moment diagrams

C_d Coefficient accounting for increased required bracing stiffness at inflection point

C_t Coefficient to account for load location relative to centroidal axis

E Modulus of elasticity of steel

F Force in brace or spring representing brace

I Moment of inertia for axis about which buckling is considered

L_b Unbraced length for flexural buckling

M Moment of forces about a point

M_r Required moment strength

N_i Coefficient to account for number of nodal braces or presence of relative braces

P Axial force on a column

P_e Column elastic buckling strength known as the Euler buckling strength

P_f Beam compressive flange force

P_n Nominal compressive strength

P_r Required compressive strength

P_{rb} Required brace strength

n Number of springs or braces

β Spring or brace stiffness

β_{br} Brace stiffness

β_{ideal} Ideal brace stiffness

β_{req} Required brace stiffness

δ Additional deflection at buckling

δ_o Initial displacement due to imperfection

δ_T Total deflection at buckling

η_0 Coefficient for determination of ideal spring stiffness with only intermediate nodal braces

η_1 Coefficient for determination of ideal spring stiffness with intermediate and column end nodal braces

λ Coefficient for determination of ideal spring stiffness based on Zhang et al. (1993)

ρ Coefficient for determination of ideal spring stiffness for relative braces

ρ_0 Coefficient for determination of ideal spring stiffness with only intermediate relative braces

ρ_1 Coefficient for determination of ideal spring stiffness with intermediate and column end relative braces

ϕ Resistance factor

REFERENCES

AISC (2000), *Load and Resistance Factor Design Specification for Structural Steel Buildings*, American Institute of Steel Construction, Chicago, IL.

AISC (2010a), *Specification for Structural Steel Buildings*, ANSI/AISC 360-10, American Institute of Steel Construction, Chicago, IL.

AISC (2010b), *Code of Standard Practice*, American Institute of Steel Construction, Chicago, IL.

CSI (2011), SAP2000 Ultimate 15.0.0, Structural Analysis Program, Computers and Structures Inc., Berkeley, CA.

Plaut, R.H. (1993), "Requirements for Lateral Bracing of Columns with Two Spans," *Journal of Structural Engineering*, Vol. 119, No. 10, October, pp. 2913–2931.

Timoshenko, S.P. (1936), *Theory of Elastic Stability*, McGraw-Hill, New York, NY.

Timoshenko, S.P. and Gere, J.M. (1961), *Theory of Elastic Stability*, McGraw-Hill, New York, NY.

Winter, G. (1958), "Lateral Bracing of Columns and Beams," *Journal of the Structural Division*, ASCE, Vol. 84, No. ST2, March, pp. 1561-1–1561-22.

Yura, J.A. (2001), "Fundamentals of Beam Bracing," *Engineering Journal*, AISC, Vol. 38, No. 1, First Quarter, pp. 11–26.

Zhang, H.-Y., Beliveau, J.-G. and Huston, D.R. (1993), "Minimum Lateral Stiffness for Equally Spaced Braces in Columns," *Journal of Engineering Mechanics,* ASCE, Vol. 119, No. 9, pp 1888–1897.

A Flexibility-Based Formulation for the Design of Continuity Plates in Steel Special Moment Frames

ANDY T. TRAN, PATRICK M. HASSETT and CHIA-MING UANG

ABSTRACT

This paper introduces a rational approach for the design of continuity plates and associated welds in steel special moment frame (SMF) connections. The current AISC *Seismic Provisions* require welds attaching continuity plates to develop the full strength of the plate, resulting in the need to use complete-joint-penetration (CJP) groove welds. The combination of continuity plate thickness requirements, welding process and weld inspection often leads to costly detailing that may be overly conservative. The proposed design procedure, which is based on the relative flexibility between the column flange and continuity plate, aims to quantify the seismic force demand on continuity plates, thus allowing designers to efficiently size both the continuity plate thickness and the associated welded joints. In addition, the design procedure may allow the use of fillet welds or partial-joint-penetration groove welds as opposed to CJP welds, leading to a more economical design and fabrication. Formulation of the design procedure through analytical studies, including finite element analysis, is outlined.

Keywords: special moment frame, continuity plate, relative flexibility, RBS, WUF-W.

INTRODUCTION

Continuity plates are commonly used in moment connections of steel moment frames to increase the local strength and stiffness of the column flange and web (see Figure 1). These transverse plates are attached to the column. They are utilized in both gravity and lateral load applications. The basic design requirements for continuity plates have been provided in the AISC *Specification for Structural Steel Buildings* (AISC 2005a, 2010a), hereafter referred to as AISC *Specification*. For seismic applications, additional requirements are provided in the AISC *Seismic Provisions for Structural Steel Buildings* (AISC 2005b, 2010b) and the AISC *Prequalified Connections for Special and Intermediate Steel Moment Frames for Seismic Applications* (AISC 2005c, 2010c), hereafter referred to as AISC *Seismic Provisions* and AISC 358, respectively.

Current seismic design provisions take a conservative approach for sizing and attaching continuity plates to the column due to the lack of a rational procedure to apportion the beam flange force to the continuity plate welded joints and limitations in tested geometries. For seismic design applications, this leads to continuity plates that maybe thicker than necessary and require complete-joint-penetration (CJP) welds to the column flanges, detailing that adds cost to fabrication and quality control. Thus, there is a need for the development of a rational design methodology such that a more economical continuity plate and weld design can be achieved.

Andy T. Tran, P.E., Director of Research and Development, SidePlate Systems Inc., Laguna Hills, CA; E-mail: atran@sideplate.com

Patrick M. Hassett, S.E., President, Hassett Engineering Inc., Castro Valley, CA. E-mail: pat@hassettengineering.com

Chia-Ming Uang, Ph.D., Professor, Department of Structural Engineering, University of California, San Diego, La Jolla, CA (corresponding author). E-mail: cmu@ucsd.edu

BACKGROUND

Section J10 of the AISC *Specification* provides requirements for continuity plate design for gravity, wind, and low seismic load applications. AISC *Seismic Provisions* and AISC 358 provide additional requirements for seismic load applications. The application of these design requirements are well documented in AISC Design Guide 13, *Stiffening of Wide-Flange Columns at Moment Connections: Wind and Seismic Applications* (Carter, 1999). These documents contain equations to compute the force demand and column limit state capacities that determine whether continuity plates are required. If required, these documents also provide requirements to size and detail continuity plates. A review of these equations and requirements are presented in the following sections.

Concentrated Beam Flange Force

Figure 2 shows concentrated beam flange forces acting on a column. Consider cases (a) and (b) where beams frame into the column from both sides. Assuming $P_{uf,1} = P_{uf,2} = P_{uf}$ under the gravity load case, the flow of stress from beam 1 to beam 2 is relatively direct and uniform (see Figure 3a). The continuity plate welded joint to the column flange (defined hereafter as "flange weld") is required to transmit part of the tensile force, P_{uf}; however, there is a negligible force transferred from continuity plate to the column web. In Figure 3b,

a different flow of stress is shown under a lateral load case. Because one loaded edge of the continuity plate is in tension while the other edge is in compression, shear forces exist along the web edge. To satisfy equilibrium, two additional shear forces along the loaded column flange edges also result. These transverse shear forces, which are not trivial in magnitude, are not numerically addressed in current design.

According to AISC Design Guide 13 (Carter, 1999), the concentrated beam flange force, P_{uf}, is calculated as shown in Equation 1:

$$P_{uf} = \frac{M_u}{d_m} \tag{1}$$

where M_u = beam end moment and d_m = moment arm between the flange centroids ($d_b - t_{bf}$). Note that Equation 1 assumes the entire beam moment is transferred to the column through the beam flanges. While this assumption may be reasonable for the more flexible, bolted beam web connection, it may be too conservative for moment connections where the beam web is welded directly to the column flange. This issue will be discussed later. The demand from the beam flange force is checked against a series of limit states to determine the need for continuity plates.

Limit States and Design Strengths

In continuity plate design for a lateral load case, the following two limit states need to be checked per AISC *Specification*.

(1) *Flange Local Bending (FLB) of Column*

When an unstiffened column flange is pulled out-of-plane by the tensile beam flange force, P_{uf}, stress concentrations in the beam flange weld will occur due to the differential

(a) *(b)*

Fig. 1. RBS moment connection: (a) with continuity plates; (b) without continuity plates.

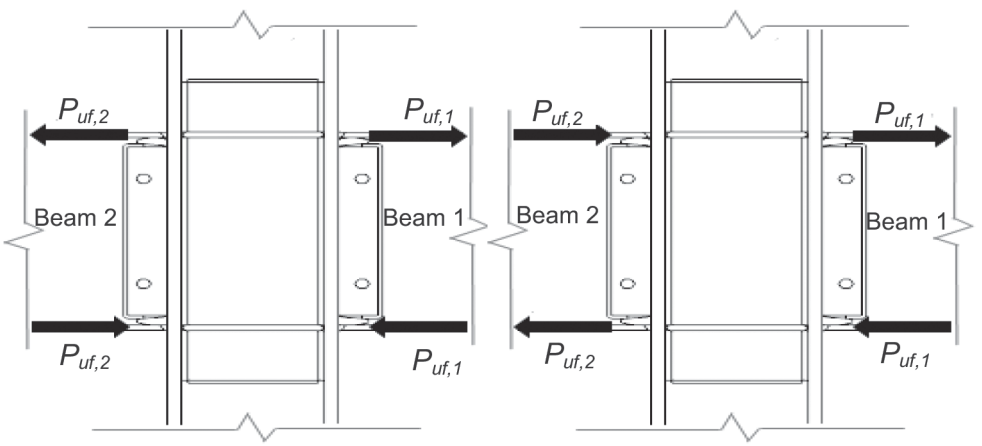

(a) *(b)*

Fig. 2. Moment connection flange forces: (a) gravity load case; (b) lateral load case (adapted from Carter, 1999).

stiffness across the column flange width (see Figure 4a). To minimize the effect of stress concentration, AISC *Specification* specifies the following design strength for FLB beyond which continuity plates are required:

$$\phi R_n = \phi 6.25 t_{cf}^2 F_{yc} \quad (2)$$

where $\phi = 0.9$, t_{cf} = column flange thickness and F_{yc} = specified minimum yield stress of the column.

To prevent weld fracture due to stress concentrations, Equation 2 was derived based on a limit state defined by a ¼-in. relative deformation between two opposing column flanges. A recent study by Hajjar et al. (2003) observed that this equation is conservative for design.

(2) *Web Local Yielding (WLY) of Column*

AISC *Specification* assumes the concentrated beam flange force, P_{uf}, is transmitted to the web of an unstiffened column as shown in Figure 5. The associated design strength is

$$\phi R_n = \phi(5k + N) F_{yc} t_{cw} \quad (3)$$

where $\phi = 1.00$, k = distance from the outer face of the column flange to the web toe of the fillet, N = beam flange thickness and t_{cw} = column web thickness.

Required Strength for Continuity Plates and Welds

When the concentrated beam flange force, P_{uf}, exceeds either the FLB or WLY limit state strengths, a pair of continuity plates is needed to strengthen and stiffen the column. Here, $\phi R_{n(\min)}$ is denoted as the lesser of the design strengths for FLB and WLY limit states. The AISC *Specification* specifies the required strength for a pair of continuity plates as

$$R_{u(st)} = P_{uf} - \phi R_{n(min)} \quad (4)$$

AISC Design Guide 13 notes that Equation 4 is a simplified approach, whereby only the force in excess of the governing limit state strength is assumed to be transmitted to the continuity plates. In an exact solution, the design guide also noted that "…this force would be apportioned between the web and transverse stiffeners on the basis of relative stiffness and effective area" (Carter, 1999). It will be shown in subsequent sections that the simplified approach can lead to a large difference between the required design strength, $R_{u(st)}$, and the actual force transmitted to the continuity plates.

Each full-depth continuity plate is welded to the column on three sides, with two flange welds and one web weld. It is critical to evaluate the required strength of these welds

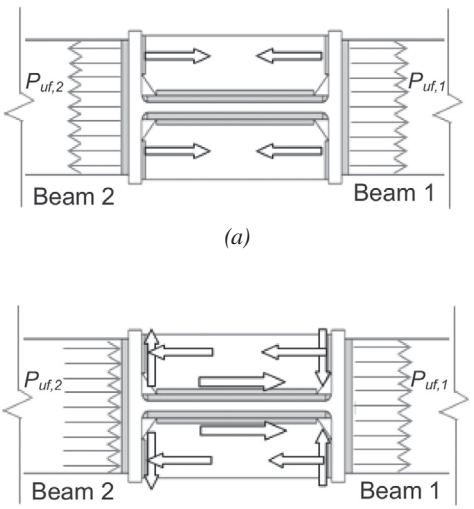

Fig. 3. Stress flow in continuity plates: (a) gravity load case; (b) lateral load case.

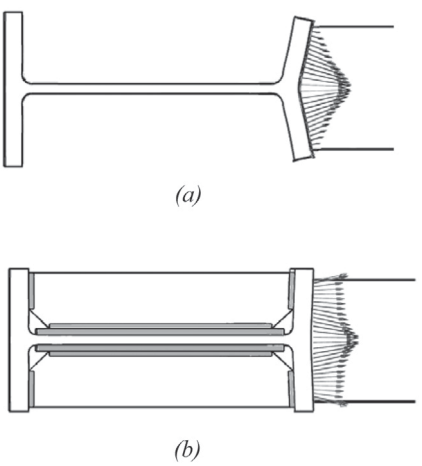

Fig. 4. Beam flange stress distribution: (a) unstiffened column flange; (b) stiffened column flange.

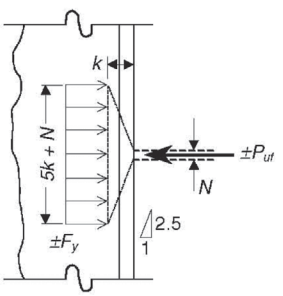

Fig. 5. Local force transfer for WLY limit state (Carter, 1999).

properly because a conservative estimate can lead to expensive welds (e.g., CJP groove welds). The past and current procedures for welding of continuity plates detailed in the AISC *Specification* is summarized later.

Section K1 of the AISC LRFD *Specification* (AISC, 1999) specifies a conservative approach to design continuity plate flange welds that require them to develop the welded portion of the stiffener. This conservatism is unavoidable when using this simplified approach because the actual force transmitted to the continuity plates is not calculated by a method that considers the relative stiffness. Section K1 of the AISC LFRD *Specification* requires the web weld to transmit the unbalanced force in the stiffener to the web.

The requirement for flange weld design is relaxed in the AISC *Specification* (2005a, 2010a) for nonseismic applications, which stipulates in Section J10 that the required strength is the difference between the beam flange force and available strength (i.e., Equation 4). Thus, the required design strengths for both continuity plates and flange welds are the same; flange welds, therefore, do not have to develop the flange welded portion of the continuity plates.

Seismic Design Provisions for Continuity Plates

For seismic applications, additional provisions are presented in the AISC *Seismic Provisions*. For pre-Northridge-type moment connections that feature welded beam flanges and a bolted web, the 1992 AISC *Seismic Provisions* assume the maximum beam moment developed at the face of the column is 1.3 times the nominal plastic moment of the beam. The 1.3 factor is used to account for the effect of material overstrength and cyclic hardening. Furthermore, it assumes that the flexible, bolted beam web is ineffective in transferring moment to the column. Assuming the flange-only plastic sectional modulus, $Z_f \left(\approx b_{bf} t_{bf} d_b\right)$, is approximately 70% of the beam plastic sectional modulus, Z_x, the concentrated tensile beam flange force is thus computed as

$$P_{uf} = \frac{M_u}{d_m} \approx \frac{1.3M_p}{d_b} = \frac{1.3\left(Z_x F_{yb}\right)}{d_b} = \frac{1.3\left(Z_f / 0.7\right)F_{yb}}{d_b} = \frac{1.3\left(b_{bf} t_{bf} d_b / 0.7\right)F_{yb}}{d_b} = 1.8 b_{bf} t_{bf} F_{yb} \quad (5)$$

To check FLB, the 1992 AISC *Seismic Provisions* use Equation 5 as the required strength, P_{uf}, and Equation 2 as the available strength, but with $\phi = 1.00$. Therefore, continuity plates are not required for the FLB limit state if the following condition is satisfied:

$$6.25 t_{cf}^2 F_{yc} \geq 1.8 b_{bf} t_{bf} F_{yb} \quad (6a)$$

or

$$t_{cf} \geq 0.4\sqrt{\frac{1.8 b_{bf} t_{bf} F_{yb}}{F_{yc}}} \quad (6b)$$

$$= 0.54\sqrt{\frac{b_{bf} t_{bf} F_{yb}}{F_{yc}}} \quad (6c)$$

Because of the damage of moment connections observed after the 1994 Northridge, California, earthquake, the 1997 and 2002 AISC *Seismic Provisions* simply stated, "[C]ontinuity plates shall be provided to match the tested specimens." Based on a study conducted after the Northridge earthquake by the SAC Joint Venture (a project headed by SEAOC, ATC, and CUREE), FEMA-350 (2000a) recommends that Equation 7, which is a slightly modified form of Equation 6b to account for the difference between nominal and expected yield stresses, be used for special moment frame (SMF) design:

$$t_{cf} \geq 0.4\sqrt{\frac{1.8 b_{bf} t_{bf} R_{yb} F_{yb}}{R_{yc} F_{yc}}} \quad (7)$$

where R_{yb} and R_{yc} are the ratio of the expected yield stress to specified minimum yield stress for the beam and column, respectively. That is, Equation 7 implies a beam flange force as in Equation 5 except that F_{yb} is replaced by $R_{yb}F_{yb}$. It is interesting to note that FEMA-355D (FEMA, 2000c) commented that Equation 7 is "…not a precise indicator of the need for continuity plates or of connection performance. There is room for considerable improvement in the continuity plate design requirements." In the SAC study on continuity plates, one welded unreinforced flange-welded (WUF-W) web moment connection tested by Ricles et al. (2000) provided satisfactory performance, although Equation 7 was not satisfied.

Equation 7 is the same as Equation 6b if the same grade of steel (e.g., ASTM A992 steel) is used for both the beams and columns. Both equations are based on a conservative assumption that the beam web is ineffective in transferring moment, and the beam flanges transfer 1.3 times the nominal plastic moment at the face of the column. For application to prequalified SMF moment connections (AISC, 2010c) where the web is fully welded to the column flange [e.g., reduced beam section (RBS) and WUF-W connections], the implied concentrated beam flange force used to determine the need for continuity plates may be too high. It is also noted that FEMA 350 (2000a) recommends another requirement based on the research of Ricles et al. (2000):

$$t_{cf} \geq \frac{b_{bf}}{6} \quad (8)$$

For SMF design, the required force for continuity plate

design is not quantified as in Equation 4. Instead, a prescriptive procedure is used to determine the thickness of the continuity plates. When required, FEMA 350 (2000a) recommends that the thickness of continuity plates satisfy the following requirements:

- For one-sided (exterior) connections, continuity plate thickness should be at least one-half of the thickness of the two beam flanges.
- For two-sided (interior) connections, the continuity plates should be equal in thickness to the thicker of the two beam flanges on either side of the column.

The recommended design procedure outlined in FEMA 350 (2000a) has been adopted by the 2005 and 2010 AISC 358 and is promulgated in the 2010 AISC *Seismic Provisions* for SMF design.

AISC 358 takes a conservative approach for weld design, requiring that the welds develop the strength of the continuity plates. The requirements are as follows:

- Continuity plates, if provided, shall be welded to column flanges using CJP groove welds.
- Continuity plates shall be welded to column webs using groove welds or fillet welds. The required strength of the sum of the welded joints of the continuity plates to the column web shall be the smallest of the following:
  - The sum of the design strengths in tension of the contact areas of the continuity plates to the column flanges that have attached beam flanges.
  - The design strength in shear of the contact area of the plate with the column web.

The current continuity plate and weld design requirements indicate that the design procedure may be more conservative than necessary. Thus, a rational approach that considers the relative stiffness to apportion the concentrated beam flange force to the continuity plates such that the welded joint can be properly and economically designed is desirable.

Experimental Evidence

A significant number of full-scale moment connections have been tested as a result of the 1994 Northridge, California, earthquake. A comprehensive summary of moment connection testing programs (pre- and post-Northridge) that feature either fillet or CJP welded continuity plates are provided by Hajjar et al. (2003). Recommendations from these studies suggest that fillet-welded continuity plates may provide adequate performance for seismic and nonseismic applications. In addition, a testing program conducted by Lee et al. (2005) featured two out of a total of eight full-scale RBS specimens with continuity plates that were fillet welded to the column (see Figure 6). Both specimens achieved an interstory drift angle of 0.04 radian with no observed failure in the continuity plate welds. Therefore, it is not always necessary to use CJP welds to connect the continuity plates to the column.

FORCE DEMAND ON CONTINUITY PLATES: A PARAMETRIC STUDY

To identify significant factors affecting the force demand on continuity plates, parametric nonlinear, finite element analyses (FEAs) were performed for an interior (two-sided) and exterior (one-sided) WUF-W moment connection (Uang, Tran and Hassett, 2011). The nonlinear FEA software

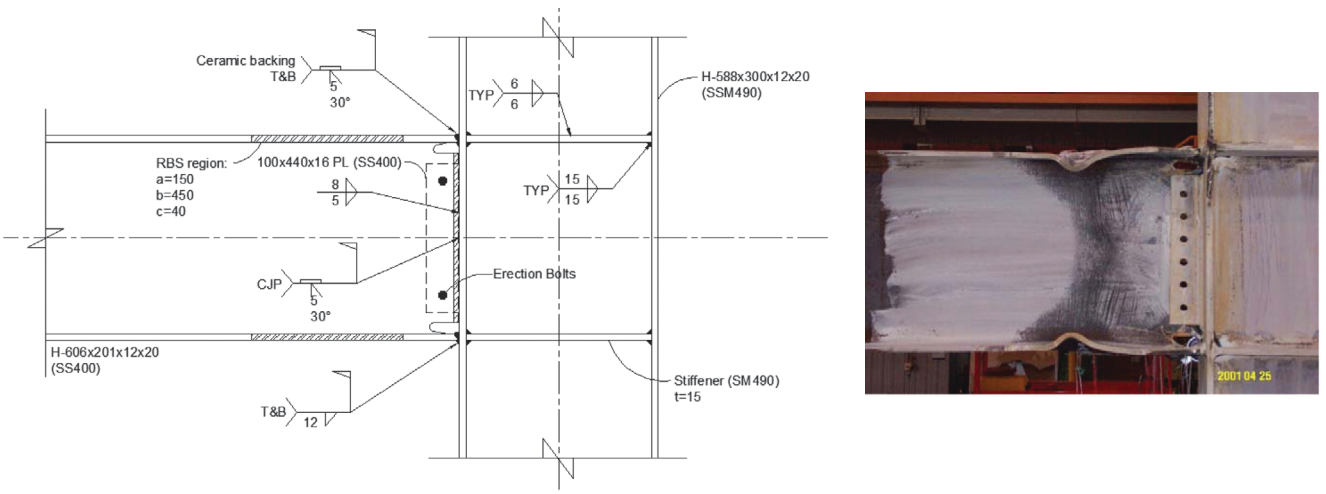

(a) *(b)*

Fig. 6. RBS moment connection with fillet-welded continuity plates: (a) connection details (in milimeters); (b) yielding pattern and deformed configuration (Lee et al., 2005).

ABAQUS was used (ABAQUS, 2005). Two base models were first established, then an additional nine interior connection cases and seven exterior connection cases were created (see Table 1) in which the continuity plate, column flange or column web were varied in thickness. For these analysis cases, four-node, thick-shell brick elements were used with mesh size ranging from 0.5 in. in the connection region to about 2 in. in the outer regions. A piecewise linear material model from FEMA (2000b) was used with a yield stress, F_{yn} = 50 ksi (see Figure 7).

A WUF-W specimen tested by Ricles et al. (2000) was used for the interior base model. The test specimen featured W36×150 beams along with a W14×398 column, all of A572 Grade 50 steel. The specimen simulated an interior connection in a SMF with a bay width of 29.5 ft and a story height of 13 ft. Column reinforcement included two ¾-in.-thick doubler plates and 1-in.-thick continuity plates. Figure 8 shows the finite element mesh (FEM) of the specimen, and Figure 9 shows the mesh at the connection. Assuming inflection points at the midspan of the beams and mid-height of the column, the free end of the beams were supported by simulated horizontal rollers. The base of the column was pin supported, and the top end of the column was loaded by a horizontal actuator to impose a monotonic displacement load. Lateral bracing of the beams was provided 10 ft from the column centerline.

The exterior WUF-W base model was designed in accordance with the AISC *Seismic Provisions*. A W33×130 beam was selected with a span of 14.75 ft (equal to half of the 29.5-ft bay width). A 13-ft-long W24×192 deep column was chosen to investigate the effects of thinner flanges. The connection features a pair of ¼-in.-thick doubler plates along with ⅞-in.-thick continuity plates to satisfy the FLB limit state. The column was pin-supported at both ends, and a load was applied to the end of the beam. The beam included lateral bracing of the flanges 10 ft from the column centerline. ASTM A992 steel was specified for the beam and column.

For each of the 16 parametric cases, the beam flange force, P_{uf}, at the face of the column is computed by integrating the tensile stresses of the bottom beam flange (beam 1 for interior connections) across its width. The forces acting on the flange weld edge of the continuity plates are also computed in a similar manner. The percentage of the beam flange force allocated to a pair of continuity plates are computed at 0.5 and 3% interstory drift to compare elastic and inelastic force distribution, respectively (inelastic force demand at 4% interstory drift tends to be lower for the beams used in this parametric study and thus were not used).

Effect of Continuity Plate Thickness

The continuity plate thickness for the interior base model was 1 in. Two additional cases corresponding to 33 and 67% of the base model thickness were considered. The continuity plate thickness for the exterior base model was ⅞ in. Three additional exterior cases were analyzed with a continuity plate thickness equal to 50, 75 and 125% of the exterior base model.

Figure 10 shows the percentage of the concentrated beam flange force that is transmitted to the continuity plates for the interior and exterior cases. It is observed that the percentage of the normal force acting on the flange weld increases with an increase continuity plate thickness; that is, thicker continuity plates attract more force from the beam flange.

Effect of Column Flange Thickness

The thickness of the column flange was 2.85 and 1.46 in. for the interior and exterior base models, respectively. Three

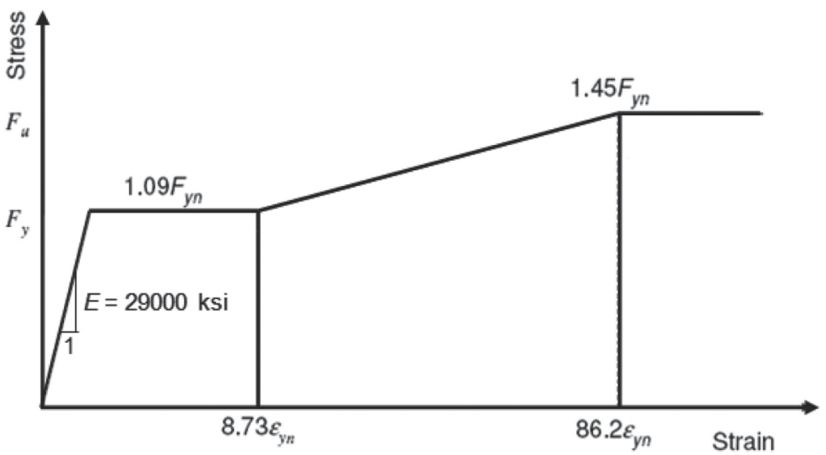

Fig. 7. Assumed steel stress-strain relationship.

Table 1. Cases for Parametric Study								
(a) Interior WUF-W Moment Connections								
	Continuity Plate Thickness		**Column Flange Thickness**		**Column Web Thickness**		**Strong Column–Weak Beam**	**Panel Zone Strength**
Case	(in.)	(%)	(in.)	(%)	(in.)	(%)	$\sum M_{pc}^{*} / \sum M_{pb}^{*}$	$\phi R_n / R_u$
I-1[†]	1.00	100	2.85	100	1.77	100	1.08	0.96
I-2	0.67	66.7	2.85	100	1.77	100	1.08	0.96
I-3	0.33	33.3	2.85	100	1.77	100	1.08	0.96
I-4	1.00	100	3.56	125	1.77	100	1.32	0.96
I-5	1.00	100	2.14	75	1.77	100	0.85	0.96
I-6	1.00	100	1.43	50	1.77	100	0.62	0.96
I-7	1.00	100	2.85	100	2.21	125	1.11	1.10
I-8	1.00	100	2.85	100	1.33	75	1.06	0.83
I-9	1.00	100	2.85	100	0.89	50	1.04	0.69
(b) Exterior WUF-W Moment Connections								
	Continuity Plate Thickness		**Column Flange Thickness**		**Column Web Thickness**		**Strong Column–Weak Beam**	**Panel Zone Strength**
Case	(in.)	(%)	(in.)	(%)	(in.)	(%)	$\sum M_{pc}^{*} / \sum M_{pb}^{*}$	$\phi R_n / R_u$
E-1[†]	0.88	100	1.46	100	0.81	100	1.68	1.37
E-2	1.09	125	1.46	100	0.81	100	1.68	1.37
E-3	0.66	75	1.46	100	0.81	100	1.68	1.37
E-4	0.44	50	1.46	100	0.81	100	1.68	1.37
E-5	0.88	100	1.83	125	0.81	100	2.02	1.37
E-6	0.88	100	1.10	75	0.81	100	1.35	1.37
E-7	0.88	100	0.73	50	0.81	100	1.02	1.37

[†] Refers to base model.

additional cases were considered for each base model with a column flange thickness equal to 125, 75 and 50% of the base model thickness. It is recognized that according to AISC *Seismic Provisions,* reducing the column flange thickness may violate some requirements (e.g., strong column–weak beam condition), and increasing the column flange thickness may result in a condition where continuity plates are no longer required. However, the purpose of this parametric study was primarily to evaluate the effect of column flange thickness on the force demand in continuity plates.

Figure 11 shows the percentage of the beam flange force that is transmitted to the continuity plates for the interior and exterior cases. The results show that an increase in column flange thickness decreases the force demand to continuity plates. It is also observed that at 3% interstory drift, the forces apportioned into the continuity plate varied from 35 to 87% of the beam flange force for the interior case and from 71 to 88% for the exterior case.

Effect of Column Web Thickness

The thickness of the column web was 1.77 in. for the interior base model. Three additional cases were considered with a column web thickness of 125, 75 and 50% of the interior base model web thickness. The results are shown in Figure 12. As expected from Equation 3 for the WLY limit state, a thicker column web will reduce the force demand on continuity plates. The percentage of force to the continuity plate, however, is shown to not be sensitive to variance in the column web thickness at the elastic level (0.5% interstory drift) and only marginally sensitive at inelastic levels (3% interstory drift). Thus, no similar parametric study was conducted for the exterior base model.

STRESS DISTRIBUTION ON FLANGE AND WEB WELDS

Figure 13a shows the normal stress distribution along the flange weld at 3% drift for the interior base model (case I-1). The figure shows that the normal stress is the highest near the column flange tip. Because the stress distribution is not uniform, to compute the maximum tensile stress, f_{max}, occurring near the column flange tip, it is necessary to idealize the distribution. A trapezoidal distribution varying from $0.25f_{max}$ at the web to f_{max} at the column flange tip is proposed (see Figure 13a). This idealized stress distribution has a resultant force located at $0.6b$ from the column web. For an exterior case, the stress is more uniform, varying from $0.40f_{max}$ near the web to f_{max} at the column flange tip (Uang et al., 2011). For the proposed design procedure that follows, it is conservative to set the location of the resultant force at $0.6b$ from the column web for both the interior and exterior cases. Figure 13b shows the stress distributions along the web weld for the interior control case. The shear stress is high but relatively uniform along this edge.

REVISED BEAM FLANGE FORCE DEMAND

It was shown in the presentation of Equation 7 that the current seismic codes (AISC 2005c, 2010c) assume all moment in the beam is transferred to the column by the beam flanges only. While this may be more consistent with the pre-Northridge-type connections that feature a bolted beam web and welded beam flanges, post-Northridge SMF connections with a welded beam web have been shown to reduce force demand on the beam flanges. Nonlinear FEA also demonstrated that welded beam webs of RBS and WUF-W

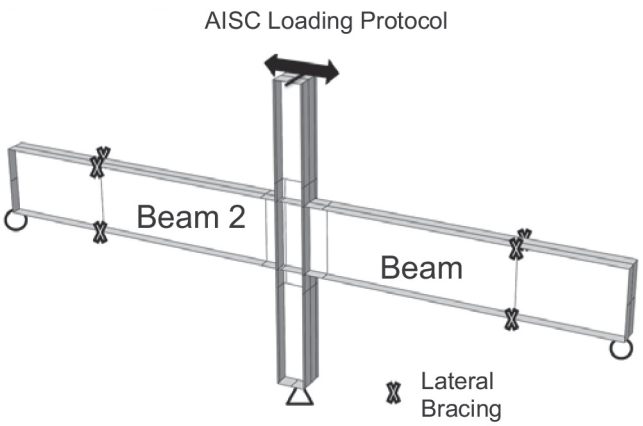

Fig. 8. Two-sided WUF-W model.

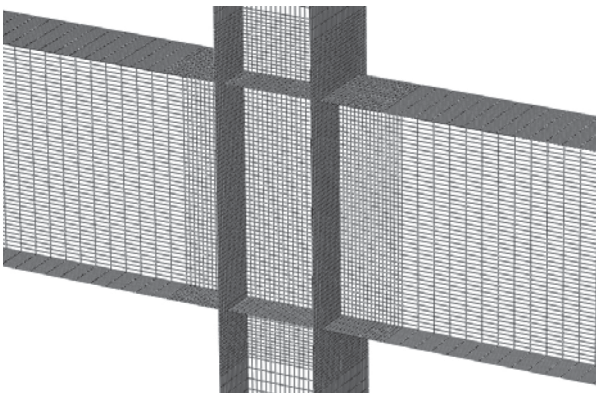

Fig. 9. Finite element mesh in the connection region.

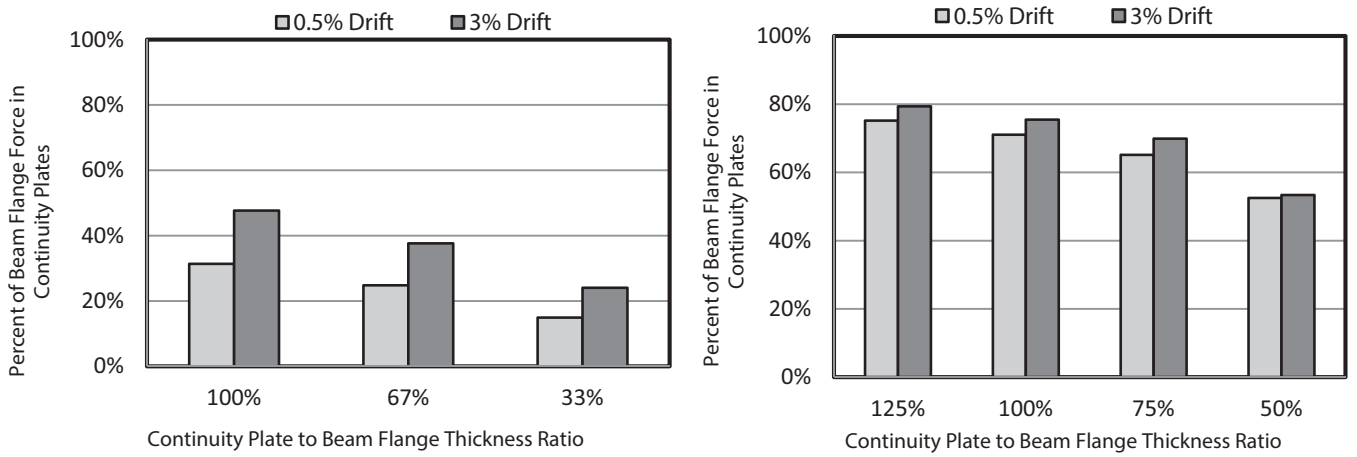

(a) interior connection

(b) exterior connection

Fig. 10. Continuity plate thickness effect on continuity plate normal force demand: (a) interior connection; (b) exterior connection.

connections can transfer a significant portion (up to 15 to 20%) of the beam moment at the column face.

Therefore, in lieu of using a factor of 1.8 in Equation 5 to compute the beam flange force, a reduced value can be used for moment connections with a welded beam web. The following is proposed to replace Equation 5:

$$P_{uf} = C_{pf} R_y F_{yb} b_{bf} t_{bf} \quad (9)$$

where C_{pf} is the beam flange force adjustment factor. Note that C_{pf} is different from C_{pr} used in AISC 358. The former is used to compute the expected beam flange force, while the latter is for computing the expected plastic hinge moment. A derivation of the C_{pf} factor for both the RBS and WUF-W connections is presented later.

RBS Moment Connection

Based on AISC 358, the beam moment at the column face is limited to

$$M_f = R_y F_{yb} Z_x \quad (10)$$

where Z_x is the plastic section modulus of the beam. Based

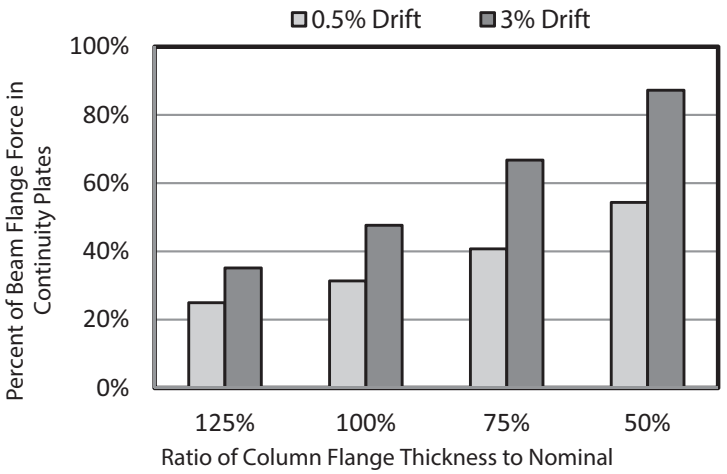

(a) interior connection

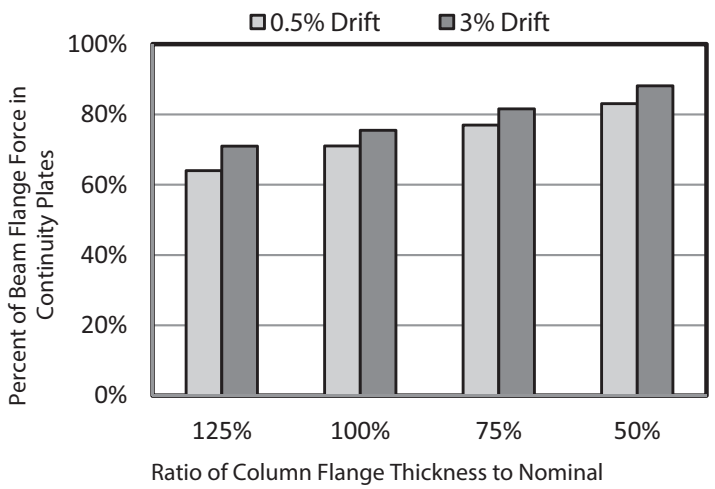

(b) exterior connection

Fig. 11. Column flange thickness effect on continuity plate normal force demand: (a) interior connection; (b) exterior connection.

on previously conducted FEA, it is conservative to assume that the beam web resists only 15% of M_f (i.e., the beam flange resists 85% of M_f). Thus, the beam flange force is

$$P_{uf} = \frac{0.85M_f}{d_b - t_{bf}} = \frac{0.85R_yF_{yb}Z_x}{d_b - t_{bf}} \tag{11}$$

Multiply both the numerator and denominator of Equation 11 by the beam flange area:

$$P_{uf} = \frac{0.85R_yF_{yb}Z_x\left(b_{bf}t_{bf}\right)}{\left(d_b - t_{bf}\right)\left(b_{bf}t_{bf}\right)} = 0.85\left(\frac{Z_x}{Z_f}\right)R_yF_{yb}\left(b_{bf}t_{bf}\right) \tag{12}$$

where Z_f [= $(d_b - t_{bf})b_{bf}t_{bf}$] is the plastic section modulus of the beam flanges.

AISC 358-10 prequalifies the RBS moment connection with the following limitations for the beam size and weight:

1. Beam depth is limited to W36 for rolled shapes.
2. Beam weight is limited to 300 lb/ft.
3. Beam flange thickness is limited to 1¾ in.

Figure 14a shows the values of the Z_x/Z_f ratio for all seismically compact rolled shapes of W12 or deeper that satisfy the preceding beam size limitations. If an upper-bound value of Z_x/Z_f taken as 1.47, only 10 out of the 127 shapes in the figure exceed this value; 6 shapes exceed the upper-bound value of 1.47 by less than 3%, and 4 shapes (W21×44, W21×50, W24×55 and W24×62) exceed this upper-bound value by a range of 5 to 11%. With this upper-bound value, Equation 12 can be taken as follows:

$$P_{uf} = 0.85(1.47)R_yF_{yb}\left(b_{bf}t_{bf}\right) = 1.25R_yF_{yb}\left(b_{bf}t_{bf}\right) \tag{13}$$

This represents a 30% reduction in beam flange force as compared to that implicitly assumed in Equation 7. That is, using Equation 7 as a criterion to determine the need for continuity plates is very conservative because it does not recognize the significant reduction of beam flange force by introducing the reduced section in the beam.

WUF-W Moment Connection

Based on AISC 358, the beam moment at the column face is

$$M_f = 1.4R_yF_{yb}Z_x \tag{14}$$

Assuming that the beam flanges resist 85% of M_f, the beam flange force is

$$P_{uf} = \frac{0.85\left(1.4R_yF_{yb}Z_x\right)\left(b_{bf}t_{bf}\right)}{\left(d_b - t_{bf}\right)\left(b_{bf}t_{bf}\right)} = 1.19\left(\frac{Z_x}{Z_f}\right)R_yF_{yb}\left(b_{bf}t_{bf}\right) \tag{15}$$

AISC 358-10 prequalifies the WUF-W moment connection with the following limitations for the beam size and weight:

1. Beam depth is limited to W36 for rolled shapes.
2. Beam weight is limited to 150 lb/ft.
3. Beam flange thickness is limited to 1 in.

Figure 14b shows the values of the Z_x/Z_f ratio for all

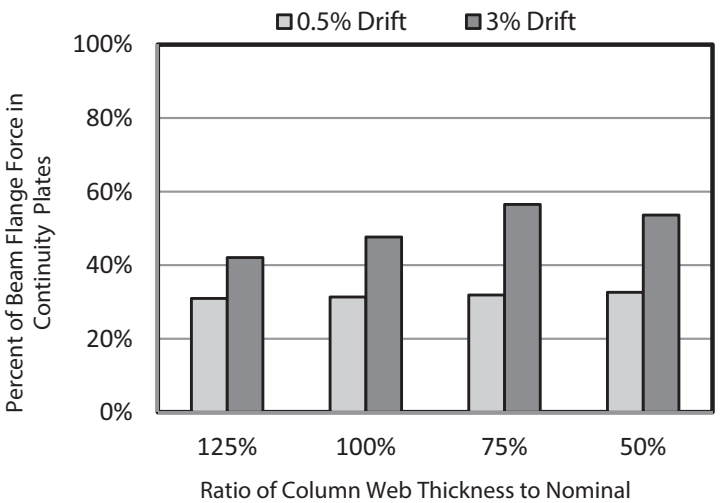

Fig. 12. Column web thickness effect on continuity plate normal force demand (interior connection).

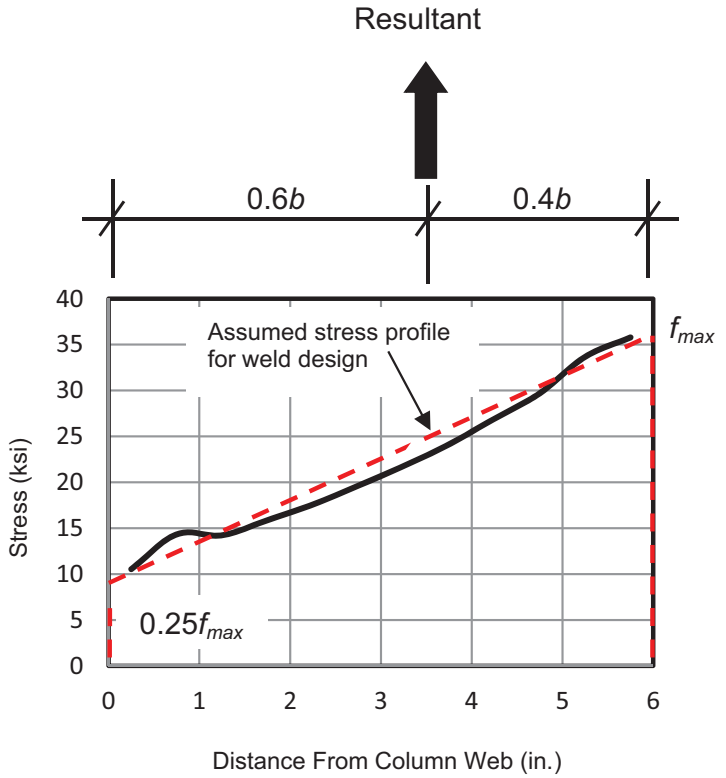

(a)

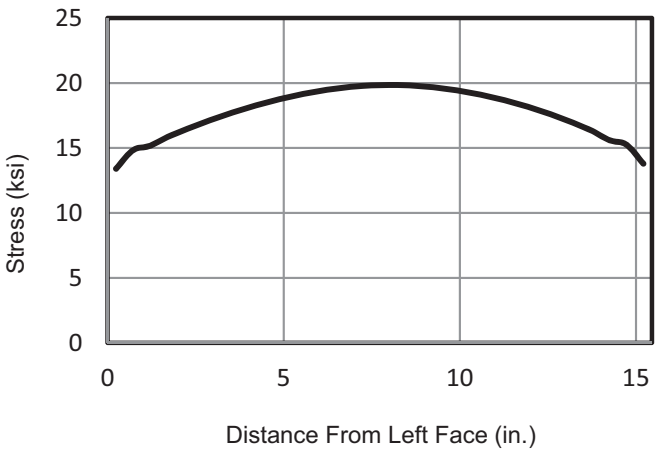

(b)

Fig. 13. Stress distribution along continuity plate welds at 3% drift (interior base model): (a) normal stress along flange weld; (b) shear stress along web weld.

seismically compact rolled shapes of W12 or deeper that satisfy the preceding beam size limitations. Again, with 1.47 as the upper-bound value for Z_x/Z_f, Equation 15 can be conservatively taken as follows:

$$P_{uf} = 1.19(1.47)R_y F_{yb}\left(b_{bf}t_{bf}\right) = 1.75R_y F_{yb}\left(b_{bf}t_{bf}\right) \quad (16)$$

Because the beam section is not reduced, the preceding beam flange force is about 40% higher than that in Equation 13. This beam flange force is also similar to that implicitly assumed in Equation 7.

To summarize, the beam flange force can be expressed as Equation 9, where the beam flange force adjustment factor, C_{pf}, is

For RBS connection: $C_{pf} = 1.25$ (17)

For WUF-W connection: $C_{pf} = 1.75$ (18)

RELATIVE FLEXIBILITY OF COLUMN FLANGES AND CONTINUITY PLATES

Results from the parametric studies indicate that the seismic force demands on continuity plates depend not only on the beam flange force, but also on the relative flexibility (or stiffness) between the continuity plate and column flange. This section describes the formulation of an analysis procedure for computing the amount of beam flange force allocated to continuity plates by considering the relative flexibility between the column flange and the continuity plate. The flexibility coefficients for both components are established from analytical studies, including FEA of individual components.

Figure 15 depicts the force flow from the beam flange to the column web for an exterior connection with continuity plates. A portion of the beam flange force in line with the column web is transferred directly into the column web. The remaining force is distributed between the continuity plates and column flange based on their relative flexibility. Force allocated to the column flange is transferred to the column web mainly through out-of-plane bending of the column flange, while force allocated to the continuity plates is transferred to the column web mainly through shear. Equation 19 computes the force allocated to one continuity plate, P_{cp}, from the beam flange force, P_{uf},

$$P_{cp} = \frac{P_{uf}}{2}\left(\frac{b_{bf} - t_{pz} - 2t_{cf}}{b_{bf}}\right)\left(\frac{B_{cf}}{B_{cf} + B_{cp}}\right) \quad (19)$$

where b_{bf} is the beam flange width, t_{pz} is the panel zone thickness and t_{cf} is the column flange thicknesses.

The term in the first parentheses accounts for the portion of the beam flange force, which is in line and transferred directly through to the column panel zone; it includes a 45-degree projection through the column flange thickness. The term in the second parentheses accounts for the flexibility of the continuity plate (B_{cp}) relative to the total flexibility ($B_{cf} + B_{cp}$) of the column flange and continuity plate, where B_{cf} is the flexibility of the column flange. The ½ term represents one of the two continuity plates at each beam flange level. The formulation of the column flange and continuity plate flexibility coefficients follows.

Flexibility Coefficient of Column Flange

When continuity plates are used, it is reasonable to assume the beam flange applies a uniform line load across its width and causes the column flange to deform out-of-plane (see Figure 16). Each column flange can be treated as a long, cantilever plate with a support along the column web. Considering symmetry, only half of the width of the column flange

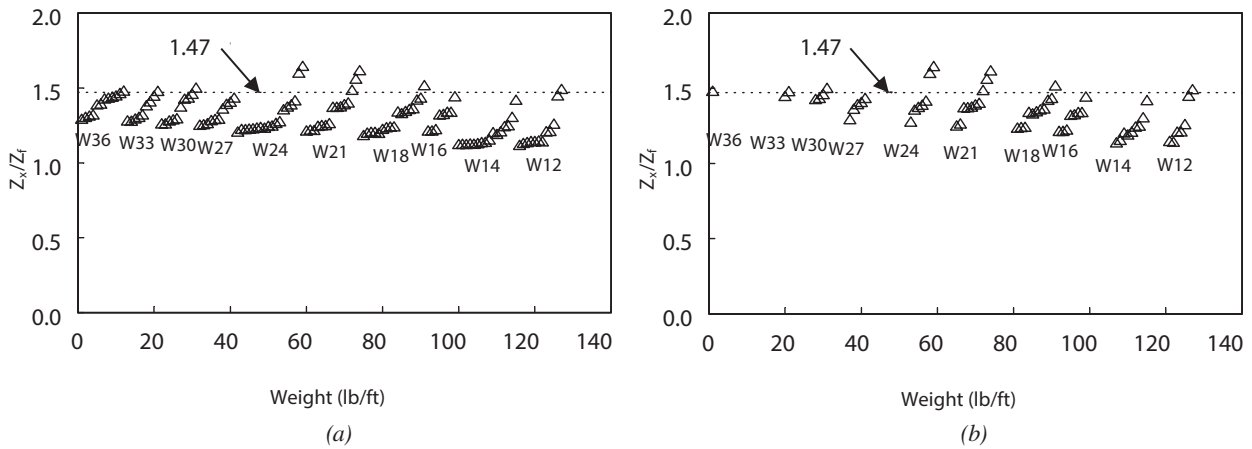

Fig. 14. Z_x/Z_f ratios for seismically compact sections: (a) RBS beam sections; (b) WUF-W beam sections.

needs to be considered in the analysis with a fixed support. The line load acts on the cantilever plate transversely with a loaded length of b, as defined in Figure 16. The flexibility of the column flange is defined as the out-of-plane displacement at the mid-width of the dimension b produced by a total line load of unity. Using the analogy of two springs in series, the column flange flexibility coefficient is

$$B_{cf} = f_{cf,b} + f_{cf,s} \tag{20}$$

where $f_{cf,b}$ and $f_{cf,s}$ are the flexibility coefficients due to bending and shear deformations, respectively.

(1) Flexibility Coefficient Due to Bending

Based on elastic plate theory (Timoshenko and Woinowsky-Krieger, 1959), the flexibility coefficient due to flexure can be expressed in the following form:

$$f_{cf,b} = C_1 \frac{b^2}{Et_{cf}^3} \tag{21}$$

To establish the constant C_1, the flexibility of long plates with varying thickness (t_{cf}) and width (b) was analyzed using FEA. Figure 17a shows the correlation of Equation 21 with $C_1 = 0.26$. Equation 21 correlates well for slender plates with a larger b/t_{cf} ratio, but for stockier plates, the effect of shear becomes significant and must be accounted for.

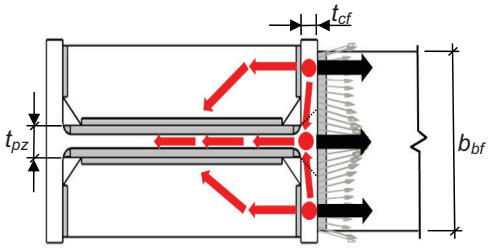

Fig. 15. Flow of beam flange force to column.

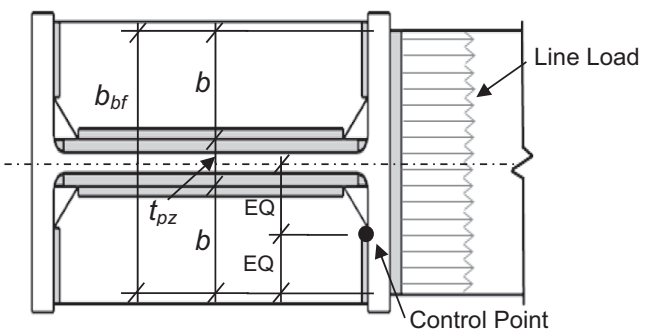

Fig. 16. Definition of column flange flexibility.

(2) Flexibility Coefficient Due to Shear

The flexibility coefficient due to shear can be expressed as

$$f_{cf,s} = \frac{C_2}{Gt_{cf}} \tag{22}$$

where C_2 is a constant.

Curve fitting shows that the following expression for C_2 produces good correlation with FEA results:

$$C_2 = 0.4\left[1 + 0.09\ln\left(\frac{b}{t_{cf}}\right)\right] \tag{23}$$

Figure 17b shows the correlation of Equation 20 with FEA results. Equation 20, which accounts for both bending and

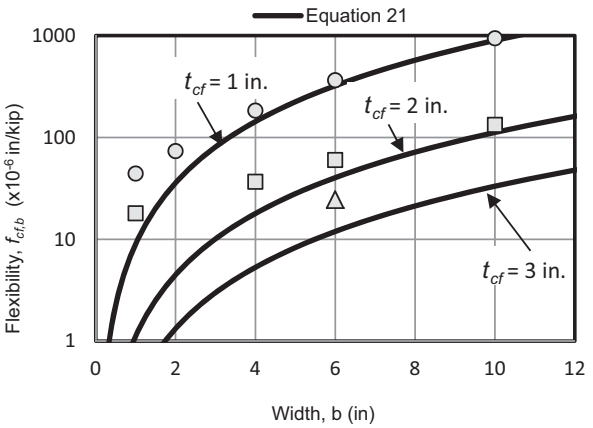

(a)

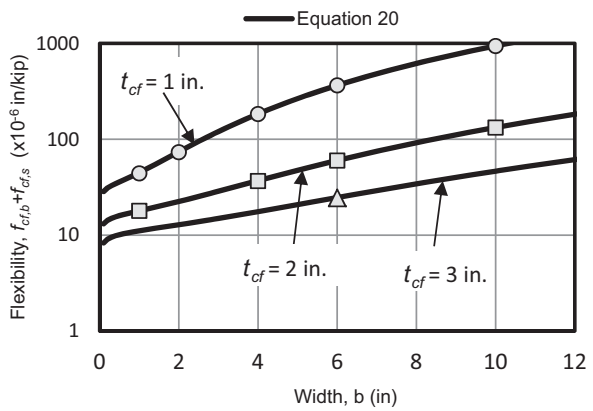

(b)

Fig. 17. Correlation of column flange flexibility: (a) flexural component only; (b) flexural and shear components.

shear deformations, provides good correlation for both stocky and slender column flanges.

Flexibility Coefficient of Continuity Plate

Finite element analysis shows that the normal force distribution varies almost linearly along the flange weld of a continuity plate (see Figure 13a). A simplification is made by assuming that the normal force is uniform, and the flexibility, B_{cp}, is defined as the deflection at the mid-width of the continuity plate due to a total edge load of unity. A continuity plate under the assumed edge load can be treated as a deep beam cantilevered from the column web (see Figure 18). For the purpose of computing the flexibility coefficient, the width of the continuity plate is taken to be equal to the length of the line load, b, as defined in Figure 16.

The applied unit load produces both shear and flexural deformations (shear being the dominant component), which are the shear ($f_{cp,s}$) and flexural ($f_{cp,b}$) flexibilities, respectively. Figure 19a shows the combined deformation from shear and flexure. Note that because the continuity plate has been idealized as a cantilever plate, the edge opposite the load also deforms by an amount, $f_{cp,r}$. In reality, the continuity plate is bounded by both column flanges. FEA shows that the rigidity of the nonloaded column flange restrains the opposite edge from deforming (see Figure 19c). A deformation pattern accounting for the restraint from the free flange is defined as having a magnitude $f_{cp,r}$ in the opposite direction, as shown in Figure 19b.

The superposition of the deformed shapes shown in Figures 19a and 19b results in a deformation pattern shown in Figure 19c. Therefore, the total flexibility coefficient of one continuity plate is:

$$B_{cp} = f_{cp,s} + f_{cp,b} - f_{cp,r} \tag{24}$$

(1) Flexibility Coefficient Due to Shear

Applying the beam theory to the cantilever plate in Figure 18, the shear flexibility is

$$f_{cp,s} = C_3 \frac{b}{Gdt} \tag{25}$$

However, for very small aspect ratios, the shear force does not transfer to the full depth (d) of the plate, but instead to an effective depth proportional to dimension b. Substitution of d with an effective depth proportional to b results in the following expression:

$$f_{cp,s} = C_4 \frac{1}{Gt} \tag{26}$$

The value of constant C_4 is determined by correlating with the FEA data. With $C_4 = 0.42$, Figure 20a shows that Equation 26 provides a good correlation for aspect ratios (b/d) less than 0.4. Above this value, however, the FEA data diverges from Equation 26 due to flexural deformation, which is considered next.

(2) Flexibility Coefficient Due to Bending

Applying the beam theory, the flexibility due to a unit total load is

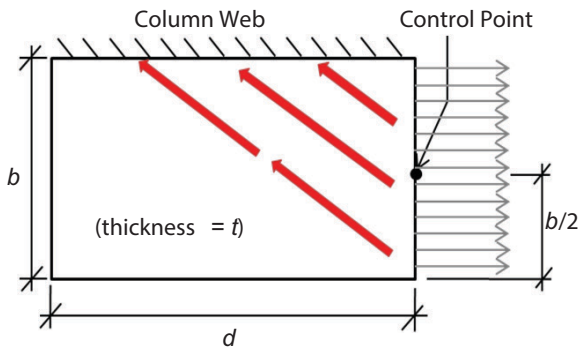

Fig. 18. Definition of continuity plate flexibility.

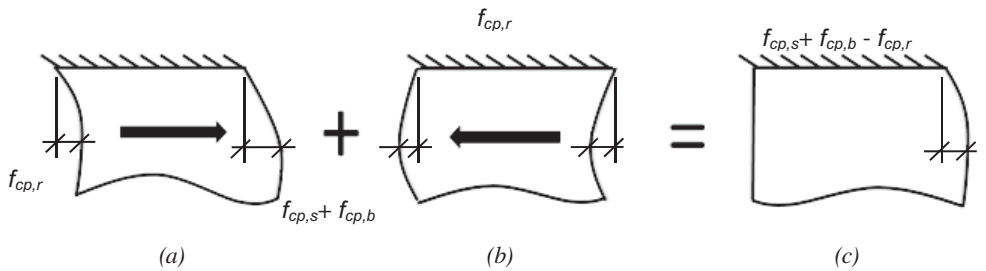

Fig. 19. Superposition of flexibility components for continuity plate: (a) shear and bending flexibility; (b) subtract restraint; (c) total flexibility.

$$f_{cp,b} = C_5 \frac{b^3}{Ed^3 t} \tag{27}$$

FEA data is again used to determine the constant C_5. In the curve-fitting process, the bending flexibility is computed as the difference between the total flexibility determined from FEA and the shear flexibility from Equation 26. By including the bending flexibility term with $C_5 = 1.0$, a satisfactory correlation of continuity plate flexibility is achieved with results from FEA over a wider range of aspect ratios, as shown in Figure 20b.

(3) Flexibility Coefficient Due to Restraining Effect

For an exterior connection, resistance by the opposite column flange decreases the flexibility by $f_{cp,r}$ (see Figure 19). The empirical Equations 28a and 28b are correlated with results from FEA:

$$f_{cp,r} = \frac{C}{Gt} \tag{28a}$$

where

$$C = 0.6\left(\frac{b}{d}\right) - 0.14 \geq 0 \tag{28b}$$

Equation 28b implies that the opposite edge does not deform when the aspect ratio is less than 0.23; that is, the effect of shear is negligible for low-aspect ratios.

(4) Total Flexibility

Combining Equations 26, 27, and 28a, the total flexibility of the continuity plate is

$$B_{cp} = f_{cp,s} + f_{cp,b} - f_{cp,r} = \frac{0.42 - C}{Gt} + \frac{b^3}{Ed^3 t} \tag{29}$$

where $C = 0$ for interior connections, and C is defined in Equation 28b for exterior connections.

PROPOSED DESIGN PROCEDURE

The proposed design procedure incorporates requirements of AISC 358 with some modifications to determine the need for continuity plates. If required, an iterative process is used to ensure that the design strength of the continuity plates is sufficient to transfer load from the beam flange to column web; the force apportioned to the continuity plates is determined based on the relative flexibility of the column flange and continuity plate. Welds connecting the continuity plates to the column are also sized according to the expected force calculated from this flexibility-based procedure. The proposed design procedure is suitable for moment connections where the beam web and flange are fully welded to the column flange. These include RBS and WUF-W moment connections.

Step 1. Continuity plates need not be provided if

$$t_{cf} \geq 0.4\sqrt{\frac{C_{pf} b_{bf} t_{bf} R_{yb} F_{yb}}{R_{yc} F_{yc}}} \tag{30}$$

$$t_{cf} \geq \frac{b_{bf}}{6} \tag{31}$$

where the beam flange force adjustment factor, C_{pf}, is

For RBS connection: $C_{pf} = 1.25$ (32)

For WUF-W connection: $C_{pf} = 1.75$ (33)

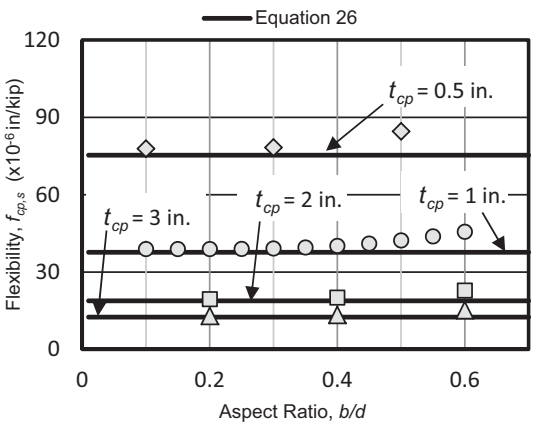

(a)

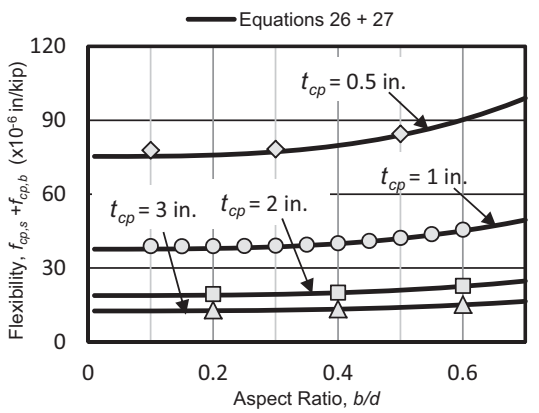

(b)

Fig. 20. Correlation of continuity plate flexibility: (a) shear component only; (b) flexural and shear components.

Note: Equation 30 is derived based on the following beam flange force:

$$P_{uf} = C_{pf} R_{yb} b_{bf} t_{bf} F_{yb} \tag{34}$$

It was previously demonstrated that the upper-bound C_{pf} values can be conservatively used for all seismically compact rolled shapes satisfying the AISC 358 size and weight limitations, except for four sections (W21×44, W21×50, W24×55 and W24×62).

Step 2. If continuity plates are needed, perform preliminary sizing based on the following:

$$R_{u(st)} = P_{uf} - \phi R_n \tag{35}$$

where ϕR_n is the design strength of the governing limit state (e.g., FLB or WLY). The required continuity plate cross-sectional area is:

$$A_{cp(req'd)} = \frac{R_{u(st)}}{F_{ycp}} \tag{36}$$

where and F_{ycp} is the specified minimum yield stress of the continuity plate.

The width-thickness ratio also needs to satisfy the following requirement:

$$\frac{b_{cp}}{t} \le 0.75\sqrt{\frac{E}{F_{ycp}}} \tag{37}$$

where b_{cp} and t are the actual (not effective) continuity plate width and thickness, respectively.

Note: AISC 358 requires the continuity plate thickness to be at least equal to one-half of the beam flange thickness for exterior connections and full beam flange thickness for interior connections. In this design procedure, it is suggested that the continuity plate thickness be at least equal to one-half of the beam flange thickness for both exterior and interior connections.

The limiting width-thickness ratio in Equation 37 is the same as that in Section B4 of 2005 AISC *Specification* for the stem of a tee in uniform compression because one edge of the continuity plate is free. Use of this limiting ratio for a continuity plate check is judged to be conservative.

The width of the continuity plate should be selected to extend at least to the end of the beam flange. It may be necessary to extend the continuity plate beyond the beam flange width to increase contact area with the column flange and account for the loss of contact area due to clipped corners to clear the *k*-area. Clipping of corners should be detailed in accordance with Section 3.6 of AISC 358. The net contact width used to calculate the net contact area should not extend a distance one column flange thickness beyond the end of the beam flange (see Figure 21). The width of the column flange may also limit the maximum net contact width. Equation 38, which is used to compute the net width of the continuity plate, takes into account cases where either the beam flange or column flange width is the limiting dimension.

$$b_n = \min\begin{cases} \dfrac{b_{bf} - t_{pz}}{2} - b_{clip} + t_{cf} \\ \dfrac{b_{cf} - t_{pz}}{2} - b_{clip} \end{cases} \tag{38}$$

where t_{pz} = thickness of panel zone and b_{clip} = continuity plate clipped corner dimension parallel to column flange.

Equation 38 assumes that doubler plates, if used, extend beyond the continuity plates. In the case where doubler plates are detailed to stop at the continuity plates, set t_{pz} to the width of the column web.

Step 3. Design continuity plates.

1. Calculate the column flange out-of-plane flexibility coefficient, B_{cf}.

$$B_{cf} = 0.26\frac{b^2}{Et_{cf}^3} + \frac{0.4\left[1 + 0.09\ln\left(\dfrac{b}{t_{cf}}\right)\right]}{Gt_{cf}} \tag{39}$$

2. Calculate the continuity plate in-plane flexibility coefficient, B_{cp}.

$$B_{cp} = \frac{0.42 - C}{Gt} + \frac{b^3}{Ed^3 t} \tag{40}$$

where $C = 0$ for interior connection, and for exterior connection:

$$C = 0.6\left(\frac{b}{d}\right) - 0.14 \ge 0 \tag{41}$$

In Equations 39, 40 and 41, $b = b_n + b_{clip}$, and d and t are defined as the depth and thickness of the continuity plate, respectively.

3. Apportion the beam flange force to one continuity plate:

$$P_{cp} = \frac{P_{uf}}{2}\left(\frac{b_{bf} - t_{pz} - 2t_{cf}}{b_{bf}}\right)\left(\frac{B_{cf}}{B_{cf} + B_{cp}}\right) \tag{42}$$

4. Check if FLB and WLY limit states are satisfied with the addition of continuity plates:

$$\phi R_n \geq P_{uf} - 2P_{cp} \tag{43}$$

where ϕR_n is the design strength of the governing limit state (e.g., FLB or WLY). Resize the continuity plates if the preceding condition is not satisfied.

Note: The continuity plates are initially sized for the required force $R_{u(st)}$ in Equation 35. When continuity plates are added, the force transferred into a pair of continuity plates is $2P_{cp}$. Equation 43 ensures that FLB and WLY limit states of the column are satisfied with a reduce beam flange force demand due to the alternative load transfer mechanism provided by the continuity plates.

Step 4. Design continuity plate flange welds.

Refer to Figure 22 for the free-body diagrams of the continuity plate for the interior and exterior connection configurations.

1. Calculate the required shear force in the flange weld:

$$V_{cp} = \left(\frac{0.6b}{d}\right)\Sigma P_{cp} \tag{44}$$

Note: Based on an idealized trapezoidal normal stress distribution shown in Figure 13a, the resultant normal force, P_{cp}, is located at a distance $0.6b$ from the column web. To satisfy moment equilibrium, in-plane shear forces are present in the flange welds.

2. Either fillet, partial joint penetration (PJP), or a combination of PJP with reinforcing fillet welds can be used to connect the continuity plates to the column flanges if the following condition is satisfied:

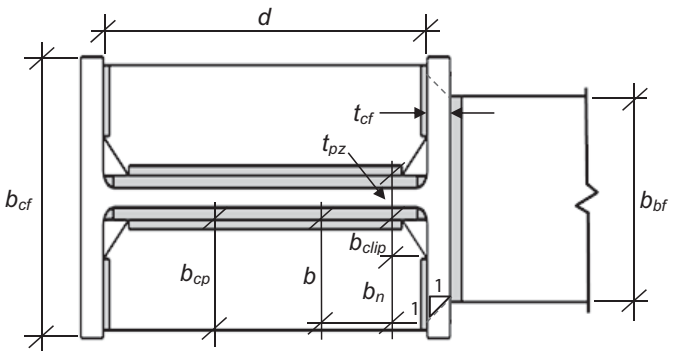

Fig. 21. Net bearing width of continuity plate.

$$\left(\frac{P_{cp}}{F_{ycp}A_{net}}\right)^2 + 3\left(\frac{V_{cp}}{F_{ycp}A_{net}}\right)^2 < 1 \tag{45}$$

Otherwise, CJP welds are required.

Note: The continuity plates may yield, similar to the portion of the beam flanges that are CJP welded to the column. Unlike the beam flange, however, continuity plate is not subjected to shear through its thickness, which causes additional stress. It is proposed in this design procedure that CJP welds still be used if continuity plates are likely to experience significant yielding similar to the beam flanges. Otherwise, PJP, fillet welds, or a combination thereof can be used. Equation 45 is based on the von Mises yield criterion for plane stress and is used to check the net cross section strength of the continuity plate.

3. When either fillet or PJP welds are used, welds are to be designed to satisfy the following:

   a. Design the flange weld for the required resultant force, R_{cp}:

$$\phi_n R_n \geq R_{cp} \tag{46}$$

where

$$R_{cp} = \sqrt{P_{cp}^2 + V_{cp}^2} \tag{47}$$

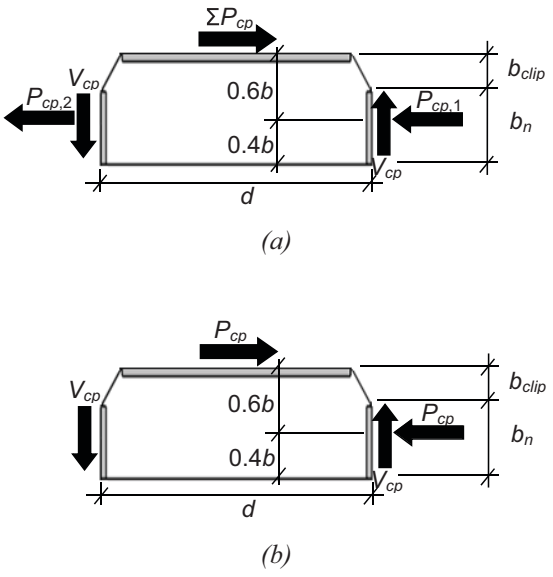

Fig. 22. Free-body diagram of a continuity plate: (a) interior connection; (b) exterior connection.

The design strength for two-sided flange fillet welds is

$$\phi_n R_n = 2(\phi_n)(0.6)t_e b_n F_{EXX}\left(1.0+0.5\sin^{1.5}\theta\right) \quad (48)$$

where t_e is the effective throat of one fillet weld, F_{EXX} is the minimum specified ultimate strength of the weld and ϕ_n is 0.9 per AISC 358. The angle of the resultant force, R_{cp}, measured from the weld longitudinal axis is

$$\theta = \tan^{-1}\frac{P_{cp}}{V_{cp}} \quad (49)$$

b. Check the flange weld at the location of maximum tensile stress, q_{max} (kips/in):

$$q_{max} = \frac{1.6P_{cp}}{b_n} \quad (50)$$

Note: The maximum stress is based on the assumed trapezoidal normal stress distribution in Figure 13a. If two-sided fillet welds are used, the value of q_{max} cannot exceed the unit-length design strength, which can be computed by using Equation 48 and setting $b_n = 1.0$ in.

If fillet welds are used, the design weld strength can be based on $\theta = 90°$.

c. Check maximum shear stress in the flange weld, τ_{max} (kips/in):

$$\tau_{max} = \frac{2V_{cp}}{b_n} \quad (51)$$

Note: Use $\theta = 0°$ to compute the weld design strength.

Step 5. Design continuity plate web weld.

Design the web weld for a required shear force equal to the summation of force allocated to the continuity plate, ΣP_{cp}, as shown in Figure 22. For exterior moment connections (Figure 22b), the required shear force is simply P_{cp}.

$$\phi_n R_n \geq \Sigma P_{cp} \quad (52)$$

If two-sided fillet welds are used, the design strength is computed as

$$\phi_n R_n = 2(\phi)(0.6)t_e l_w F_{EXX} \quad (53)$$

where $\phi_n = 0.9$, t_e = effective throat of one fillet weld and l_w = length of the web weld.

The column panel zone base metal shear strength should also be checked to ensure it has the capacity to develop the force demand allocated to a pair of continuity plates (on each side of the column web).

Figures 23 and 24 show a comparison of two designs for an RBS moment connection with a W14 column. A similar comparison is presented in Figure 24 when a deep column (W33) is used. See Uang et. al (2011) for step-by-step calculations. Compared with the current seismic code requirements, these two design examples show that the proposed flexibility-based design approach often leads to thinner continuity plates and smaller welds. In addition, the option to use fillet, PJP, or PJP with reinforcing fillet flange welds versus CJP flange welds reduces the cost of fabrication and inspection. Also, the significantly reduced beam flange force demand for RBS connections will lead to cases where continuity plates that are required based on the current design code are not needed.

CONCLUSIONS

A historical review of code developments and past full-scale testing programs have suggested that conservatisms exist in the sizing and weld criteria of continuity plates in SMF moment connections. The two main areas of conservatism identified were (1) the beam flange force demand and (2) the force allocation into continuity plates.

Nonlinear FEA suggests that for moment connections with the beam web welded to the column flange—for example, RBS and WUF-W connections—the web transfers a noticeable portion of the moment, thus reducing the beam flange force to the column face. A revised beam flange force demand is introduced (see Equations 32, 33 and 34).

Results of parametric studies demonstrated a reduction of demand force to the continuity plates with increased column flange thickness. Likewise, an increased continuity plate thickness reduced the demand on the column flange. As a result, flexibility coefficients for the column flange and continuity plates were corroborated with FEA to introduce a means by which the beam flange force into the continuity plates can be apportioned.

A design procedure is proposed that provides a rational approach to (1) determine the need for continuity plates, (2) size the thickness of continuity plates and (3) size the flange and web welds to attach the continuity plates. Like other welded moment connection details, however, verification by full-scale testing is needed before the proposed procedure can be adopted for practical design.

ACKNOWLEDGMENTS

This study was made possible by the Structural Steel Educational Council, financially supported by the California Field Iron Workers Administrative Trust (CFIWAT). The authors also would like to acknowledge Mr. Kevin Moore for his constructive comments on this study.

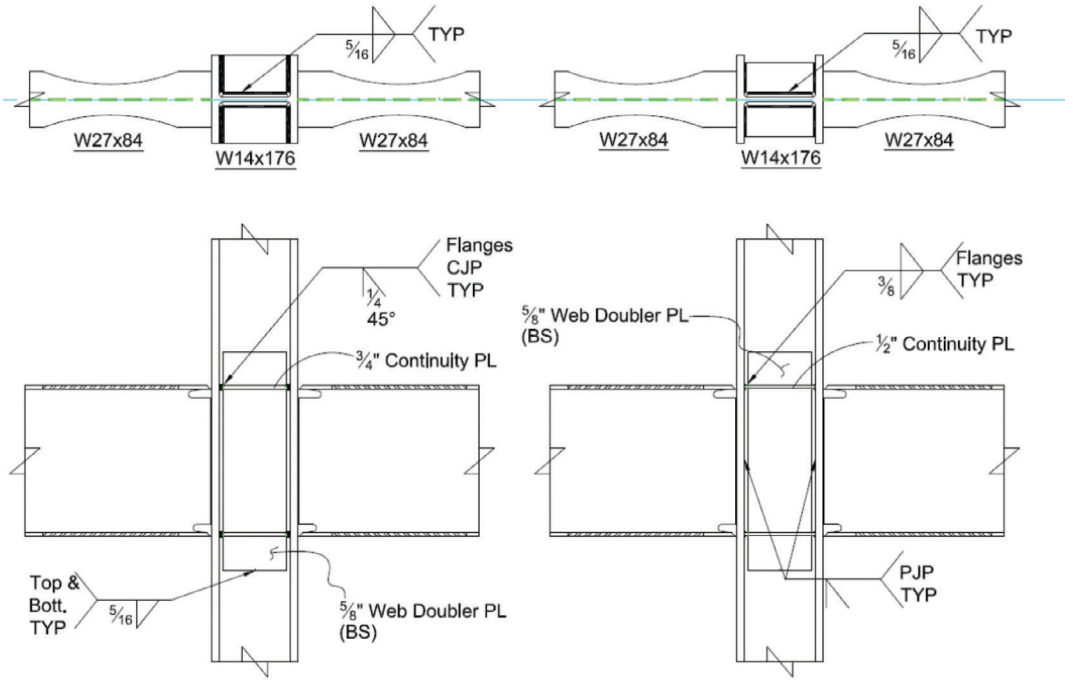

(a) current design practice *(b) proposed design procedure*

(a) *(b)*

Fig. 23. Comparison of continuity plate and weld design of an RBS moment connection with a W14 column: (a) current design practice; (b) proposed design procedure.

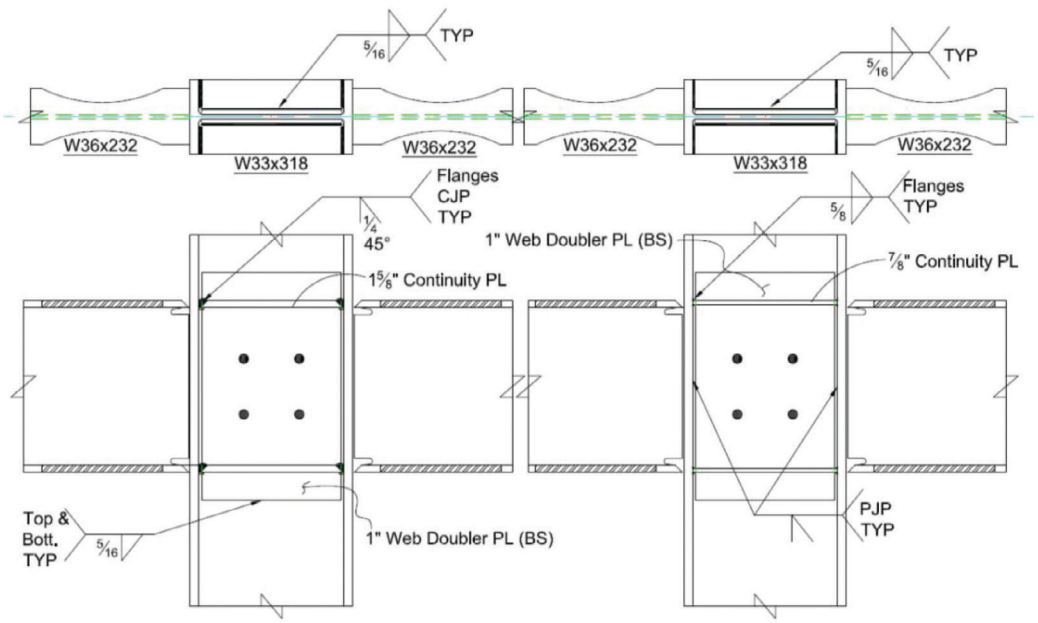

(a) current design practice *(b) proposed design procedure*

(a) *(b)*

Fig. 24. Comparison of continuity plate and weld design of an RBS moment connection with a deep column: (a) current design practice; (b) proposed design procedure.

REFERENCES

ABAQUS (2005), *ABAQUS Standard Users Manual*, Version 6.7, ABAQUS Inc., Providence, RI.

AISC (1999), *Load and Resistance Factor Design Specification for Structural Steel Buildings*, American Institute of Steel Construction, Chicago, IL.

AISC (2005a), *Specification for Structural Steel Buildings*, ANSI/AISC 360-05, American Institute of Steel Construction, Chicago, Illinois.

AISC (2005b), *Seismic Provisions for Structural Steel Buildings*, ANSI/AISC 341-05, American Institute of Steel Construction, Chicago, IL.

AISC (2010a), *Specification for Structural Steel Buildings*, ANSI/AISC 360-10, American Institute of Steel Construction, Chicago, Illinois.

AISC (2010b), *Seismic Provisions for Structural Steel Buildings*, ANSI/AISC 341-10, American Institute of Steel Construction, Chicago, IL.

AISC (2005c), *Prequalified Connections for Special and Intermediate Steel Moment Frames for Seismic Applications*, ANSI/AISC 358-05, American Institute of Steel Construction, Chicago, IL.

AISC (2010c), *Prequalified Connections for Special and Intermediate Steel Moment Frames for Seismic Applications*, ANSI/AISC 358-10, American Institute of Steel Construction, Chicago, IL.

Carter, C.J. (1999), *Stiffening of Wide-Flange Columns at Moment Connections: Wind and Seismic Applications, Design Guide 13*, AISC, Chicago, IL.

FEMA (2000a), "Recommended Seismic Design Criteria for New Steel Moment-Frame Buildings," Report No. FEMA-350, Federal Emergency Management Agency, Washington, DC.

FEMA (2000b), "State of the Art Report on Base Metals and Fracture," Report No. FEMA-355A, Federal Emergency Management Agency, Washington, DC.

FEMA (2000c), "State of the Art Report on Connection Performance," Report No. FEMA-355D, Federal Emergency Management Agency, Washington, DC.

Hajjar, J.F., Dexter, R.J., Ojard, S.D., Ye, Y. and Cotton, S.C. (2003), "Continuity Plate Detailing for Steel Moment-Resisting Connections," *Engineering Journal*, AISC, Vol. 40, No. 4, pp. 189–211.

Lee, C.H., Jeon, S.W., Kim, J.H. and Uang, C.M. (2005), "Effects of Panel Zone Strength and Beam Web Connection Method on Seismic Performance of Reduced Beam Section Steel Moment Connections," *Journal of Structural Engineering*, ASCE, Vol. 131, No. 12, pp. 1854–1865.

Ricles, J., Mao, C., Lu, L. and Fisher, J.W. (2000), "Development and Evaluation of Improved Details for Ductile Welded Unreinforced Flange Connections," Report No. SAC/BD-00/24, SAC Joint Venture, Bethlehem, PA.

Timoshenko, S. and Woinowsky-Krieger, S. (1959), *Theory of Plates and Shells,* McGraw-Hill, New York, NY.

Uang, C.M., Tran, A. and Hassett, P. (2011), "Design of Continuity Plate Welds in Special Moment Frames," *Steel Tips*, Structural Steel Education Council, Moraga, CA.

ERRATA

Bond Behavior of Concrete-Filled Steel Tube (CFT) Structures

Paper by JIE ZHANG, MARK D. DENAVIT, JEROME F. HAJJAR and XILIN LU

(4th Quarter, 2012)

After this paper had gone to press, it was determined that four specimens were accidentally included twice in the databases for push-out tests without shear tabs. These duplicate specimens have been removed, and two other specimens that were inadvertently excluded have been added. Additionally, for four of the specimens, the measured tube thickness has been included in place of the nominal tube thickness that was reported in the original paper. Tables 1 and 2 have been revised to reflect these corrections.

These corrections result in minor changes to the empirical bond stress formulas, Equations 3, 4, 7, 8, 13c, and 14c, as well as Figure 4, have been revised to reflect the corrections:

$$F_{in} = 1.15\times10^{6}\left(H/t\right)^{-2.90} \quad R^2 = 0.69 \tag{3}$$

$$F_{in} = 12800\left(t/H^2\right) \quad R^2 = 0.62 \tag{4}$$

$$F_{in} = 27900\left(D/t\right)^{-1.59} \quad R^2 = 0.32 \tag{7}$$

$$F_{in} = 30900\left(t/D^2\right) \quad R^2 = 0.50 \tag{8}$$

$$F_{in} = 12.8\left(t/H^2\right) \le 0.1 \tag{13c}$$

$$F_{in} = 30.9\left(t/D^2\right) \le 0.2 \tag{14c}$$

The corrections to the database also result in minor changes to the proposed resistance and safety factors. Table 9 has been updated to reflect the corrections; values of $\phi = 0.50$ and $\Omega = 3.00$ are recommended for both CCFT and RCFT.

The data and formulas were used elsewhere in the paper; however, the resulting changes are slight and do not affect the conclusions. Specifically:

- Equation 8 was used in the computation of the last three columns of Table 6. The original and corrected numbers differ by less than 1%.
- Equations 13c and 14c were used in the mechanistic analysis to determine the minimum transfer lengths presented in Tables 7 and 8. Table 7 has been revised to reflect the corrections. In Table 8, the original and corrected numbers differ by less than 1%. The resulting recommendation for C_{in} has not changed.
- Equation 8 was used to compute the bond stress and the load applied at the connection for the analysis presented in Figure 7. The original and corrected numbers differ by less than 1%. The observations from the analyses have not changed.

Table 1. RCFT Push-Out Tests without Shear Tabs								
Reference	Number of Specimens	L (in.)	H, B (in.)	t (in.)	H/t, B/t	F_y (ksi)	f'_c (ksi)	F_{in} (psi)
Shakir-Khalil, 1993a	10	8–24	3.1–5.9	0.20	16–30	43.0	5.6–5.9	48–193
Shakir-Khalil, 1993b	3	16	5.9	0.20	30	43.0	5.2–5.7	29–61
Parsley et al., 2000	4	48–60	8.0–10.0	0.23	35–43	48.0	5.9–6.5	25–42

Table 2. CCFT Push-Out Tests without Shear Tabs								
Reference	Number of Specimens	L (in.)	D (in.)	t (in.)	D/t	F_y (ksi)	f'_c (ksi)	F_{in} (psi)
Virdi and Dowling, 1975	82	6–18	5.8–12.0	0.22–0.40	15–32	mild steel	3.2–6.7	75–431
Shakir-Khalil, 1993a	6	8–24	6.6	0.20	34	43.0	6.1	95–135
Shakir-Khalil, 1993b	3	16	6.6	0.20	34	43.0	5.6–5.7	63–135
Roeder et al., 1999	18	30–76	10.8–24.0	0.22–0.53	20–109	not given	4.0–6.9	1.5–114
Xu et al., 2009	3	20	6.1–6.3	0.11–0.18	35–57	not given	6.8	87–97
Aly et al., 2010	14	16	4.5	0.13	36	50.8	5.9–13.2	51–181

Table 7. RCFT Minimum Transfer Lengths from Mechanistic Analysis									
	Case	H (in.)	B (in.)	t (in.)	H/t	F_y (ksi)	f'_c (ksi)	$L_{transfer}$ (in.)	$L_{transfer}/H$
Square CFT	Load on steel, column extends both sides	4.00	4.00	0.067	59.5	36.0	3.0	45.78	11.45
	Load on steel, column extends below only	4.00	4.00	0.125	32.0	36.0	3.0	15.80	3.95
	Load on concrete	4.00	4.00	0.125	32.0	36.0	3.0	15.80	3.95
RCFT	Load on steel, column extends both sides	4.00	4.00	0.067	59.5	36.0	3.0	45.78	11.45
	Load on steel, column extends below only	8.00	4.00	0.667	12.0	36.0	3.0	23.12	2.79
	Load on concrete	8.00	4.00	0.667	12.0	36.0	3.0	23.12	2.79

Table 9. Computation of Resistance and Safety Factors					
Type	Number of Experiments	R_m/R_n	V_R	ϕ	Ω
RCFT	17	0.94	0.39	0.50	3.02
CCFT	126	1.27	0.50	0.56	2.70

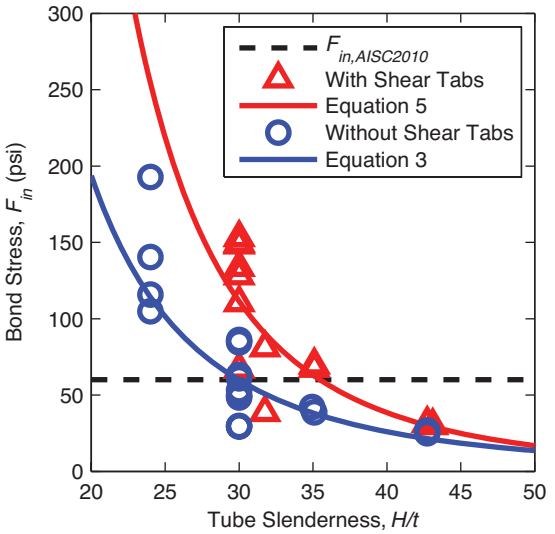

(a) Bond stress of RCFT as a function of H/t

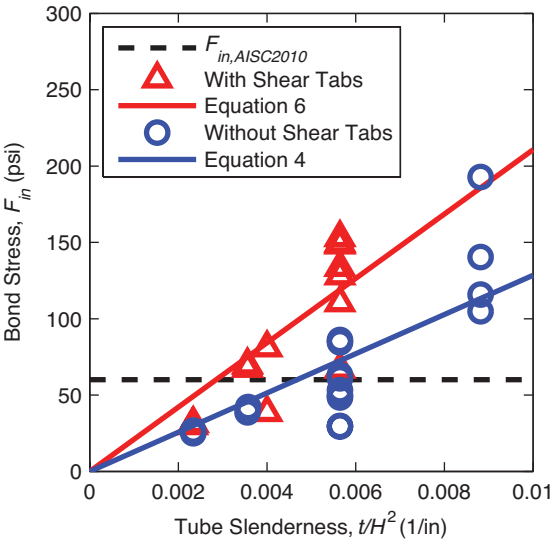

(b) Bond stress of RCFT as a function of t/H^2

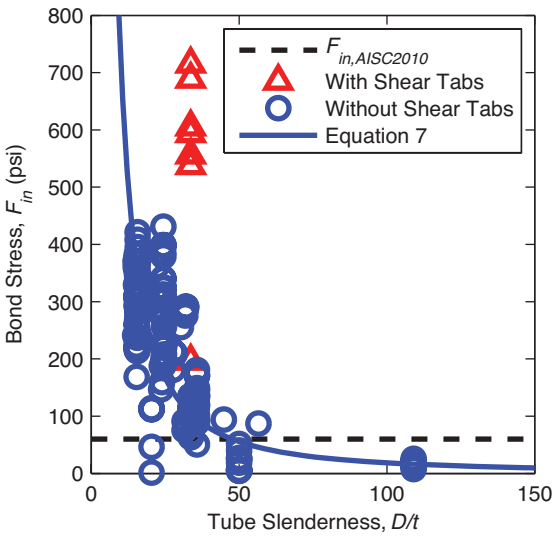

(c) Bond stress of CCFT as a function of D/t

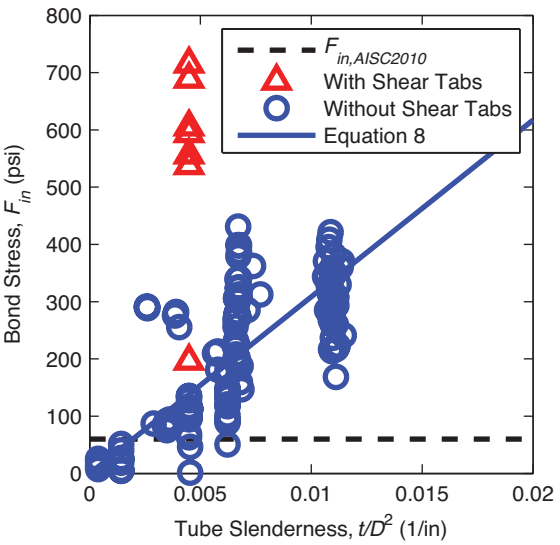

(d) Bond stress of CCFT as a function of t/D^2

Fig. 4. Bond stress for CFT as a function of tube slenderness.

ERRATA

Flange Bending in Single Curvature

Paper by BO DOWSWELL

(2nd Quarter, 2013)

The second to last sentence of the first column on page 81 should read:

> Therefore, the spacing effect can be neglected if the distance between adjacent wheel loads is more than the flange width.